The Dissertation Committee for David Samuel Smith
certifies that this is the approved version of the following dissertation:

Astrophysical Radiation Environments of Habitable Worlds

Committee:

John M. Scalo, Supervisor

Neal J. Evans II

Joe Giacalone

Theodore A. von Hippel

J. Craig Wheeler

Astrophysical Radiation Environments of Habitable Worlds

by

David Samuel Smith, B.S., B.A., A.M.

Dissertation

Presented to the Faculty of the Graduate School of

The University of Texas at Austin

in Partial Fulfillment

of the Requirements

for the Degree of

Doctor of Philosophy

The University of Texas at Austin

August 2006

To my parents, for building the foundation.

And to Diana, for making it livable.

Acknowledgments

I was gratified to be able to answer promptly. I said I don't know. — Mark Twain

Projects of this magnitude cannot be done alone, and I gratefully recognize those who've contributed to this one:

- My wife, Diana, and my parents, James and Mary, are my constant allies and have provided ceaseless care and support.
- John Scalo and Craig Wheeler directed my scientific maturation.
- Stephanie Crouch kept the administrative train on the tracks.
- And, finally, the Donald D. Harrington Graduate Fellows Program and the NSF Graduate Research Fellowship Program provided financial support that freed me to pursue more speculative ideas.

David Samuel Smith

The University of Texas at Austin
August 2006

Astrophysical Radiation Environments of Habitable Worlds

Publication No. _____

David Samuel Smith, Ph.D.
The University of Texas at Austin, 2006

Supervisor: John M. Scalo

Numerous astrophysical sources of radiation affect the environment of planets orbiting within the liquid-water habitable zone of main-sequence stars. This dissertation reaches a number of conclusions about the ionizing radiation environment of the habitable zone with respect to X-rays and gamma-rays from stellar flares and background Galactic cosmic rays. Gamma-rays and X-rays incident on terrestrial-like exoplanet atmospheres can be efficiently reprocessed into diffuse UV emission that, depending on the presence of atmospheric UV absorbers, can reach the surface. Extreme solar X-ray flares over the last 4.6 Gyr could have delivered large enough radiation doses to the Martian surface to sterilize any unprotected organisms, depending on the largest energy releases possible. These flares also pose a significant hazard to manned space missions, since a large flare can occur with little or no warning during an extravehicular activity. A flare as large as the largest observed could deliver radiation doses exceeding safety limits to an astronaut protected

by only a spacesuit. With respect to particle radiation, the nature of Galactic cosmic-ray modulation by astrospheres means that habitable-zone cosmic-ray fluxes change by much larger magnitudes when passing through low-densities regions of the interstellar medium. In contrast to the popular idea that passages through dense molecular clouds are required to significantly enhance Galactic cosmic-ray fluxes and affect planets' electrical circuits, background mutation rates, and climates, we find that densities of only 0.1–10 cm^{-3}, the densities of most interstellar clouds, are sufficient to bring fluxes close to the full, interstellar level. Finally, passages through dense molecular clouds are necessary to shrink astrospheres to within the habitable zone, but such events produce even higher interstellar hydrogen and dust accretion rates than have been estimated because of the combination of enhanced charge-exchange rates between stellar-wind ions and interstellar neutrals and the growing importance of the central star's gravity on particle trajectories as the astrosphere shrinks.

Contents

Chapter 1

Transport of Ionizing Radiation in Terrestrial-like Atmospheres

Chapter Synopsis: Gamma-rays and X-rays from astrophysical sources, such as stellar flares, can be reprocessed in planetary atmospheres into aurora-like ultraviolet spectra. The physical mechanism of reprocessing involves an ionization cascade that starts with incident, high-energy photons that ionize atmospheric molecules through Compton scattering and atomic photoabsorption and ends with multiple, low-energy collisional ionizations by electrons liberated from the original photoionizations. The energy deposited finally causes excitation of UV lines that radiatively de-excite, resulting in auroral-like spectra. The fraction of this auroral emission that reaches the surface depends on the abundance of UV absorbers, such as ozone. For Earth with an ozone layer, roughly 0.2% of incident gamma-rays and X-rays can reach the ground in the 200–320 nm band; for Earth without ozone, the number rises to 4%.

1.1 Introduction

Planets orbiting the sun and other stars are occasionally subjected to large ionizing fluxes from astronomical sources, such as gamma-ray bursts, supernovae, and flares from the parent star. During these highly stochastic events, γ-ray, X-ray, and UV irradiation affects

planetary atmospheric chemistry through ionization and heating, and biological activity through direct mutational enhancement or sterilization.

The frequency of the some types of these events has been estimated by Scalo and Wheeler (2002) and Scalo et al. (2004); see also §1.4. Rates and fluences for intense parent star flares are much more frequent for planets in the conventional habitable zone (continuous liquid water, see Kasting et al. 1993) of low-mass stars; this is discussed briefly in §1.4.1. Whatever the radiation source, the significance of the above phenomena depends strongly on the transparency of the atmosphere to the high-energy radiation. For this reason, we have studied the propagation of ionizing radiation (X-rays and γ-rays in our case) through a suite of model terrestrial-like exoplanet atmospheres of various column densities subjected to irradiation by various incident spectra. We also considered effects due to the angle of incidence.

Previous work has considered atmospheric irradiation by specific X-ray and γ-ray events (Brown 1973, Kasturirangan et al. 1976, Omongain and Baird 1976, Gehrels et al. 2003, and references therein), but only in a terrestrial context and, except for Gehrels et al. who studied the O_3 chemistry, were aimed at estimating only the altitude-dependent ionization. Some treated the radiative transfer in full detail while others used a simple exponential attenuation approximation. No past work has considered the electron excitation of atomic and molecular lines as a channel for redistribution of the ionizing flux to the biologically important ultraviolet spectral range, a major theme of the present work. We also explore a large range of atmospheric column densities, follow the energy transfer in detail using a Monte Carlo approach, including accurate Compton and photoabsorption cross sections, and are generally concerned more with events that may affect planetary life. In particular, we are interested in events strong enough to result in biologically significant doses of radiation at the ground, as well as observable atmospheric chemical effects (e.g., photolysis, ionization, and heating).

In this work, we do not attempt to couple the radiative transfer to the atmospheric chemical or thermal structure; instead we assume an isothermal exponential atmosphere of given composition, column density, and scale height. This is an excellent approximation

for the high-energy radiative transfer, in which the energies considered are much greater than typical molecular electronic binding energies, so the radiative transfer is basically independent of the chemical composition or thermal structure. We postpone a calculation of the impact on the chemical and thermal structure of the atmospheres, since our focus is the radiation that reaches the planetary surface. Specific application of the results of this work for Earth and Mars is given in §1.3.1. Additionally, we are concerned with photon irradiation only. Energetic particles from the parent star or the Galaxy would induce similar processes and their energetics are briefly summarized in §1.4.3.

Note that recent studies of irradiated "hot Jupiters" (e.g., Seager and Sasselov 1998) are concerned with the effect of the mostly visual radiation of the central star on giant planet atmospheres, not irradiation of terrestrial-like atmospheres by high-energy radiation. The present work has more in common with studies of irradiation of accretion disk atmospheres by compact high-energy radiation sources (Ross, 1979; Kallman and McCray, 1982; Ross and Fabian, 1993). In addition, we confine our study to ionizing photons and neglect radiation produced through high-energy particle cascades (see Molina-Cuberos et al. 2001 and references therein for the case of Mars).

The kinds of events we are considering are of interest for their effects on the stability of planetary chemistry, but our primary motivation is the question of how and whether evolution would proceed on habitable planets immersed in a highly variable radiation environment. This question certainly includes the Earth, since it is likely that the terrestrial radiation environment has varied significantly over timescales from millennia to eons due to a variety of phenomena. Would an intermittently enhanced and stochastic radiation field and mutation rate inhibit or sterilize life, or instead accelerate its occurrence and evolution? In the simplest theoretical models for evolution at the level of allele frequencies, the rate of evolution is proportional to the variance of the allele probabilities, and this variance is increased by mutations. Thus one might reason that hypermutation events greatly widens the degree of variability on which selection can operate. The genetic response to hypermutation events or sudden environmental change, and the rate of evolution of the mutation rate itself, is complex (see for example Sniegowski et al. 2000). Already some experimental

evidence shows that evolutionary rates can be increased by enhanced rates of mutation (Itoh et al., 2002).

We are envisioning planetary biospheres in which environmental novelty and exogenous mutational variation is the norm. Some tantalizing lines of evidence and arguments suggest that diversity and hence evolution might be enhanced by an environment that is complex. Directed in vitro and artificial life evolution experiments both indicate that genome lengths (one metric of complexity) grow only in information-rich environments (see Adami et al. 2000). That the rate of evolution increases with environmental diversity or novelty has been demonstrated in organisms as simple as the yeast *Pseudomonas fluorescens* (Rainey and Travisano, 1998) and as complex as guppies (Reznick et al., 1997). See also Moxon et al. (1994); Peak et al. (1996); van Belkum et al. (1998); Pinaud et al. (2002); Chesson and Huntly (1997). The recognition of the existence of hypermutability mediated by heat-shock proteins (see Rutherford and Lindquist 1998; Feder and Hofmann 1999, and the overview by Pugliucci 2002) and mutator mutases (e.g., Giraud et al. 2001; Radman et al. 1999, 2000) are particularly relevant to the present work. Another line of evidence comes from considering evolution as a learning process. Experiments using neural networks as the phenotype for digital genomes show that learning is more efficient in the presence of bursts of strong mutation compared to a constant mutation rate (Moriarty and Miikkulainen, 1995, 1999; Gomez and Miikkulainen, 1997). From one perspective, mutations that increase fitness can be regarded as random measurements on the environment, and genomes as selection-imprinted genetic memory of past environments (Adami et al., 2000). Flares, supernovae, and other stochastic radiation events may provide a wide information channel on which natural selection can operate.

This point of view contrasts with the assumption of Ward and Brownlee (2000) and Gonzalez et al. (2001) that development of complex organisms primarily requires self-regulated stability of the environment. Surely stability at some level (especially with respect to temperature) is desirable for the continuance and evolution of life, but between the extreme limits of tolerance, it is possible that development of complexity is enhanced by fluctuations, as the above examples suggest. If so, accelerated evolution and development

of complexity may occur on habitable planets subjected to a strongly fluctuating radiation environment. This possibility is crucially important for selection of targets in SETI searches (Turnbull and Tarter, 2003). While we cannot yet demonstrate whether this occurs, or whether such an environment simply retards evolution or sterilizes life, the arguments given above suggest that an acceleration of evolution is plausible, and in any case motivates us to quantify the nature of the fluctuations themselves, in particular how well atmospheres of various column densities on terrestrial-like exoplanets are buffered from jolts of ionizing radiation.

1.2 Methods

1.2.1 Exoplanet atmosphere model

Our work assumes an isothermal, plane-parallel atmosphere having an exponential vertical density distribution. Because of the high energies of the photons compared to the molecular thermal energies in the atmosphere, the value of the temperature is irrelevant for our calculations except insofar as it affects the scale height. Similarly, the photon energies are so large compared to electronic binding energies of atoms or molecules that the radiative transfer and secondary electron energy budget is approximately independent of the composition of the atmosphere; in effect the photons "see" free electrons at these energies. The particular density values at each grid point are determined by specifying the total column density in g cm^{-2}, which determines the number density of particles at the ground n_0. Using n_0 and h, we build up the grid according to $n_i = n_0 \exp(-z_i/h)$, where z_i is the altitude of the i-th grid point.

Choosing the scale height is fairly straightforward when using an exponential density distribution. In all quantities related to the radiative transfer, the scale height appears only in the product $n_0 h$ and the quotient z/h. The total column density of the atmosphere is $n_0 h$, so fixing the column density (and hence the optical depth) and adjusting the scale height only changes the number density of molecules at the ground, which is irrelevant for our work. The one effect of choosing a particular scale height is that it sets the altitude

scale in terms of z/h, i.e., the altitudes corresponding to given optical depths from the top of the atmosphere are determined by h. In this work, we use the sea-level terrestrial scale height value of 8 km. The altitudes in our results for any other desired scale height may be determined according to

$$z' = \left(\frac{h}{8\ \mathrm{km}}\right) z, \tag{1.1}$$

where z is the altitude given by our results, and z' is the altitude on the exoplanet with a scale height h.

If the habitability of an exoplanet is adequately defined by the presence of liquid water, the lower limit to the column density of a planet with surface liquid water is given by considerations of water vapor photodissociation followed by atmospheric escape (Ingersoll, 1969; Kasting, 1988; Kasting et al., 1993). An estimate of the lower limit is 30–100 g cm^{-2} for a terrestrial mass planet, depending on the temperature (J. Kasting, private communication). This is also coincident with the smallest column density required to prevent atmospheric collapse on synchronously rotating planets ($\gtrsim$ 30 g cm^{-2}, as given by Joshi et al. 1997).

Avoiding speculation about the origins or robustness of life, for illustrative purposes we assume that planets possessing even thin atmospheres are indeed habitable—given enough warming flux from the parent star.

Selecting atmospheric constituents for terrestrial-like exoplanets is extremely speculative. Fortunately, we can neglect atmospheric composition effects on the radiative transfer of the incident ionizing radiation because the energies considered here are so much larger than any internal atomic or molecular transition energies of interest. The composition matters only in that it determines the column abundances of electrons, which are the primary scatterers. For simplicity, we chose an inert N_2 atmosphere for the transfer of ionizing radiation. None of the results for the ionizing radiation would change significantly if the primary constituent were CO_2 or O_2.

The transfer of the UV reemission *does* depend on assumed composition and is discussed in §1.2.5. For this calculation, we chose two simple UV opacity sources that probably bracket the extremes of UV transparency. For present-day Earth analogues, we

included O_2 and O_3 absorption, distributed in an abundance profile similar to Earth's (taken from Appendix C of Brasseur et al. 1999 for altitudes up to 60 km and from Table 14-7 of Champion et al. 1985 for larger altitudes). For column densities other than Earth's, we scaled the terrestrial O_3 altitude profile to match the vertical O_3 column density from the top of the exoplanet atmosphere, i.e., the peak of the O_3 profile is always at the same column density from the top. This could be a severe approximation—see §1.2.5. For Archean Earth analogues, we removed molecular absorption and included only Rayleigh scattering, although we recognize the possibility of other Archean UV screens (e.g., Sagan and Chyba 1997), especially aerosols. These two idealizations are useful to gauge the surficial UV fluence in different limits.

1.2.2 Incident radiation spectra

Given that we are interested in such sources as supernovae, gamma-ray bursts, and stellar flares, we chose incident spectra characteristic of these. For supernovae we assumed monoenergetic spectra of energies 0.125, 0.25, 0.5, 1, and 2 MeV (1 MeV = 1.24×10^{-3} nm), which correspond to the energy ranges of ^{56}Co and ^{56}Ni decay lines (Höflich et al., 1998). We chose not to model specific supernovae spectra—they are merely the motivation for using a monoenergetic spectrum, which is instructive in its simplicity. In order to model the effects of stellar flares and gamma-ray bursts, we included two types of continuous spectra.

To represent the lower-energy spectra of flares, we adopted the following parameterized formula which is actually the energy dependence expected for a high-temperature thermal plasma, such as the solar corona (Tucker and Koren, 1971):

$$\frac{dN}{d\lambda} \propto \lambda^{-2} \exp(-\lambda_p/\lambda), \tag{1.2}$$

where $dN/d\lambda$ is the number of photons per unit wavelength. Our adopted spectral form for flares is also consistent with the 0.9–10 keV spectrum of the giant X-ray flare in the dMe star EV Lac presented by Favata et al. (2000). We are unaware of the expected or observed form of generic solar or stellar flare spectra; the problem is complicated by the fact

that flares peak in different wavelength regimes at different times. For the energy spectrum corresponding to Eq. 1.2, the photon number distribution can be shown to be

$$\frac{dN}{dE} = \frac{N_\gamma}{E_p} \exp\left(-\frac{E}{E_p}\right), \tag{1.3}$$

where N_γ is the total number of photons in the model and $E_p = hc/\lambda_p$ is the energy corresponding to the peak of the wavelength spectrum (Eq. 1.2). We calculated models irradiated by flare spectra with peak energies, E_p, of 2.2, 22, and 220 keV, corresponding to average energies of 1, 10, and 100 keV (see Krucker and Lin, 2002). For these spectra, the lower and upper photon energy cutoffs are $0.01E_{\rm inc}$ and $4E_{\rm inc}$, respectively, where $E_{\rm inc}$ is the specified average incident energy, from which the peak energy, E_p, was calculated. We chose to place the above arbitrary limits on the flare spectra for computational reasons: photons of higher energy than about $4E_{\rm inc}$ are too improbable, and photons of energy much lower than $0.01E_{\rm inc}$ are of little physical significance because of the low energies.

For the gamma-ray burst spectra, we used a broken power law with an exponential cutoff known as a Band spectrum (Band et al., 1993). The photon number distribution is given by

$$\frac{dN}{dE} = k \left(\frac{E}{100 \text{ keV}}\right)^\alpha \exp(-E/E_0) \tag{1.4}$$

for $E \leq (\alpha - \beta)E_0$ and

$$\frac{dN}{dE} = k \left[\frac{(\alpha - \beta)E_0}{100 \text{ keV}}\right]^{\alpha-\beta} e^{\beta-\alpha} \left(\frac{E}{100 \text{ keV}}\right)^\beta \tag{1.5}$$

for $E \geq (\alpha - \beta)E_0$, where $E_0 = 250$ keV is the turnover energy, α and β are the power law indices. We adopt for this particular spectrum upper and lower wavelength limits of 50 keV and 3 MeV, respectively, with an average energy of 200 keV (constrained by observations, e.g., Preece et al. 2000). The empirical power law indices lie in the range $-1.6 \lesssim \alpha \lesssim 0.0$ and $-4.5 \lesssim \beta \lesssim -1.5$ (Tavani et al., 2000). For our calculations, we adopt $\alpha = -0.9$ and $\beta = -2.3$, which are roughly the averages in the histograms given by Tavani et al.

We examined Band spectra, but for simplicity our results are given only for the

model flare spectra and monoenergetic spectra. Since both the model flare spectra and Band spectra decline in photon number at higher energies, the results are very similar if the average energies are equal. Indeed, some of our results will be shown to be completely independent of the form of the incident spectrum. Additionally, gamma-ray bursts are such infrequent events that their contribution to the mutational environment of an exoplanet is much smaller than supernovae and stellar flares.

The angle of incidence was taken to be normal to the atmospheric boundary surface for most of the calculations. Given a point source in the sky, the angle of incidence will be roughly perpendicular for most of the planet. But the spherical symmetry of the problem still makes a calculation for normal incidence slightly more optimistic than one that included the full radiative transfer effects of varying the angle of incidence. We tested varying the angle of incidence and its effects on the transmitted fraction and discuss the results briefly in §1.3.5 below.

1.2.3 Incident ionizing radiation transfer

The transfer of the incident X-rays and γ-rays was handled via a Monte Carlo code that was written for this work and that accurately accounts for the complicated angular and energy dependences of the cross sections. Section 1.2.4 explains the algorithm in detail.

The initial step of the calculation involves Compton scattering and photoabsorption of γ-rays and X-rays. Compton scattering was implemented as an inelastic scattering cross section given by the Klein-Nishina formula (Lingenfelter and Rothschild, 2000). Photoabsorption was included as a purely absorptive cross section of the empirical form

$$\sigma_{\rm pa}(E,Z) = 2.04 \times 10^{-30}(1+0.008Z)\frac{Z^3}{E^3}\ {\rm cm}^2, \tag{1.6}$$

where Z is the atomic number of the absorber and E is the photon energy in units of the electron rest mass (Setlow and Pollard, 1962). We found that Eq. 1.6 reasonably represented the detailed cross section measurements (Henke et al., 1993) for a variety of elements for energies greater than the corresponding K photoabsorption edge (480 eV for nitrogen).

Since terrestrial-like exoplanet atmospheres can be very optically thick to high-energy radiation (e.g., the optical depth is 65 at 1 MeV on the Earth), two weighting procedures were used to more efficiently track photon statistics (see Watson and Henney 2001 for a summary of weighting and other variance reduction techniques). In our model, approximately 10^6 photons are initialized at the top of the atmosphere heading downward with energies sampled according to the specified incident spectrum. Supernovae and flare spectra were sampled by inversion, while the Band spectrum was sampled by a rejection technique (Hammersley and Handscomb, 1979; Kalos and Whitlock, 1986). Every photon carries a statistical weight, which signifies the probability that it is still scattering in the atmosphere after each interaction. Each photon is propagated to a random optical depth, sampled from $e^{-\tau}$, since the probability that the photon will travel a distance corresponding to τ without interaction is $e^{-\tau}$. The photon is then statistically forced to scatter by subtracting a fraction of its weight equal to the probability, $e^{-\tau}$, that it did not scatter before exiting the grid. This technique is known as "forced scattering" (Witt, 1977). In this way, the statistics are more accurately tracked for a discrete number of photons, and each Monte Carlo interaction explores many possible outcomes. Mersenne Twister (Matsumoto and Nishimura, 1998) was used for pseudo-random number generation.

During the above process, we tracked the spectra of photon energy deposited at the ground, electron energy deposited (via Compton recoil and photoabsorption) at various layers in the atmosphere, and photons lost to space. Later this information is used to calculate the UV reemission fluxes and ionization fractions.

1.2.4 Radiation Transport Code

Weighted Monte Carlo Algorithm with Forced Scattering

An outline of the structure of the Monte Carlo code is as follows:

1. **Initialize**

   (a) Assign each photon an initial incident energy E_0 drawn randomly from the specified incident spectrum.

(b) Initialize the direction of propagation, θ_p. The angle of incidence, θ_i, is defined with respect to the plane of the atmosphere, but θ_p is oriented toward the ground. Hence for a normally incident ray $\theta_p = 0$ and $\theta_i = \pi/2$. We track the direction of propagation in three dimensions by a unit vector (v_x, v_y, v_z) that represents the direction of travel with respect to the ground, where the z-axis points downward to the ground. For the physics in this work, however, only the projection of the vector onto the z-axis (v_z) matters, where $v_z = \cos\theta_p$.

(c) Set the statistical weight, w, of each photon to unity. Higher weights imply that the photon represents a packet of w photons, rather than one photon, which alters only normalizations.

2. **Propagate**

(a) Recalculate the total cross sections for absorption and scattering.

(b) For downward traveling photons, add a portion of the photon energy equal to $w\exp(-\tau/v_z)$ to the spectrum of flux received at the ground, where w is the current weight of that photon, τ is the optical depth from the photon's current altitude to the ground, and v_z is the downward component of the direction vector from above. This is the forced scattering procedure (cf. Witt 1977). This fraction of the weight removed represents the probability that the photon is still scattering (which we are forcing it to do) is simply one minus the probability that it did not scatter. If the photon is directed upward, the procedure is identical except the peeled-off weight is added to the spectrum of photons reflected by the planet and τ corresponds to the optical depth from the photon's altitude to the top of the atmosphere.

(c) Sample a random optical depth to the interaction location from an exponential probability distribution $p(\tau) = \exp(-\tau)$ by generating a uniform deviate $R \in [0, 1]$ and inverting p to find the corresponding optical depth: $\tau = -\log R$. We choose an exponential distribution with unit mean because the photon behaves as part of a beam subjected to extinction and so has an intensity following Beer's

Law, or $I(\tau) = I_0 \exp(-\tau)$. Thus the probability that a photon will traverse a distance corresponding to an optical depth τ unimpeded is $\exp(-\tau)$.

(d) Move the photon a distance in the atmosphere corresponding to the randomly sampled optical depth. Since the atmosphere is based on an exponential density profile, the new altitude can be found analytically, eliminating one of the most computationally intensive procedures in Monte Carlo radiative transport—sampling a density field along a ray. From the sampled optical depth τ, we update the altitude z to z' according to

$$z' = -h \log \left[\exp\left(-\frac{z}{h}\right) + \frac{v_z \tau}{\chi h} \right], \tag{1.7}$$

where χ is the total extinction coefficient, including Compton scattering and photoabsorption, and h is the scale height.

3. **Interact**

(a) At the new location z', multiply the statistical weight w by the scattering albedo a, which represents the probability that the photon still exists after the interaction. (If the photon were instead replaced by a continuous energy stream, a fraction a of the flux that interacted would be scattered, while a fraction $1 - a$ would be absorbed.)

(b) Add the fraction of energy that was photoabsorbed to the spectrum of energy deposited at this layer. This represents the fraction of photons that would not have been scattered. Rather than absorbing all the energy of a fraction $1 - a$ of a packet of photons, the weighting technique stipulates instead to absorb that fraction of the energy of a single photon.

(c) Choose a new propagation direction θ_p by sampling by a rejection technique from the differential Klein-Nishina formula, where the forward direction is parallel to (v_x, v_y, v_z). The angular distribution is symmetric about this direction, so the angle about that axis is chosen from a uniform distribution. The sampled angle

gives the direction change after the scattering event, so the a new direction vector must be calculated.

(d) Update the photon energy based on the change in direction and the corresponding Compton energy loss. Add the Compton recoil electron energy to the spectrum of energy deposited in this layer. This energy is multiplied by the scattering albedo and the current photon weight in order to conserve energy.

(e) Remove the current photon from the model if the updated weight is smaller than a predetermined minimum value, since the photon is now statistically insignificant; otherwise, go to step 2 and repeat.

Code Benchmark: Pure Scattering Atmosphere

A standard solution to the radiative transfer equation can be obtained for pure scattering in the two-stream approximation. The approximation of pure scattering given by Schuster (1905) assumes (i) a plane-parallel atmosphere, (ii) a diffuse source incident at the top of the atmosphere, (iii) no sources inside the atmosphere, and (iv) a perfectly absorbing ground. With these conditions, the fraction of the incident flux transmitted through the atmosphere is $T \simeq 2/(2 + \tau/\mu)$, where τ/μ is the total optical thickness of the atmosphere divided by an angle cosine which represents the average angle of incidence of the radiation field. The actual value of μ can only be obtained by iteratively solving the radiation field until a value for μ converges; however, as can be seen in our benchmarks, the approximation $\mu \simeq 1$ for normally incidence radiation is sufficiently accurate.

To compare our code, which includes more complicated physics than pure scattering, to a known scattering solution, we removed photoabsorption and altered the treatment of Compton scattering to make it conservative. Thus the photons were allowed to scatter with a cross section equal to the Compton cross section, but the energy changes were ignored. Figure 1.1 shows the comparison between the Monte Carlo code and the Schuster solution as a function of column density. The agreement is quite good for a Monte Carlo code, even for thick atmospheres, where the discrepancy is $\lesssim 15\%$. For reference, the μ required to bring the Schuster transmittance into agreement with ours is shown.

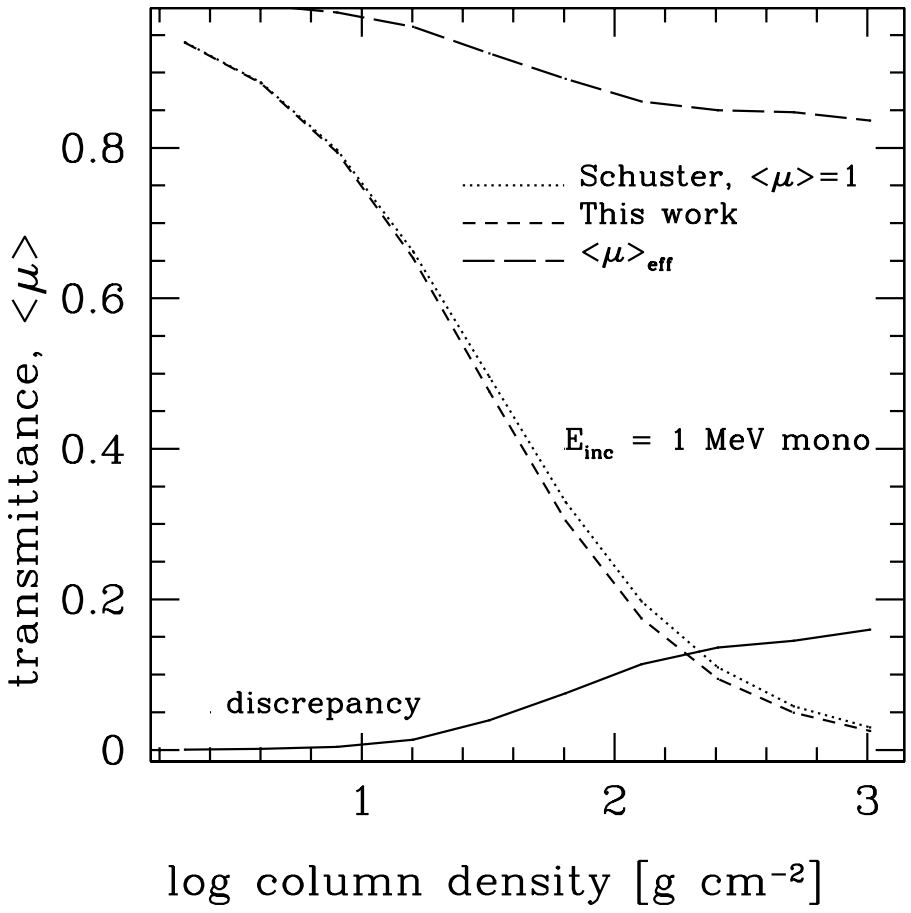

Figure 1.1: Comparison of the Monte Carlo code with the Schuster (1905) pure scattering solution. The agreement is quite good, even for thick atmospheres, where the radiation field deviates most from being monodirectional. The fractional discrepancy between the two results is due to the approximation of $\langle\mu\rangle = 1$ for the Schuster result, which would tend to overestimate the transmittance. The value of $\langle\mu\rangle_{\rm eff}$ required to bring the Schuster data down to ours is shown and is $\gtrsim 0.8$ even for the thick atmospheres, implying that $\langle\mu\rangle \sim 1$ is an acceptable approximation. In our calculations, we assume normal incidence.

Code Benchmark: Beer-Lambert Absorption

In the case of pure absorption, photons interact only once and then are removed from the model. To simplify the calculation, we treated the extinction coefficient as purely absorptive and removed all photons upon the first scattering. We found the agreement between the exponential attenuation approximation of the Beer's law and the Monte Carlo code to be excellent. The Monte Carlo code shows an exponential dependence and matches Beer's Law to better than 1 part in 10^4 for even the thickest atmospheres. This test is somewhat trivial, but disagreement would nevertheless indicate problems with the radiative transfer code.

Code Benchmark: Comptonization by Cold Electrons

A third test was performed to test solely the non-conservative, Compton scattering aspect of the code. We removed all photoelectric absorption and allowed each photon to Compton scatter a fixed number of times (100 in this case). In the limit of large scattering number, the Compton energy losses become small, and the photon energy spectrum approaches a Gaussian. Based on the results of Xu et al. (1991), we can write an analytic approximation for the spectrum as a function of initial energy and scattering number. The energy spectrum after the n-th scattering is given by Eq. 10 of Xu et al. (1991):

$$F_n(\lambda) = (2\pi\sigma_n^2)^{-1/2} \exp[-(\lambda - \lambda_n)^2/2\sigma_n^2], \tag{1.8}$$

where

$$\lambda_n = \lambda_{n-1} + 1 - \frac{4}{5\lambda_{n-1}} + O\left(\frac{1}{\lambda_{n-1}^2}\right), \tag{1.9}$$

$$\sigma_n^2 = \left(1 + \frac{8}{5\lambda_{n-1}^2}\right)\sigma_{n-1}^2 + \frac{2}{5} + O\left(\frac{1}{\lambda_{n-1}^2}\right), \tag{1.10}$$

and λ is in units of the Compton wavelength ($\lambda_c \equiv h/m_e c$).

Figure 1.2 shows a comparison of the Monte Carlo code and the Xu et al. formula for $n = 100$ scatterings of 2^{19} photons, each with an initial dimensionless wavelength (λ/λ_c) of 51.1 (equivalent to an energy of 10 keV). The correspondence is excellent. The slight shift to longer wavelengths of the Monte Carlo results compared to the analytic approximation

is due to the neglect of the higher order terms in the above formula for λ_n and σ_n^2, which leads to an underestimation of the peak wavelength and variance when using the Xu et al. formula. The Monte Carlo code uses the full Compton energy shift formula and energy dependent cross section and thus should be more accurate.

1.2.5 UV redistribution

Physical process

The Earth receives a steady flux of solar wind ions with very high kinetic energies. Energetic electrons produced via a variety of mechanisms (fast particles, magnetohydrodynamic flows, etc.) excite atmospheric constituents, resulting in dynamic auroral displays that extend from the ultraviolet to the infrared. Chamberlain (1961) discusses the detailed physical mechanisms.

When astrophysical bursts of radiation, such as stellar flares, supernovae, and gamma-ray bursts irradiate a terrestrial-like exoplanet with a sufficiently thick atmosphere, analogous phenomena will occur. The initial ionizing radiation creates primary electrons as a photoproduct. These very energetic charged particles then produce secondary photoelectrons which excite molecules and create aurora-like emission in much the same way the solar wind and EUV does on Earth. Figure 1.3 illustrates this process.

Since the energies considered here are so high, an incident photon can cause the ionization of tens of thousands of molecules before being absorbed. Primary Compton-recoil electrons and photoelectrons are responsible for the ionization as they are slowed by collisions with neutral N_2 molecules. Each of these ionizations results in a secondary electron, and it is these liberated electrons which dominate the particle flux from the incident radiation (see Evans 1974 for direct observations of auroral electron spectra). The average energy of secondary electrons released by primary ionization of N_2 is about 35 eV (Fano, 1963), with only a very weak dependence on primary electron energy or charge of the target. For example the average energy per ion pair for air, argon, and water are 34, 26, and 30 eV, respectively (see, for example, Fano 1963). The distribution of secondary energies has been studied experimentally by Peterson et al. (1971, 1972).

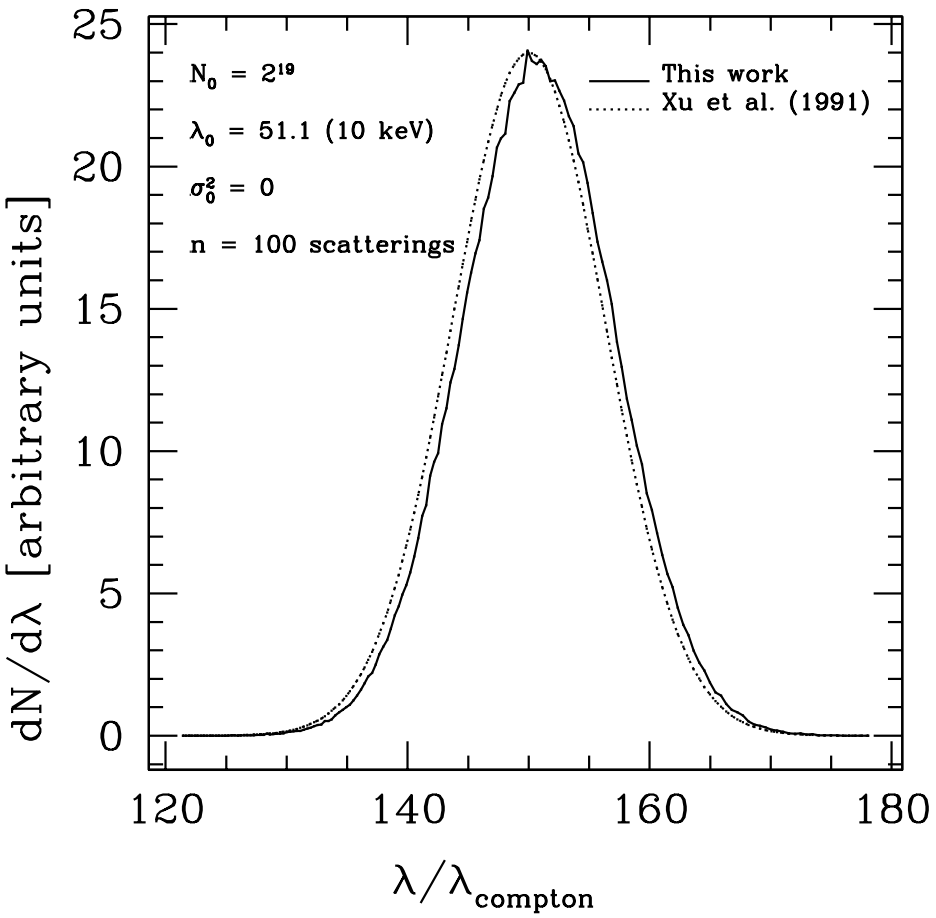

Figure 1.2: Comparison of the Monte Carlo code with the results of Xu et al. (1991). The slight shift to longer wavelengths of our code compared to the analytic approximation is due to the neglect of the higher order terms in the analytic expression for λ_n and σ_n^2 (see text), which leads to an underestimation of the peak wavelength and variance when using the Xu et al. formula (Eq. 1.8).

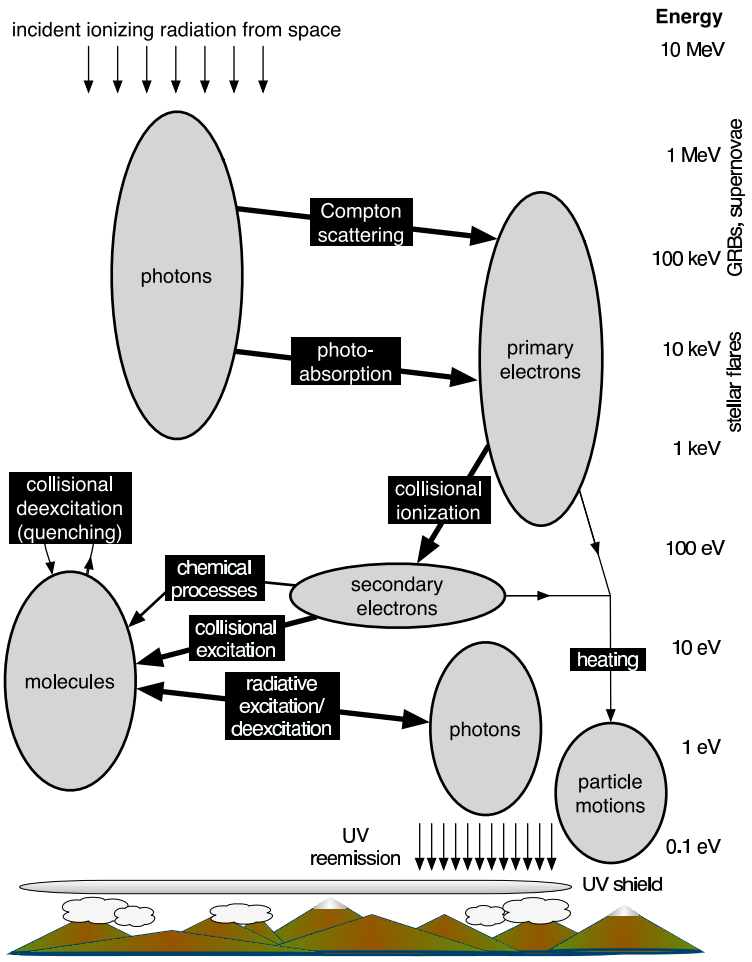

Figure 1.3: Schematic illustration of the physical processes that mediate the redistribution of the incident energy from ionizing gamma- and X-ray photons (arrows at top left) to UV aurora-like reemission (arrows at bottom right). Thick lines indicate processes found to be important and/or included in the present study. Chemical processes are not included, not because they will not be affected by the irradiation events, but because the redistribution process is relatively insensitive to the detailed atmospheric abundances. "Heating" refers to sharing of primary and secondary electron kinetic energy with thermal energies of other particles through Coulomb or neutral-neutral collisions. "Quenching," or collisional deexcitation of the levels excited by secondary electrons, was found to be unimportant for lifetimes and deexcitation cross sections representative of various N_2 electronic levels associated with transitions leading to ultraviolet emission. A detailed discussion of heating and quenching is presented in §1.2.5.

As each secondary electron moves through the atmosphere, it can exchange energy with other particles by (i) elastic Coulomb interactions and elastic collisions with neutrals (both of which lead to thermalization of the electron energy) or (ii) excitation of internal degrees of freedom in the target molecules. In case (ii), secondary electron impact excitation of electronic, vibrational, and rotational levels will result in a rich line spectrum extending from the UV (electronic transitions) to the radio (pure rotational transitions). This excitation by secondary electrons and subsequent line emission is equivalent to the main process giving rise to the terrestrial auroral spectra. In our case the process redistributes some of the energy of the X-ray and γ-ray photons into UV and longer wavelengths. This redistribution is also analogous to that which occurs in gases of cosmic abundances in accretion disks around compact stellar remnants (Ross, 1979; Kallman and McCray, 1982; Ross and Fabian, 1993) and in interstellar clouds where secondaries from cosmic-ray ionization events can result in a rich UV line spectrum (Prasad and Tarafdar, 1983; Gredel et al., 1989). An important difference between the molecular and atomic cases is that in the atomic case the secondary electron energy must be thermalized once its energy falls below the excitation potential of the first excited state of the atom, whereas the molecular case has a broad spectrum of excitation channels at lower energies.

Excitation dominates heating

In a highly ionized plasma, most of the electron energy would be thermalized by electron-electron collisions because of the long-range nature of the Coulomb interaction—very little of the energy would go into excitation and line radiation. The importance of electron-electron collisions depends on the ionization fraction, however, and for a nearly neutral planetary atmosphere, most of the secondary electron energy goes into excitation, not heating. Fox and Victor (1988) presented detailed calculations of the dependence on the ionization fraction of the number of excitations to various electronic levels of N_2.

We can derive an order of magnitude condition for excitation to be more important than Coulomb interactions by comparing the respective collision frequencies. The characteristic Coulomb collision frequency can be expressed as (Spitzer 1978, Eqs. 4.13 and

4.14)

$$\nu_{\rm ee} = \frac{4\pi e^4 n_e}{m_e^2 w^3} \ln\left(\frac{\Lambda m_e w^2}{3kT}\right), \tag{1.11}$$

where w is the relative velocity between test and field electrons and the factor

$$\Lambda \equiv \left(\frac{9k^3T^3}{4\pi n_e e^6}\right)^{1/2} \tag{1.12}$$

is the usual approximate cutoff factor in the Coulomb logarithm—see Spitzer (1962) and Mitchner and Kruger (1973) for derivations. The extra ratio of energies in the logarithm accounts for the fact that the test particles follow a non-Maxwellian velocity distribution. Noting the $w^{-3} \propto E^{-3/2}$ dependence, we see that this agrees very well with the analytical fit to more detailed calculations given by Swartz et al. (1971):

$$\nu_{\rm ee} = 2.0 \times 10^{-4} n_e^{0.94} E^{-1.44} {\rm sec}^{-1}, \tag{1.13}$$

where E is the energy of the secondary electrons in eV and $E \gg kT$. We adopt this convenient fit here. We neglect electron-ion Coulomb scattering because the time scale for thermalization by electron-ion scattering is larger than for electron-electron scattering because the high electron-ion mass ratio reduces the per-collision energy transfer efficiency.

We estimate the inelastic collision frequency to be

$$\nu_{\rm inel} = n\sigma_{\rm inel}(2E/m_e)^{1/2}. \tag{1.14}$$

The cross sections for ionization and excitation of N_2 and other atmospheric gases are energy dependent, with much structure due to resonances with dominant electronic and vibrational transitions as the secondary electron energy decreases. A useful plot of cross sections for N_2, O_2, and O from 1 to 100 eV is given in Banks and Kockarts (1973), and cross sections for N_2 at low energies are given in Fig. II.43 of Mitchner and Kruger (1973). Edgar et al. (1973) give cross sections for five ionization continua of N_2 due to electron impact, with cross sections of 10^{-16} to 10^{-17} cm^2 at 100 eV. The cross sections are smaller by about a factor of three at 35 eV and decline rapidly at still lower energies. (The first ionization potential

of N_2 is 14.5 eV.) Similar behavior is expected for other candidate dominant constituents of planetary atmospheres. For N_2, below about 20–30 eV typical inelastic cross sections are of order 10^{-16} cm^2 down to about 1.5 eV, with variations of a factor of a few (e.g., the local peak at about 2 eV due to excitation of vibrational levels within the ground electronic states). Similar cross sections occur for other candidate molecules and for the thermal inelastic electron impact excitation of atoms inferred from data in Spitzer (1978). Taking this value of 10^{-16} cm^2 for the cross section, we estimate the inelastic collision frequency to be

$$\nu_{\rm inel} = 5 \times 10^{-9} n \sigma_{\rm inel,16} E^{1/2} \ {\rm sec}^{-1}, \tag{1.15}$$

where E is in eV, n is in cm^{-3}, $\sigma_{\rm inel,16}$ is in units of 10^{-16} cm^2. Comparing Eqs. 1.13 and 1.15 we find that inelastic excitation will dominate Coulomb thermalization ($\nu_{\rm ee} \ll \nu_{\rm inel}$) when

$$n_e/n \ll 4 \times 10^{-2} \sigma_{\rm inel,16} E_{35}^2, \tag{1.16}$$

where E_{35} is in units of 35 eV. According to Crisp (2000), the ionization fractions in the D ($\sim$ 90 km), E ($\sim$ 110 km), F1 ($\sim$ 170 km) and F2 ($\sim$ 300 km) layers of the Earth's ionosphere are only 10^{-12}, 10^{-7}, 10^{-5}, and 10^{-3}, respectively. As our results will show, all but the most extreme cases of irradiation (such as a 10^8 erg cm^{-2} stellar flare) will produce ionization fractions below the limit of Eq. 1.16. Thus *the secondary electrons will expend nearly all their energy in excitation, and almost none in heat.*

Another portion of the secondary electron energy will be expended in elastic, electron-neutral, molecular collisions. The electric field of the electron polarizes the charge distribution in the molecule, inducing a dipole moment, leading to an effective potential at large distance that varies as r^{-4} and a cross section that varies as w^{-1} (recall w is the relative velocity). The calculated and measured momentum transfer cross sections for such interactions are large, of order 10^{-15} cm^2 at the energies of interest (10 times larger than for inelastic collisions). Despite the large cross section, the fractional energy lost by the secondary electron in a typical electron-neutral collision is of order $2m_e/Zm_p$ (e.g., Mitchner and Kruger 1973 Eq. 7.5), which makes this process much less than a 1% effect compared

Transition	Species	Wavelength range
$A^3\Sigma_u^+$-$X^1\Sigma_g^+$ (Vegard-Kaplan)	N_2	210–540 nm
$a^1\Pi_g$-$X^1\Sigma_g^+$ (Lyman-Birge-Hopfield)	N_2	130–200 nm
$E^3\Sigma_g^+$-$A^3\Sigma_u^+$ (Herman-Kaplan)	N_2	213–274 nm
$C^3\Pi_u$-$B^3\Pi_g$ (2nd positive)	N_2	268–545 nm
$B^2\Sigma_u^+$-$X^2\Sigma_g^+$ (1st negative)	N_2^+	320–600 nm

Table 1.1: Strongest UV N_2 and N_2^+ electronic band systems (Banks and Kockarts, 1973; Lofthus and Krupenie, 1977; Huber and Herzberg, 1979).

to excitation, and so we neglect it.

Approximate treatment of UV reemission

Although the secondary electrons have a distribution of energies, their mean energy is 35 eV for N_2, a value which is known to be nearly independent of the composition, as discussed above. The electron excitation cross sections as a function of energy for N_2 have broad maxima around 10–80 eV (Jones 1974, Fig. 4.15), which neatly brackets the average energy of the secondary electrons, so we expect the collisionally excitable N_2 electronic states to be well populated among the the target molecules. This suggests that, in the UV, the sources of strong reradiation will be N_2 emission bands, similar to the case for auroral lines (Jones, 1974). Data for some of the more important band systems are given in Table 1.1 (Banks and Kockarts, 1973; Lofthus and Krupenie, 1977; Huber and Herzberg, 1979). We emphasize that we have chosen a pure N_2 atmosphere simply to keep the calculations and presentation manageable, and that any molecule which might be suspected to dominate the compositions of terrestrial-like exoplanet atmospheres has similarly spaced electronic levels and should be excited with comparable efficiency.

We ignore the complication of the full line radiative transfer, since we are interested in only estimating the transparency of atmospheres to auroral emissions. The density and amplitude of lines (in photon number per unit wavelength) in auroral spectra is roughly distributed uniformly from the UV to the near IR (see spectra in Jones 1974; Chamberlain 1961), so we assume the energy fluence $F_{\mathrm{dep,i}}$ deposited at each layer i is reradiated from

that layer in the form

$$\frac{dF_{\rm UV,i}}{d\lambda} = \frac{F_{\rm dep,i}}{\lambda \ln(\lambda_{\rm max}/\lambda_{\rm min})} \tag{1.17}$$

between the wavelengths $\lambda_{\rm min}$ and $\lambda_{\rm max}$ corresponding to the lower and upper limits of the important auroral emission lines. The Monte Carlo calculation yields the fraction of the original incident energy that is deposited by X-ray photoabsorption and Compton recoil at each layer i. From this number, we assume that all primary electron energy is transferred to secondary electrons. At each layer a spectrum of the form of Eq. 1.17 is reemitted isotropically and then attenuated either by Rayleigh scattering or molecular absorption.

We have replaced the rich and extremely complex line spectrum of N_2 (and other molecules) by a continuous spectrum that contains (roughly) the same amount of flux per unit wavelength interval as the line spectrum. This smearing of the line spectrum into an equivalent continuous spectrum was assumed because: (i) we are interested in only an order-of-magnitude estimate for the fraction of energy that reaches the ground in each wavelength interval, and (ii) the alternative would require the solution of a large number of rate equations for the level populations at each altitude, a calculation beyond the scope of the present work.

Atmospheric UV screening

Any UV reemission will be subject to a variety of opacity sources within the exoplanet atmosphere. Depending on the precise atmospheric composition, the primary UV screens might be molecular absorbers or aerosols, or in the absence of these, pure Rayleigh scattering. We take two extreme limits: pure O_3/O_2 absorption with a terrestrial abundance profile (characteristic of present-day Earth) and pure Rayleigh scattering (i.e., no molecular or aerosols absorbers, characteristic of Archean Earth). Although we recognize that there is considerable uncertainty concerning UV screening in the Archean atmosphere (e.g., Levy and Miller 1998; Cockell 2002), recent evidence concerning mass-independent isotopic fractionation in Archean sulfides (Farquhar et al., 2002) suggest the absence of a significant UV shield during this period (Wiechert, 2002), so our assumed Archean atmosphere may not be so extreme. And if fluxes are large enough to significantly erode the ozone layer (e.g.,

Gehrels et al. 2003 and references therein), then the pure scattering case may be relevant even for periods when the planet possessed an ozone layer.

To find the fraction of the reemitted flux that would reach the ground in the case of pure Rayleigh scattering, we attenuated the reemission on a layer-by-layer basis according to a modification of the Schuster (1905) solution for "foggy" atmospheres, which is a special case of the two-stream approximation. Schuster (1905) solved the problem of a pure scattering atmosphere for a source above the atmosphere and a purely absorptive base (see §1.2.4). For the problem of the transmission of UV reemission in a planetary atmosphere, we adopt an average incidence angle cosine $\langle\mu\rangle = 0.5$, since our source of reemission is isotropic, and we expect the radiation field to be roughly so. Under these boundary conditions the fraction of the incident flux transmitted through the atmosphere is

$$T(\tau) = \frac{1}{1+\tau}, \tag{1.18}$$

where τ is the total optical depth of the atmosphere. Similarly, the albedo of the atmosphere is $R \equiv 1 - T$, or

$$R(\tau) = \frac{\tau}{1+\tau}. \tag{1.19}$$

For the UV redistribution in our work, we modified this solution to accurately handle reflection from the part of the atmosphere above each UV reemission layer, which was not present in the original Schuster solution. In our case, on a layer by layer basis, we have an isotropic source (a layer at which redistribution from ionizing to UV radiation occurs) sandwiched between two atmospheres with purely absorptive boundaries (both the ground and space do not reflect). The situation is illustrated in Fig. 1.4. We denote the optical depths of the upper and lower atmospheres as $\tau_\uparrow$ and $\tau_\downarrow$, respectively.

Since we are concerned with the amount of reemitted UV which reaches the surface, we set the transmission fraction of the "sandwich" to be the sum of the flux directly transmitted from the emission layer to the ground and the flux reflected between the two atmosphere layers and finally transmitted to the ground. Each atmosphere layer obeys the Schuster solution in isolation, but together the reflection terms increase the expected

transmission by a significant margin. In a manner similar to the popular two-stream approximation, the isotropic source flux can be divided into a downward hemisphere ($\mu_+ \geq 0$) and an upward hemisphere ($\mu_- < 0$), each containing half of the total emitted flux. Starting with the downward hemisphere, the successive contributions to the surface flux from multiple reflections can be written easily. Starting with the flux transmitted without reflection, we add the contribution from the flux that has reflected once off the bottom atmospheric layer and then off the top atmospheric layer and is then transmitted through the bottom atmospheric layer. To that we add the flux that reflects off the bottom atmospheric layer, then the top, then the bottom, then the top, and then is transmitted through the bottom atmospheric layer, etc. Hence,

$$\begin{aligned} T(\mu_+) &= \frac{1}{1+\tau_\downarrow} + \frac{\tau_\downarrow}{1+\tau_\downarrow}\frac{\tau_\uparrow}{1+\tau_\uparrow}\frac{1}{1+\tau_\downarrow} \\ &\quad + \left(\frac{\tau_\downarrow}{1+\tau_\downarrow}\right)^2\left(\frac{\tau_\uparrow}{1+\tau_\uparrow}\right)^2\frac{1}{1+\tau_\downarrow} \\ &\quad + \cdots \\ &= \frac{1}{1+\tau_\downarrow}\sum_{p=0}^{\infty}\left[\frac{\tau_\downarrow\tau_\uparrow}{(1+\tau_\downarrow)(1+\tau_\uparrow)}\right]^p. \end{aligned} \tag{1.20}$$

Note that, $\forall \tau_\downarrow, \tau_\uparrow > 0$,

$$\frac{\tau_\downarrow\tau_\uparrow}{(1+\tau_\downarrow)(1+\tau_\uparrow)} < 1, \tag{1.21}$$

so this is a geometric series which can be summed to produce the transmission fraction for the downward hemisphere:

$$T(\mu_+) = \frac{1+\tau_\uparrow}{1+\tau_\uparrow+\tau_\downarrow}. \tag{1.22}$$

A similar procedure for the upward hemisphere can be carried out, arriving at the above sum plus another factor of $R(\tau_\uparrow)$ accounting for the extra reflection from the upper atmosphere required to make the flux downward directed:

$$\begin{aligned} T(\mu_-) &= \frac{\tau_\uparrow}{1+\tau_\uparrow}\frac{1}{1+\tau_\downarrow} \\ &\quad \times \sum_{p=0}^{\infty}\left[\frac{\tau_\downarrow\tau_\uparrow}{(1+\tau_\downarrow)(1+\tau_\uparrow)}\right]^p \end{aligned}$$

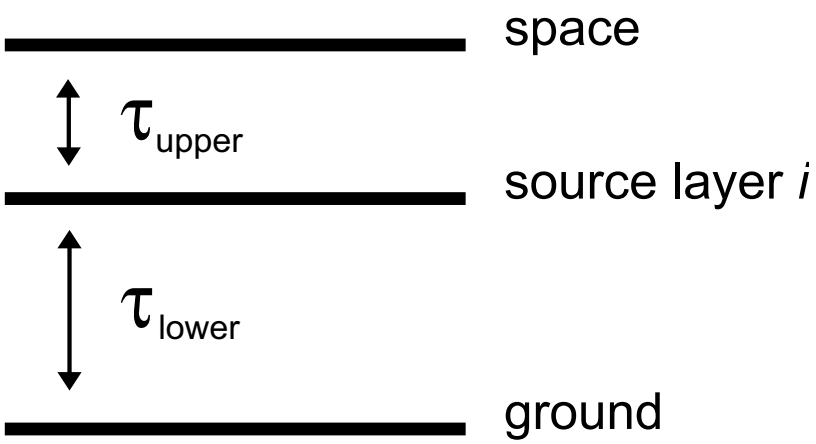

Figure 1.4: Diagram of the geometry of the UV redistribution layer and the surrounding atmosphere.

$$= \frac{\tau_\uparrow}{1+\tau_\uparrow+\tau_\downarrow}. \tag{1.23}$$

The total transmission of the source within the sandwich is

$$\begin{aligned} T &= \frac{1}{2}\left[T(\mu_+)+T(\mu_-)\right] \\ &= \frac{1/2+\tau_\uparrow}{1+\tau_\uparrow+\tau_\downarrow}. \end{aligned} \tag{1.24}$$

In the limit $\tau_\uparrow \gg \tau_\downarrow \gg 1$, we can see that $T \to 1$, which allows us to define $\tau_\uparrow \gg \tau_\downarrow$ as "close to the ground," so no matter how optically thick the atmosphere, auroral emission "close to the ground" in a pure scattering atmosphere will reach the ground. The limit $\tau_\uparrow \ll \tau_\downarrow$ is the Schuster solution limit, in which $T \to 1/(2+2\tau_\downarrow)$. Note that this limit is actually half of the Schuster transmission because the source we consider is isotropic, while Schuster defines the entire source flux to be incident on the atmosphere.

In this scheme, the fraction of the flux emitted at layer i transmitted by the atmosphere is

$$T(\lambda,z) = \frac{1/2+\tau_\uparrow(\lambda,z)}{1+\tau_\uparrow(\lambda,z)+\tau_\downarrow(\lambda,z)}, \tag{1.25}$$

where $\tau_\downarrow$ and $\tau_\uparrow$ are the optical depths of the part of the atmosphere below and above the layer of reemission, respectively. We assume, to good approximation, that the emission

layer itself is of negligible optical depth (we use 256 altitude zones per atmosphere). The redistributed UV flux received at the ground, $F_{\rm UV}$, is then

$$F_{\rm UV} = \int_0^{z_{\rm max}} \int_{\lambda_{\rm min}}^{\lambda_{\rm max}} F_{\rm UV}(\lambda, z)\ T(\lambda, z)\, d\lambda\, dz, \tag{1.26}$$

where $F_{\rm UV}(\lambda, z)$ is the differential photon number spectrum as a function of wavelength and altitude, $z_{\rm max}$ is the altitude of the highest atmosphere zone, and $T(\lambda, z)$ is the wavelength-dependent transmission function for layer at height z given by Eq. 1.25 for the optical depths above and below that layer. The surface transmitted energy fractions we calculate in this manner are upper limits, since we neglect aerosol absorption and scattering and collisional deexcitations (see §1.2.5).

A very different situation occurs if the atmosphere contains a significant source of UV molecular opacity at altitudes below the bulk of the secondary electron deposition. We use O_2 and O_3 as our prototype. To examine molecular absorption, we must neglect Rayleigh scattering, since the above treatment applies only in the pure scattering limit. We assume the transmission through each layer in the presence of molecular absorbers follows the Beer-Lambert law, so that

$$T(\lambda, z) = \exp[-\tau(\lambda, z)], \tag{1.27}$$

where $\tau(\lambda, z)$ is the wavelength-dependent optical depth to absorption from height z to the ground. The subsequent calculation of $F_{\rm UV}$ is analogous to Eq. 1.26. Integrating over atmospheric layers is equivalent to a formal solution to the transfer equation (neglecting the angular dependence), in which the source function at each layer is due only to redistributed UV radiation, since the thermal contribution at these wavelengths is negligible for any possible atmospheric temperature. For this case, we assume that half of the reemitted flux is directed straight downward and half is directed upward. We ignore the upward fraction and attenuate the downward half to obtain our estimate.

We chose terrestrial fractional abundances of O_2 and O_3 (taken from Brasseur et al. 1999 for altitudes up to 60 km and from Champion et al. 1985 for higher altitudes) for our

absorption case. Since the relative ozone is to zeroth order a photoproduct of irradiation incident on the top of the atmosphere, the ozone concentrations as a function of column density from the top of the atmosphere should be approximately invariant. Taking ozone on the Earth as the prototype, we scaled terrestrial concentrations to match our various atmosphere models. In each case, the fractional abundance of ozone at a particular altitude on the exoplanet was matched with the abundance of terrestrial ozone at an altitude corresponding to the same column density from the top of the atmosphere. In cases where the exoplanet atmospheric column density was smaller than that of Earth, we truncated the ozone profile at low altitudes. It must be noted that this is a gross simplification, since the O_3 profile depends on the O_2 column density, not the total optical depth, and even then the O_3 peak does not follow the O_2 column density linearly because of the density-dependence of the ozone production from O + O_2 (Kasting and Donahue, 1980; Kasting et al., 1985). For this reason the calculations of ozone shielding of the redistributed UV radiation must be considered as illustrative only. The wavelength-dependent O_2 and O_3 cross sections were taken from Yung and DeMore (1999). The transmitted fractions in the presence of the ozone shield presented hereafter assume an upper limit to the biologically relevant flux of 320 nm. Unfortunately, the results are very sensitive to this quantity (as shown in Fig. 1.15), but evidence from terrestrial UV-B damage (see §1.3.4) supports this conservative value.

Collisional Deexcitation

In our model, we assume all photon energy deposited in the atmosphere is reemitted as UV because of the efficiency of secondary electron excitation in a gas of very low ionization fraction. But in reality part of the reemission will be quenched by collisional deexcitation. Quenching was not included in our calculation because it would require solving the complete non-LTE level population rate equations for a variety of potential atmospheric constituents, a level of complexity and uncertainty beyond the scope of the present work. Nevertheless, we do wish to estimate its importance.

We first consider the usual two-level approximation. Rigorously, the two-level solution for the line intensity cannot be used because the principle of detailed balance between

excitation and deexcitation rates does not hold when the secondary electrons have a non-Maxwellian velocity distribution. We instead require that all electron excitations result in an emitted line photon, except for the fraction suffering collisional deexcitation.

Ionization fractions are small enough in terrestrial-like exoplanet atmospheres that deexcitation occurs primarily via neutral atoms and molecules. The exception is the highest altitudes of atmospheres subjected to very high fluence ($\gtrsim 10^8$ erg cm^{-2}) stellar flares. We assume that the quenched transition is not forbidden, which would reduce the Einstein A_{ji} value by a large factor, as in terrestrial [OI] emission. The following method also applies (with some modification) for vibrational transitions within a given electronic level.

For the following estimate, we compute the excitation-deexcitation balance and obtain the relative importance of collisional quenching and radiative deexcitation in the most important N_2 auroral emission band systems listed in Table 1.1. The N_2^+ level is important despite low ionization fractions because many of the secondary electrons will ionize N_2 to the $B^2\Sigma_u^+$ excited of state of N_2^+, and subsequent fluorescence to the $X^2\Sigma_g^+$ state yields the well-known strong 391.4 nm auroral band. The cross section for this process is large, and the efficiency of production of this band relative to all ionizations is about 6% (Banks and Kockarts 1973, p. 213). Following Jones (1974), we let dn_2/dt be the rate of excitation of the target molecule—N_2 in our case—to the upper electronic level by secondary electrons in the two-level scheme, A_{21} is the Einstein A value for the downward transition, Q_{21} is the thermally averaged collisional rate coefficient $\langle \sigma v \rangle$ for downward transitions due to collisions between the target and the dominant quenching particle M (N_2 and O_2 for the Earth), and n_2 and $n_{\rm M}$ are the number densities of the excited species and quenching species M, respectively. The balance between secondary electron excitation and the sum of radiative and collisional deexcitation can be written as

$$\frac{dn_2}{dt} = A_{21} n_2 + Q_{21} n_2 n_{\rm M}. \tag{1.28}$$

By dividing the balance equation by the unquenched rate $A_{21} n_2$, it is easy to show that the

Band	A_{ji} [s^{-1}]	Q_{ji}[cm^3 s^{-1}]	$n_{M,crit}$ [cm^{-3}]
Vegard-Kaplan	0.53	1.5×10^{-11}	3×10^{10}
L-B-H	8.3×10^3	$\lesssim 3 \times 10^{-10}$	$\gtrsim 3 \times 10^{13}$
Herman-Kaplan	5.3×10^3	$\sim 10^{-10}$	$\sim 5 \times 10^{13}$
2nd positive	2.7×10^7	$\sim 10^{-10}$	$\sim 7 \times 10^{17}$
1st negative	1×10^7	4×10^{-10}	3×10^{16}

Table 1.2: Quenching factor data for N_2 UV band systems (Banks and Kockarts, 1973; Lofthus and Krupenie, 1977; Huber and Herzberg, 1979). See Table 1.1 for definitions of the bands.

unquenched radiative deexcitation rate is reduced by a quenching factor f_Q:

$$f_Q = 1 + n_M Q_{21}/A_{21}. \tag{1.29}$$

We also define the critical density of quenching particles to be $n_{M,crit} \equiv A_{21}/Q_{21}$, at which the emission is halved.

We have estimated the critical quenching height z_Q in our models, at which $n_M(z_Q) = n_{M,crit}$, and the altitude of maximum energy deposition z_E, for two important UV transitions of N_2. We can then gauge the amount by which a line is quenched by defining the quenching ratio, $\rho_Q \equiv z_Q/z_E$. When $\rho_Q \ll 1$, excitations take place where densities are low enough that collisional deexcitation is unimportant. The results of this approach can be applied to any other molecule of interest, depending on A_{ji} and Q_{ji}. Table 1.2 lists the relevant parameters for the N_2 band systems of Table 1.1 taken from Lofthus and Krupenie (1977), Huber and Herzberg (1979), and Banks and Kockarts (1973). Since the lifetimes of the upper molecular electronic states vary by orders of magnitude, we have chosen to illustrate the situation with two representative transitions of N_2 in Table 1.2—the Lyman-Birge-Hopfield and 2nd positive systems. These bands have A_{ji} values (10^4 and 10^8, respectively) that cover the range of values for allowed transitions.

Figure 1.5 shows ρ_Q as a function of atmospheric column density for the two representative N_2 systems and two different incident photon energies. We can see from the plot that only Lyman-Birge-Hopfield (small A_{ji} value) is significantly quenched and only at very high incident energies, for which the altitude of maximum energy deposition z_E is very low.

For X-ray incident energies, neither of the lines is significantly quenched, but the reemission in the L-B-H band would be reduced by a factor of about two. We can then conclude that reemission due to stellar flares incident on thin atmospheres are the least quenched, while the highest-energy irradiation by supernovae and gamma-ray burst γ-ray lines will be the most quenched.

The quenching effect as a function of incident energy is shown in Fig. 1.6. As expected the magnitude of quenching increases with increasing incident energy, since z_E decreases roughly logarithmically with optical depth. Again we see that the L-B-H system is quenched more than the 2nd positive transition, due to its lower A_{ji}. Interestingly, we see in both Figs. 1.5 and 1.6 that the incident energy sensitivity of ρ_Q is smaller for higher column density atmospheres. This behavior can be understood from the dependence of the quenching ration on the optical depth (which is proportional to the column density). Using the Chapman solution for the energy deposition, we can approximate the height of maximum as $z_{\max} = h \log \tau$ (see §1.3.5). We defined the altitude at which quenching becomes significant as z_Q such that $n(z_Q) = n_{\mathrm{M,crit}}$. From this we have,

$$z_Q = -h \log(n_{\mathrm{M,crit}}/n_0), \tag{1.30}$$

where n_0 is the number density of quenching molecules at the planet's surface and h is the scale height. Taking the definition of the quenching ratio, we can write an approximation for it as

$$\begin{aligned} \rho_Q &= z_Q/z_E \\ &= -\frac{h \log(n_{\mathrm{M,crit}}/n_0)}{h \log \tau} \\ &= \frac{\log(Q_{ji}\Sigma/A_{ji}h)}{\log(\Sigma\sigma)}, \end{aligned} \tag{1.31}$$

where Σ is the column density and σ is the cross section for energy deposition at the original incident energy. We can see from the form of this formula that the ratio $Q_{ji}\Sigma/A_{ji}h$ determines whether the quenching ratio is smaller or larger than 1, since all atmospheres

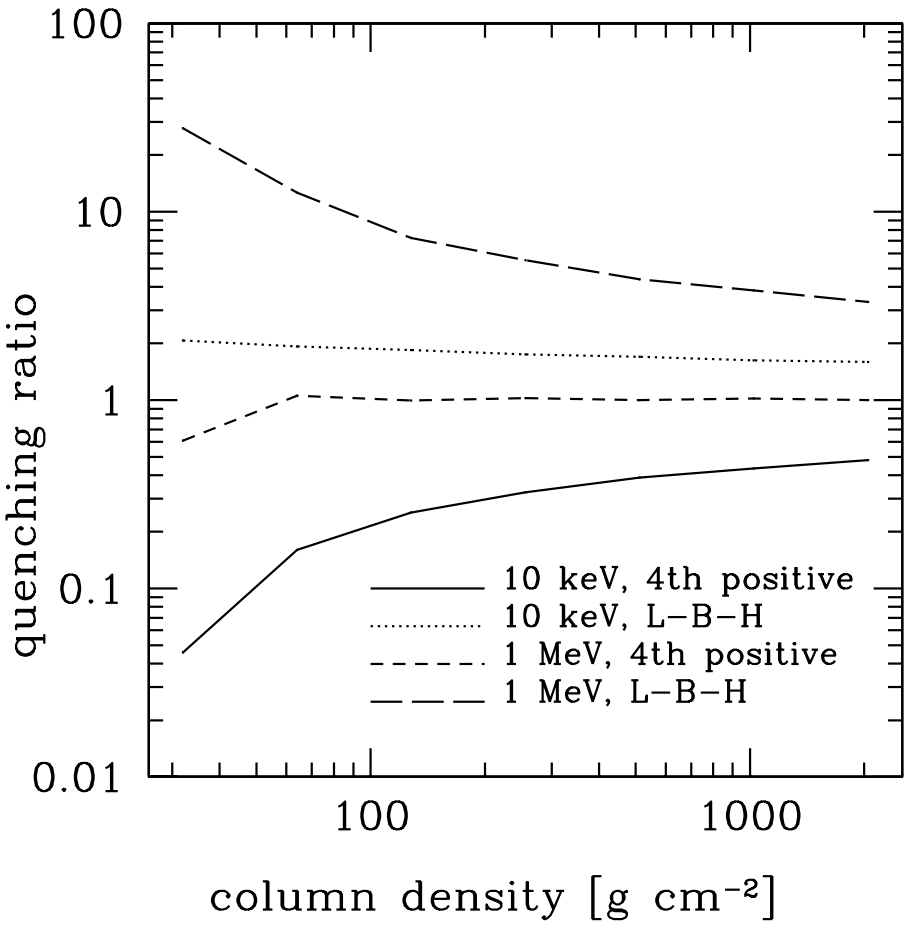

Figure 1.5: Quenching ratio ρ_Q as a function of column density for two representative molecular nitrogen systems. Only the Lyman-Birge-Hopfield system is significantly quenched and only at very high incident energies, for which the altitude of energy deposition z_E is very low. For hard X-ray incident energies, neither of the systems is completely quenched, but the reemission in the L-B-H band would be reduced by a factor of a few. The quenching ratio approaches unity for very thick atmospheres (see text for explanation).

of exoplanets considered habitable in this work have optical depths greater than unity at the incident energy. The only energy dependence enters in the denominator, in the optical depth τ. Rewriting,

$$\rho_Q = 1 + \frac{\log(Q_{ji}/A_{ji}\sigma h)}{\log \tau}. \tag{1.32}$$

Now we can see that as the column density (and hence τ) increases, the quenching ratio will approach unity. Furthermore, the quenching ratio increases as the incident energy increases because the dominant cross sections at keV to MeV energies (photoabsorption and Compton scattering) both decrease with higher energy. In other words, higher penetration of the atmosphere as the energy of the incident ionizing radiation increases reduces the UV reemission efficiency by depositing more of the energy in denser regions of the atmosphere.

Depending on the relative fluxes of the various auroral lines, the overall UV reemission will be quenched by a factor somewhere between the limits given in the plots. Since characteristic A_{ji} values and collisional deexcitation cross sections show a similar range for other molecules we can generalize our conclusions to the statement that quenching will only significantly affect the surficial fluences for transitions with A_{ji} values of $\lesssim 10^4$ s^{-1}. Given that all of the lines listed in Table 1.1 are roughly equally strong, we expect that quenching will be insignificant for stellar flare irradiation, and for supernovae and gamma-ray bursts, the emission will likely be reduced by factor of only a few, depending on the A_{ji} value and column density.

1.3 Results and Discussion

1.3.1 Examples

Archean Earth

The Archean Earth presents perhaps the simplest case of a habitable planet, with respect to the atmospheric radiative transfer. In particular, before the rise of oxygen, the atmosphere lacked the current ozone shield, and so (neglecting aerosols or other potential UV shields; see Cockell 2002 and references therein) the atmosphere may have been relatively transparent to

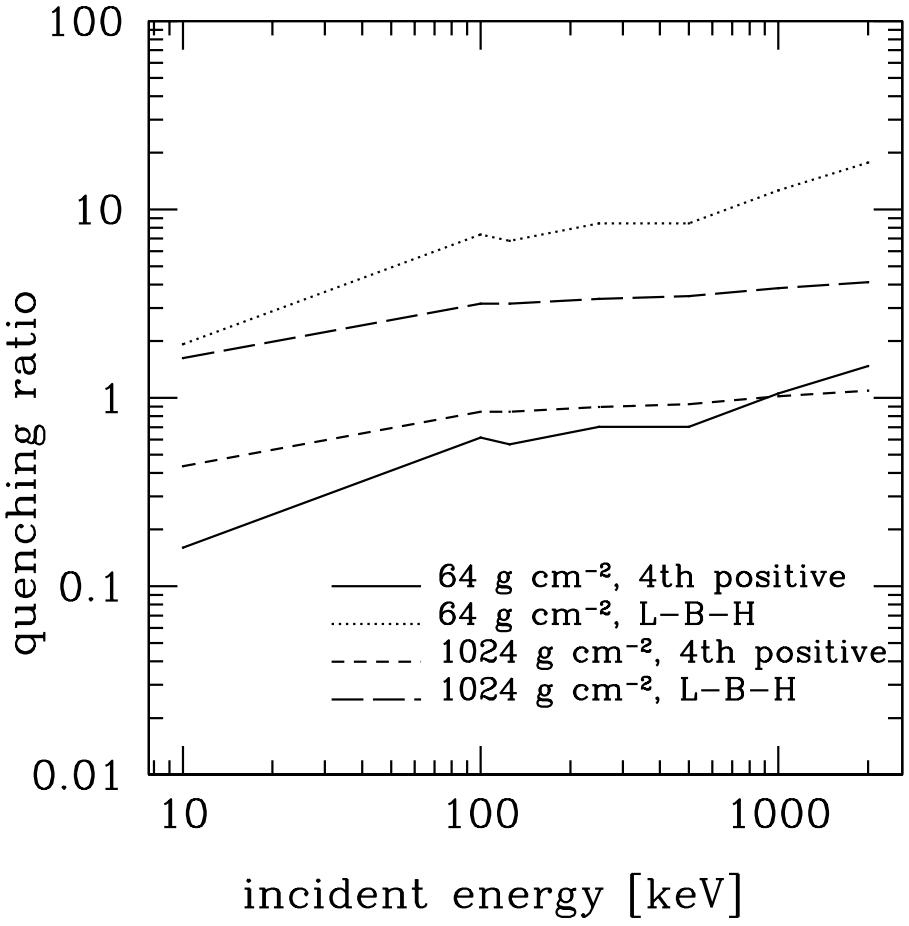

Figure 1.6: Quenching ratio ρ_Q as a function of incident energy for the two representative N_2 lines. Again we see that the L-B-H is quenched more than the 2nd positive transition, due to its lower A_{ji}. Interestingly, we again see that the difference in ρ_Q for the two lines is smaller for higher column densities, as can also be seen in Fig. 1.5 (see text for an explanation). Irregularities in the 64 g cm^{-2} curve are due to the smaller optical depth, i.e., fluctuations in the optical depth of the height of maximum energy deposition are magnified in altitude, leading to a larger uncertainty in z_E.

Spectrum Type	Ionizing Transmittance	UV Transmittance (200-320 nm)
1 keV $\langle E \rangle$ exponential	~ 0	3.9×10^{-2}
10 keV $\langle E \rangle$ exponential	1.9×10^{-110}	4.0×10^{-2}
1 MeV monoenergetic	6.4×10^{-29}	4.4×10^{-2}

Table 1.3: Fractional surficial fluences on the Archean Earth for three representative types of incident X-ray and gamma-ray spectra. In each case, the fraction of the incident radiation reaching the ground is much larger when redistribution of the ionizing radiation to the biologically effective 200–320 nm region is included.

UV in the biologically effective 200–320 nm range. With no significant molecular absorption, the re-emission due to UV redistribution is subject only to Rayleigh scattering. Using a modified two-stream approximation for a pure scattering atmosphere, we propagated the reemitted UV through an Earth-like atmosphere of pure N_2 and a column density of 1024 g cm^{-2}. Although we recognize that there is considerable uncertainty concerning UV screening in the Archean atmosphere (e.g. Levy and Miller, 1998; Cockell, 2002), recent evidence concerning mass-independent fractionation effects in Archean sulfides (Farquhar et al., 2002) suggest the absence of a significant UV shield during this period (Wiechert, 2002), so our assumed Archean atmosphere may not be so extreme. Table 1.3 shows the resulting fractions of the incident energy in both ionizing radiation and biologically effective UV received at the surface for three different incident spectra. As the incident ionizing radiation is efficiently blocked by atmospheres as thick as the Earth's, the surface fluences are completely dominated by the redistributed UV, showing the potential importance of this physical process in determining the radiation environment on the early Earth or terrestrial-like exoplanets without UV shields.

The transmittance of the direct ionizing radiation rapidly decreases by orders of magnitude with decreasing energy because the photoabsorption cross section, which scales as the inverse cube of the energy, is rapidly increasing. Thus the fraction of the incident ionizing radiation received at the ground is ridiculously small for the 1 and 10 keV average energy exponential spectra, which are characteristic of stellar flares. Including the secondary electron-mediated redistribution of the absorbed ionizing radiation to biologically effective UV raises the surficial fluxes by many orders of magnitude. As a concrete example, an

estimate of the surface environment of the Archean Earth under irradiation by a nearby supernova's radioactive decay gamma-ray lines would be too low by almost 30 orders of magnitude without including the UV redistribution. A similar estimate of the Archean Earth under irradiation by a solar superflare would be wrong by 100 orders of magnitude.

Notice that the fraction of the incident fluence redistributed to UV and reaching the surface is almost independent of the value of the mean energy of the incident photons. This occurs because the number of secondary electrons available for molecule excitation only depends on the total energy of primary electrons, which in turn depends on the total fluence of ionizing radiation.

Present-day Earth

The present-day Earth is an interesting prototype of a simple atmosphere with a single important molecular UV absorber that peaks in the 200–320 nm region. Although any planet with a thick atmosphere like Earth is well protected from gamma-rays and X-rays, the planet may or may not be protected from UV irradiation. Currently, the most important UV absorber on Earth in the biologically effective wavelength region is ozone, a byproduct of solar UV photolysis of oxygen in the lower atmosphere. The wavelengthdependent cross section of ozone to UV absorption peaks at around 260 nm, rapidly falling to higher and lower wavelengths and becomes small outside the range 210–290 nm. Not all energy in the reemitted aurora-like spectrum lies in the range of significant ozone absorption, however, and a significant amount does "leak" through the sides of the ozone absorption peak in regions where biological effects are known to be significant but ozone absorption is minimal. The choice of the upper wavelength for biological effectiveness sensitively affects the results because of the rapidly declining ozone cross section in the wavelength range 300–350 nm. While a variety of biological effects in certain organisms have been observed up to wavelengths of 350 nm and larger (e.g. Jagger, 1985; Nilsson, 1996), we conservatively placed the upper limit in our calculations at 320 nm, given that we are interested only in gauging the significance of the redistributed UV on a generic organism.

Because the altitudes of energy deposition in the case of incident gamma radiation

Spectrum Type	Ionizing Transmittance	UV Transmittance (200-320 nm)
1 keV $\langle E \rangle$ exponential	~ 0	2.1×10^{-3}
10 keV $\langle E \rangle$ exponential	1.9×10^{-110}	2.1×10^{-3}
1 MeV monoenergetic	6.4×10^{-29}	2.1×10^{-3}

Table 1.4: Fractional surficial fluences on the present-day Earth for three representative types of incident X-ray and g-ray spectra. In each case, the fraction of the incident radiation reaching the ground is much larger when redistribution of the ionizing radiation to the biologically effective 200-320 nm region is included, even in the presence of an efficient molecular absorber such as ozone.

are relatively small and overlap the Earth's ozone layer, we assumed the average vertical dependence of the ozone mixing ratio from Brasseur et al. (1999, Appendix C). We assumed that the O_2 mixing fraction is constant. The wavelength dependence of the O_2 and O_3 absorption cross sections were digitized versions of the graphical results presented by Yung and DeMore (1999).

According to our calculations, the UV transmittance in the presence of the modern ozone shield is nearly identical for any incident spectrum within the constraints of the sources addressed in this work, for the same reason as given above in the case of no UV shield. For the three spectra listed in Table 1.4, the ionizing transmittance is of course identical to that of the Archean Earth, but the UV transmittance in each case on the present-day Earth drops to 2.1×10^{-3}. This is somewhat below the value for the early Earth, but it is still orders of magnitude above the fraction of direct ionizing radiation transmitted. The surprisingly large UV transmittance leads us to conclude that the UV redistribution mechanism is extremely important even when the reemission is attenuated through molecular absorption by ozone, and that the Earth is presently unprotected from large astrophysical radiation events.

Mars as an Evolving Example

Mars presents an interesting application of the present calculations because its atmospheric column density has decreased with time and is now thin enough for a significant fraction of the incident ionizing radiation to directly reach the surface. Although the present mean

surface pressure is about 6.4 mbar (Lodders and Fegley, 1998), there are several lines of evidence, primarily from outgassing model constraints and geomorphic evidence for early liquid water, that Mars had a thick ($\sim$ 1 bar) CO_2 atmosphere about 4 Gyr ago (e.g. Carr, 1999; Jakosky and Phillips, 2001). Depletion of CO_2 by incorporation into the regolith, ice caps, and carbonates, as well as atmospheric escape by sputtering and other non-thermal and thermal processes, have been examined in a large number of studies. There has been little consensus about the evolution of the total pressure (cf. Haberle et al., 1994b; Leblanc and Johnson, 2001). Rather than a continuous pressure decrease, some models even yield a "climate collapse," involving an almost discontinuous reduction in CO_2 due to ice formation at age 2.5–3.5 Gyr, indicating that Mars has had a thin atmosphere for $\sim$ 1 Gyr (Haberle et al., 1994b). (Cockell et al., 2000) has pointed out the possibility of an "ultraviolet crisis" resulting from climate collapse, considering only the steady UV from the sun. In any case, Mars should have been subjected to brief optically thin exposures to sterilizing gamma-rays and hard X-rays from solar flares, supernovae, and gamma-ray bursts many times during the past Gyr. Similarly, if Mars began with a thick atmosphere, then its early evolution would have been punctuated with bursts of UV representing redistributed X-rays from the same astronomical sources. A study of the attenuation of steady galactic cosmic-ray and solar UV radiation at the Martian surface as a function of time has been given by Molina-Cuberos et al. (2001). Cordoba-Jabonero et al. (2003) present an accurate calculation of the radiative transfer of steady solar UV in the presence different column densities of volcanic ashes and SO_2 UV shields on present-day Mars, based on a detailed photochemical model for Mars' atmosphere.

Given the uncertainties involved in the Martian atmospheric history, we chose to calculate the fractional transmission of ionizing radiation as a function of time for simple models with a pure CO_2 atmospheric composition. We examined both power law and exponential models in which the CO_2 pressure decreased from 1 bar at 4 Gyr ago (after intense planetesimal bombardment subsided) to 6.4 mbar at present. The exponential version of this decreasing pressure is very similar to the moderate sputtering loss history favored by Luhmann et al. (1992) and the more detailed three-dimensional Monte Carlo sputtering cal-

culations by Leblanc and Johnson (2001). We neglect any UV shield other than Rayleigh scattering, since the composition and altitude dependence of such shields depends on the treatment of a complex photochemical model and assumptions about geological activity (see Cordoba-Jabonero et al., 2003) which would have to be extended to earlier epochs. This uncertainty means that, as in the case of Archean Earth calculations, the fraction of redistributed energy that is transmitted to the surface calculated here is an upper limit.

Figure 1.7 shows the fractional fluence arriving at the Martian surface as a function of time for both the direct ionizing radiation and the UV reemission in the mutationally relevant 200–320 nm region. Adopting these models, standard supernova rates, and the expression for the time between events of given fluence from Scalo et al. (2004), we conclude that the surface of Mars is likely to have been exposed to bursts of ionizing radiation strong enough to sterilize or hypermutate most terrestrial eukaryotes about 1000 times from supernovae, over 100 times from gamma-ray bursts, and over millions of times from stellar flares in the last Gyr. These numbers would be lower by roughly a factor of 10 for prokaryotes on average, although there are large variations in irradiation sensitivity in both domains.

1.3.2 Habitable exoplanet surfaces can be exposed to significant γ-ray—but not X-ray—fluences

According to our Monte Carlo calculation, exoplanet atmospheres with column densities between roughly 30 and 100 g cm^{-2} (habitable by our definition in §1.2.1) will transmit at least 1% of the incident γ-rays to the surface. Furthermore, for atmospheres between 30 and 50 g cm^{-2} and a source of MeV photons such as a supernova or gamma-ray burst, most of the surficial energy fluences will be due to the incident ionizing radiation. The characteristic energy of the radiation received at the ground on planets with thin atmospheres will be very high since the redistribution of the radiation through electron-mediated excitation processes discussed above will be small due to the low optical depths.

Even in thin atmospheres, the surficial spectrum will be altered from the incident spectrum. The relevant physics can be summarized as follows. A photon will typically start

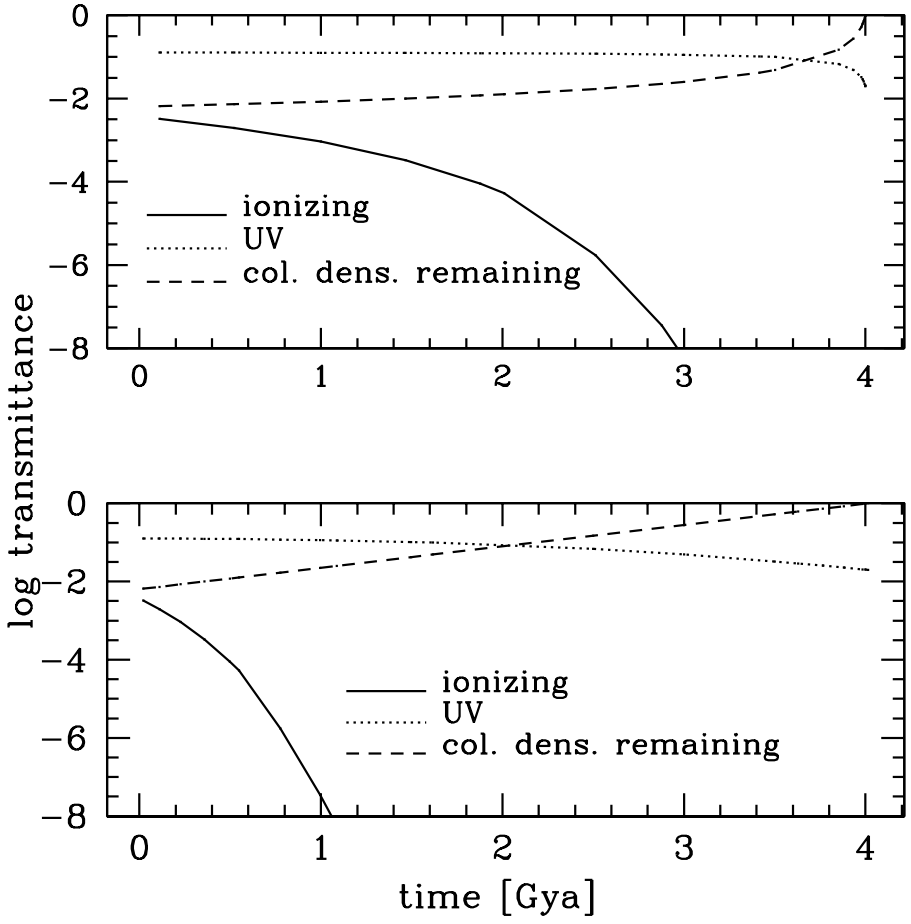

Figure 1.7: Fraction of incident energy reaching the surface of Mars as ionizing and UV radiation as a function of time in the past for two simple models of the evolution of the CO_2 pressure in the Martian atmosphere, with present time on the left. Upper and lower panels correspond to a surface pressure (and total column density) which decreases with time exponentially or as a power law, respectively. The dashed lines represent the fraction of the initial atmospheric column density remaining as a function of time. The initial column density was assumed to be 2600 g cm^{-2}, corresponding to a surface pressure of 1 bar.

with a very high energy (1 MeV, say) and lose a significant fraction of its energy to Compton recoil electrons at each interaction. This fraction depends on energy and decreases with decreasing energy, leading to a "pile-up" of photons at energies of $\lesssim 100$ keV. In the low-energy limit ($E \ll m_e c^2$), the average energy shifts are well-approximated by $\langle \Delta E \rangle \propto E^2$ (obtained by averaging the Compton energy losses weighted by the angular Klein-Nishina cross section). The photons at successively lower energies experience a photoabsorption cross section that increases rapidly ($\sigma_{\rm pa} \propto E^{-3}$) and are thus removed from the Compton downscattering peak. This is demonstrated in Fig. 1.8, which shows the energy spectra at the surface for four different column densities and an incident energy of 1 MeV. The downscatter ledge, where the photons are "piling up," can be seen ($\sim$ 50–100 keV) along with a continuum of energies between this peak and the maximum incident energy. This continuum is filled by photons that lost a smaller than average energy at one or more Compton scatterings. Also seen for the thinnest atmospheres are the peaks at the average energies corresponding to both one and two Compton scatterings from an initial energy of 1 MeV.

For stellar flare spectra, energies are in the keV range, and the dominant cross section is photoabsorption, and no downscattering occurs. Figure 1.9 shows the effect of atmospheric attenuation on an incident stellar flare model spectrum, represented by a decaying exponential with average energy of 10 keV. Unlike the γ-ray case, the X-ray flare spectrum actually shifts to higher mean energies than the incident spectrum because the flux is attenuated primarily according to the photoabsorption cross section, which is proportional to E^{-3}. The estimated fraction of ionizing radiation received at the ground for exoplanets with thin atmospheres is shown in Fig. 1.10. Interestingly, since the surficial radiation spectrum has such high characteristic energies for the thinnest atmospheres, the transmittance is nearly independent of atmospheric composition (i.e., the primary photon reprocessing occurs through Compton scattering, which is independent of composition). This makes our results quite general if indeed exoplanets with such thin atmospheres are habitable.

Even in the optically thin limit, a finite amount of energy redistribution to the UV

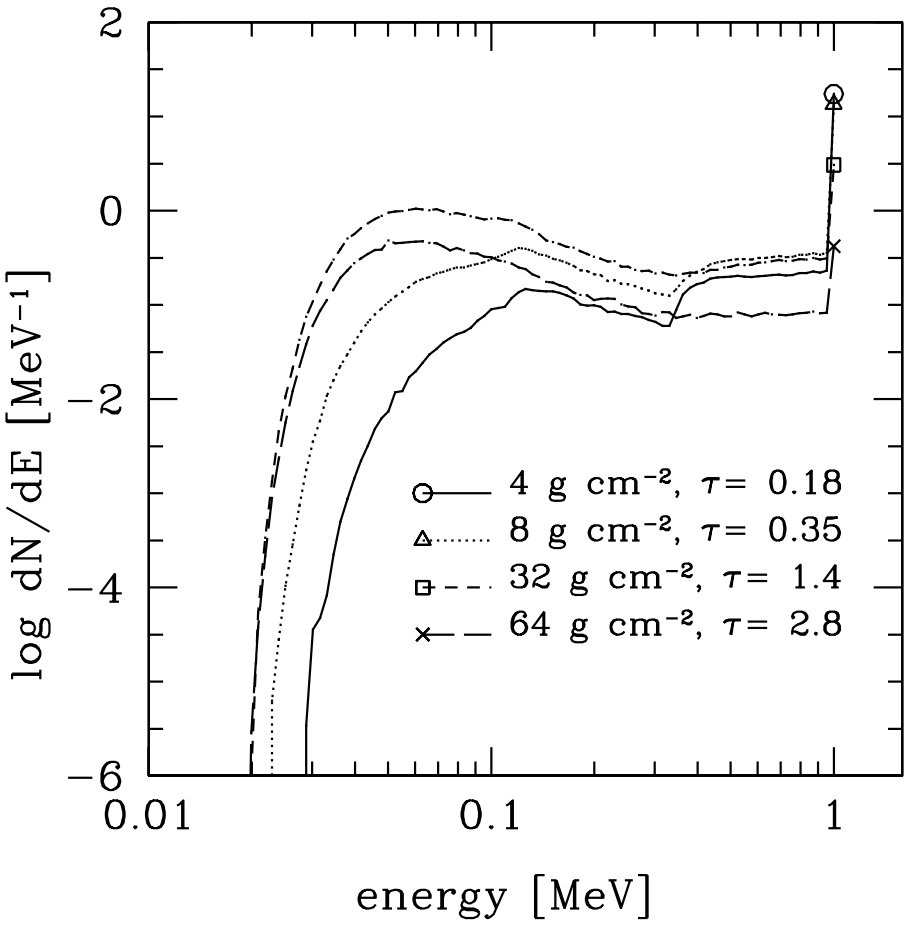

Figure 1.8: Spectra of the ionizing radiation received at the ground for four thin atmospheres and a 1 MeV monoenergetic incident spectrum. The Compton backscattering peaks for the first and second scatterings starting at 1 MeV can be seen for the two thinnest atmospheres, as well as the "piling up" at 50–100 keV due to successively smaller energy shifts.

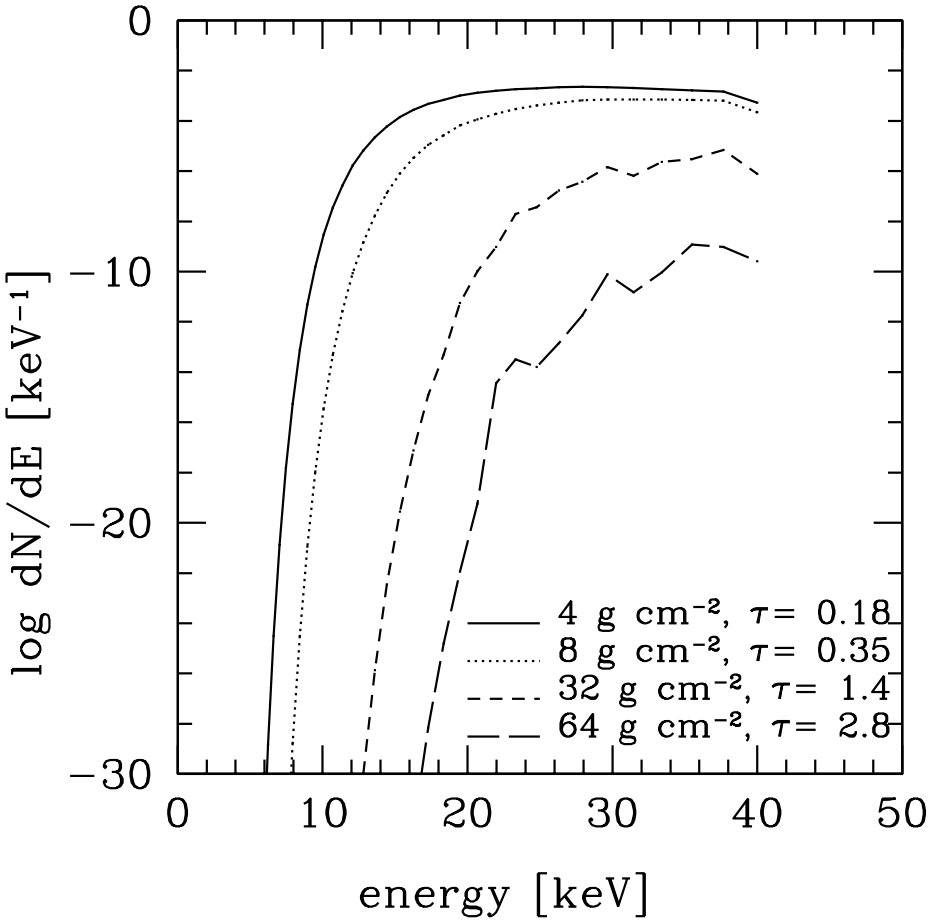

Figure 1.9: Spectra of the radiation received at the ground for four thin atmospheres and an exponential incident spectrum with an average energy of 10 keV.

occurs. As stated above, the γ-rays dominate the surface spectrum for atmospheres with column densities between 30 and 50 g cm^{-2}; above this range, the UV reemission dominates on planets without an atmospheric screen. Figure 1.10 shows the relative contributions of the incident radiation and the reemission to the fraction of incident energy received at the ground in the two extreme cases of Rayleigh scattering and absorption by an O_2/O_3 UV shield similar to the terrestrial O_3 distribution with optical depth scaled as described earlier. Even when subjected to an O_2/O_3 screen, the transmitted UV reemission still exceeds the directly transmitted ionizing radiation for column densities above about 100 g cm^{-2}, and the transmitted fraction is about 1% at that column density.

1.3.3 Secondary ionospheric layers can be produced

To justify our neglect of ion recombination on generic terrestrial-like exoplanets, we must examine the most extreme cases of irradiation. A supernova at a distance of 1 pc—which should occur very rarely, if at all, during the lifetime of a planetary system—would yield a maximum fluence of about 10^8 erg cm^{-2} of ionizing radiation (hard UV and X-rays from shock breakout and γ-ray lines); a 10^{35} erg superflare of a solar-type star would give a slightly smaller fluence for a planet at 1 AU, while a 10^{34} erg dMe flare gives a somewhat larger fluence for a planet in the conventional habitable zone ($\sim$ 0.1 AU distant for such a low mass star). These extreme events would generate electron fractions smaller than the limit given above in Eq. 1.16, even neglecting recombination. The vast majority of events will easily satisfy that strong inequality, especially if recombination timescales are not much larger than the duration of the irradiation events. We are thus able to obtain a reliable estimate of the maximum ionization fractions caused by astrophysical irradiation while neglecting recombination.

Even with moderate levels of irradiation, regions of the terrestrial-like exoplanet atmosphere can be ionized to the level of the terrestrial ionosphere. For comparison, the ionization fractions in the terrestrial ionospheric D and E layers are 1×10^{-12} and 1×10^{-7} (Crisp, 2000), respectively. The ionization profiles we calculate show nearly constant ionization levels for the monoenergetic spectra down to a characteristic altitude, below

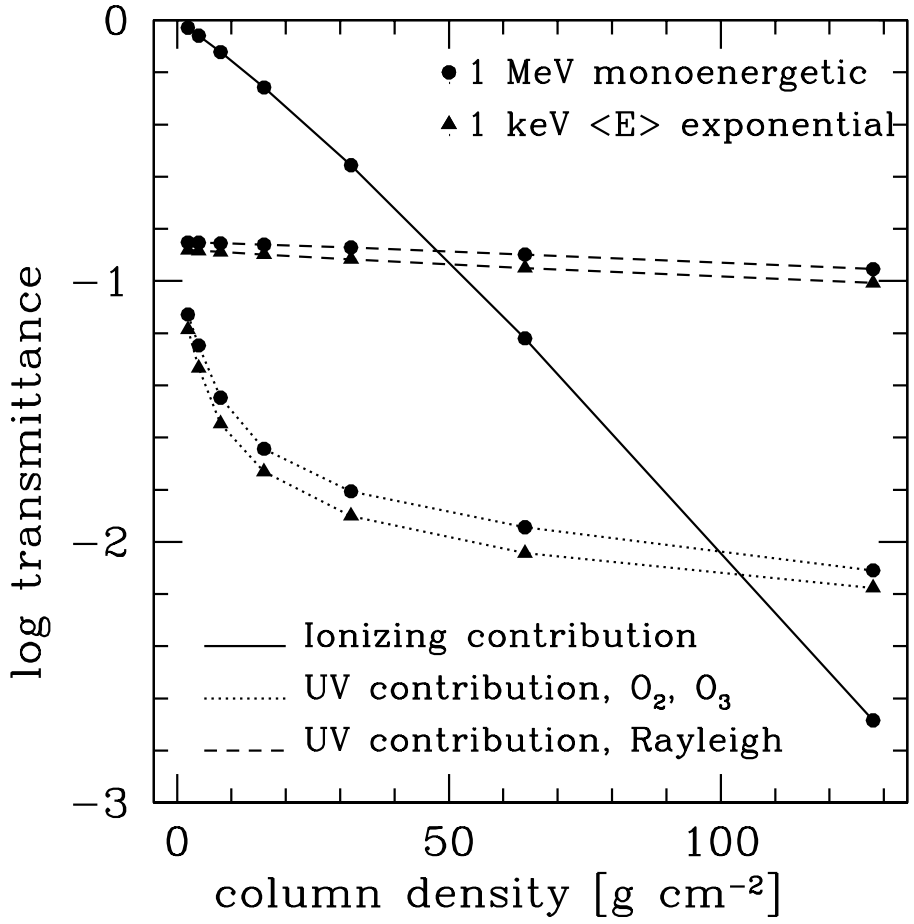

Figure 1.10: Fraction of the incident energy reaching the ground as ionizing radiation and as biologically effective UV in thin atmospheres for two incident spectra using two simple models of UV redistribution. The ionizing radiation dominates for column densities $\lesssim 50$ g cm^{-2} for hard incident radiation. For the softer, $\langle E \rangle = 1$ keV, case, photoabsorption prevents any substantial direct surficial flux; we omit the solid curve corresponding to the X-ray incident spectrum because the transmittance is far below the scale shown here. The UV reemission contribution is shown for two cases: (1) O_2 and O_3 molecular absorption only and (2) Rayleigh scattering only. In both UV cases, only the biologically effective flux (200–320 nm) is counted.

which the ionization level drops extremely rapidly. For our continuous spectra, ionization levels rise with increasing altitude because the photon number per unit energy decreases with increasing energy. Thus most photons in our continuous spectra have lower energies (and larger interaction cross sections) than the spectrum average and will be deposited at higher altitudes. Figure 1.11 shows the results for a few atmosphere models. Even for atmospheres as thick as Earth's, the ionization profiles shown as fractional ionization produced per unit incident fluence for γ-ray incident spectra show a significant effect down to altitudes below the lowest steady-state ionization layer on Earth (D layer, 60–95 km; Crisp 2000). For example fluences at the top of the atmosphere of 1 erg cm^{-2} from a stellar flare with average energy of 10 keV would be yield a transient layer of comparable ionization fraction to the D layer, but at much lower altitudes. Based on this result, we predict that additional ionization layers may be produced on a transient basis and with stochastic ionization levels in response to external radiation sources. Neglecting recombination, the maximum ionization fractions per unit incident fluence (hereafter, ionization efficiency) are independent of column density, depending only on the incident spectrum. For stellar flare irradiation with hard X-ray spectra of average energy in the range 1–10 keV, we find maximum ionization efficiencies of 10^{-5}–10^{-7} (erg cm^{-2})$^{-1}$; for supernovae and gamma-ray bursts, we find maximum ionization efficiencies of 10^{-12}–10^{-13} (erg cm^{-2})$^{-1}$. Maximum ionization efficiencies as a function of average incident energy are shown in Fig. 1.12.

As the ionization fraction at a particular layer depends on the amount of energy deposited in that layer, it is instructive to examine the energy deposition profiles, defined here as the variation in the fraction per km of the incident energy transferred to photoelectrons and Compton recoil electrons as a function of altitude. Figure 1.13 shows that our model stellar flare spectrum deposits more energy at higher altitudes than the corresponding monoenergetic incident spectrum at the same average energy. This has important implications for the ionization fractions created. Because the density of atmospheric molecules falls off exponentially with height, a higher fraction of energy deposited at higher altitudes where molecular densities are lower will result in higher ionization fractions. This is why the stellar flares may create higher peak ionization fractions than supernovae, and why the altitudes

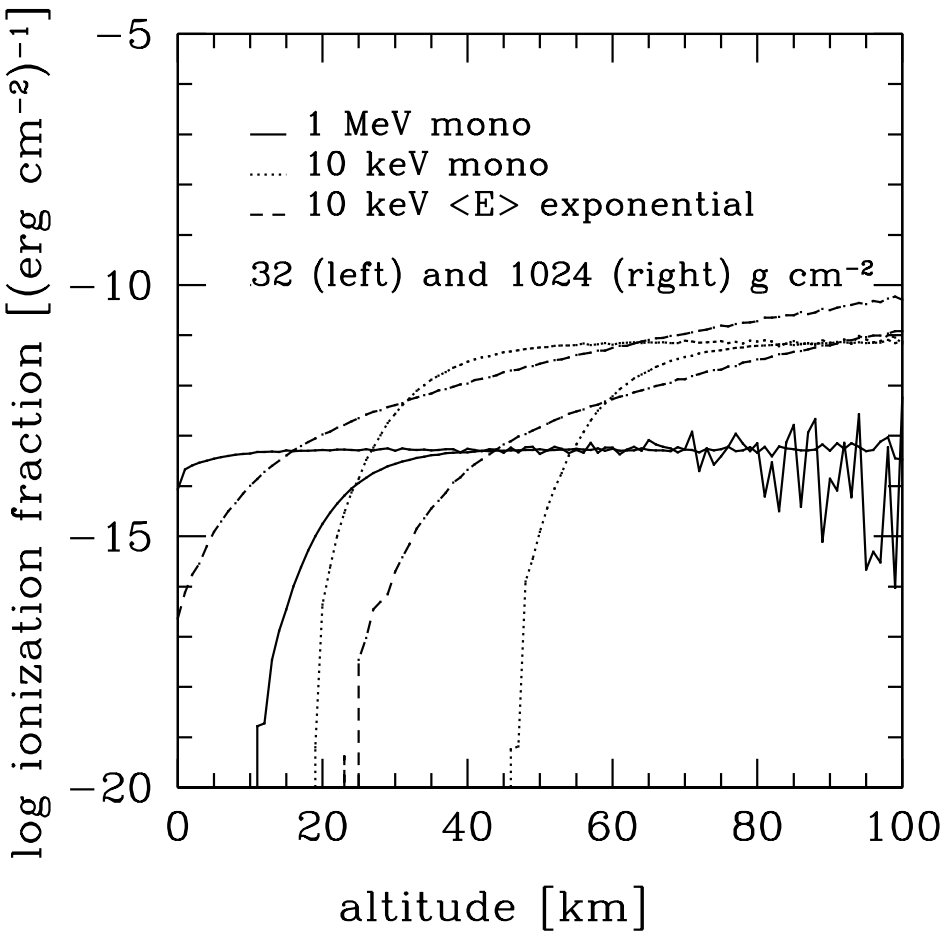

Figure 1.11: Typical ionization efficiency profiles (neglecting recombination) for three different incident spectra and two column densities. Vertical units are ionization fraction produced per cm^3 per unit incident fluence at the top of the atmosphere. For monoenergetic spectra, nearly constant ionization levels are produced down to a characteristic altitude, which roughly corresponds to the altitude of maximum energy deposition. This agrees well with the Chapman solution. The model flare spectra produce ionization levels which rise with increasing altitude because more energy is deposited at higher altitudes than in the monoenergetic case with an identical average energy . The progressively larger fluctuations at altitudes above ~ 60 km are due to small-number statistics, where the optical depths are small and photon interactions are statistically unlikely.

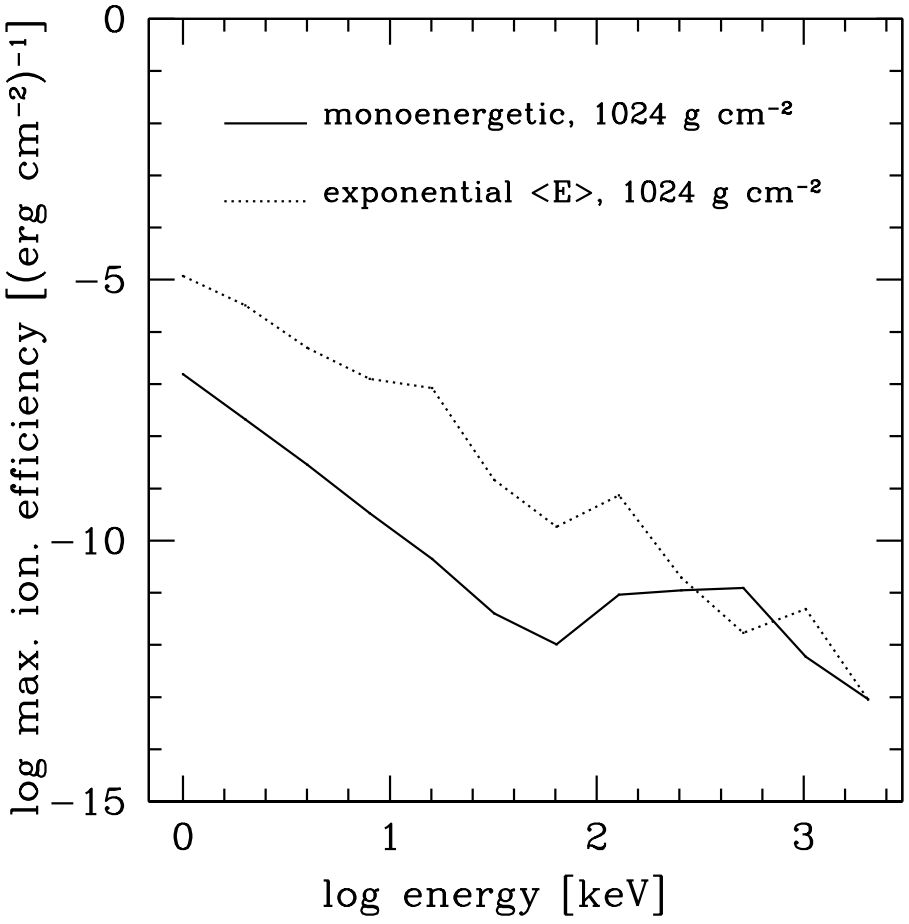

Figure 1.12: Maximum ionization efficiencies (fractional ionization produced per unit fluence of incident energy) for average incident energies between 1 keV and 2 MeV and a column density of 1024 g cm^{-2}. The efficiency declines as energy increases because most of the energy is being deposited at lower altitudes where molecular number densities are higher and hence a given amount of energy is able to ionize a smaller fraction of the molecules. Uncertainties in the curve arise from small-number statistics—only a small fraction of the incident photons are interact in the layer of maximum energy deposition, creating fluctuations in the altitude of maximum ionization.

of peak ionization will be higher.

1.3.4 Substantial diffuse UV is produced in thick atmospheres

We can estimate the intensity of aurora-like emission produced by superflares and cosmic explosions here and on other planets by comparing with terrestrial data. Auroral intensities are often classified into four "International Brightness Coefficient" (IBC) Classes I-IV, from weakest to strongest. According to data presented by Whalen et al. (1985) for IBC Class III auroral intensities, the OI 557.7 nm emission is about 1% of the total zenith auroral brightness. For the most intense auroral events with IBC Class IV the brightness in the OI line is 10^{12} photons cm^{-2} s^{-1}. Using the same scaling from OI to total brightness as for the Class III event, the total brightness must be of order 10^{14} photons cm^{-2} s^{-1}. Using 5 eV as a median energy photon for the auroral emission, this gives a rough energy flux of 8×10^2 erg cm^{-2} s^{-1}. For the Class III data, the efficiency of conversion of primary and secondary electron energy into radiation at all wavelengths is given to be 21–35%, so the corresponding photon flux for the Class IV event is about 3×10^3 erg cm^{-2} s^{-1}. We find larger efficiencies for the ratio of incident photon energy to electron energy for the very different physical process producing the electrons here (Compton scattering and photoabsorption, versus collisional ionization for standard aurorae), and similar efficiencies can be inferred from calculations of X-ray redistribution in accretion disks around compact stellar objects (Ross, 1979; Kallman and McCray, 1982; Ross and Fabian, 1993).

In comparison to these terrestrial events, we have estimated that gamma-ray burst events (Scalo and Wheeler, 2002) and supernova explosions (Scalo et al., 2004) would expose an exoplanet to incident ionizing fluences greater than 10^6 erg cm^{-2} hundreds of times per Gyr, which translates to fluxes of about 10^7 erg cm^{-2} s^{-1} and 10^2 erg cm^{-2} s^{-1}, respectively. On a planet orbiting a low-mass dMe strong flare star in the habitable zone (semimajor axis ~ 0.1 AU), a flare with an EUV energy greater than 10^{32} erg can occur 10–100 times per day (see Audard et al. 2000, Fig. 4), with a corresponding flux for a 10 minute flare of 6000 erg cm^{-2} s^{-1}. Given the energy-frequency power law relations estimated for both solar (e.g., Crosby et al. 1993 and Aschwanden et al. 2000) and dMe flares in various UV and

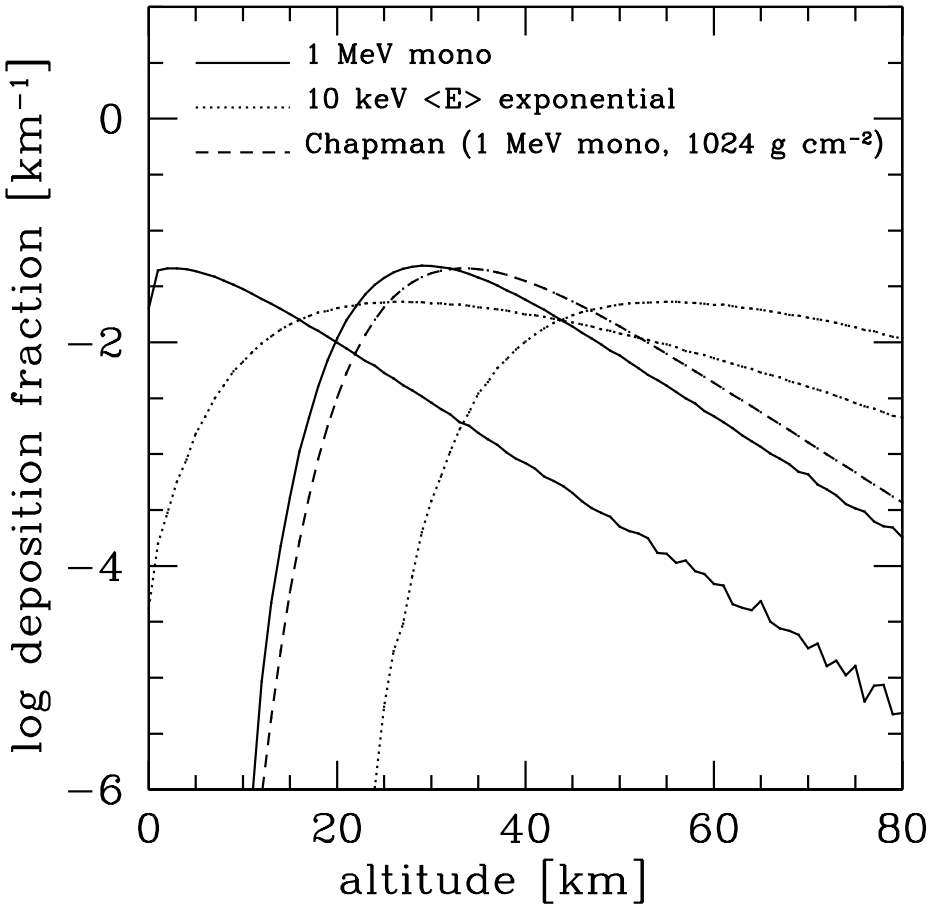

Figure 1.13: Energy deposition profiles for three different incident spectra in atmospheres with column densities of 32 and 1024 g cm^{-2}. For each spectrum, the lefthand curve is for a 32 g cm^{-2} column density and the righthand curve is for a 1024 g $^{-2}$ column density. A single curve corresponding to the Chapman solution for a 1 MeV monoenergetic incident spectrum in a 1024 g cm^{-2} atmosphere is shown for comparison. Note that our Monte Carlo results for the monoenergetic spectra are identical in shape to the Chapman solution (which assumes a monoenergetic incident spectrum) except for a shift to lower altitudes which accounts for the effects of multiple scattering. Also it can be seen that continuous spectra give different overall shapes, with our model flare spectrum depositing more energy higher in the atmosphere than a monoenergetic spectrum at the same average energy.

X-ray bands (Gershberg and Shakhovskaya, 1983; Audard et al., 2000; Güdel et al., 2003), with differential frequency distributions of -1.5 to -2.2, incident fluxes of at least 10^5 erg cm^{-2} s^{-1} should occur with a frequency of order once per day. Clearly the intensities of auroral lines generated by these events will far exceed the strongest terrestrial Class IV auroral displays.

Figure 1.14 shows the fraction of the incident fluence reaching the surface in the biologically significant range 200–320 nm for column densities up to 2048 g cm^{-2}. The original incident radiation is strongly attenuated, but the redistribution of energy toward UV emission maintains the surface fluences at significant levels. Two cases are shown: pure Rayleigh scattering and pure O_2/O_3 absorption. The pure Rayleigh scattering case represents an atmosphere with no significant molecular or aerosol UV absorbers in the biologically effective region—perhaps similar to the Archaean Earth. The transmission in this case was calculated using the modified two-stream Schuster (1905) scattering solution described in §1.2.5. The O_2/O_3 case represents an ozone and oxygen abundance similar to the present-day Earth (identical column density profiles). As can be seen in Fig. 1.14, the effect of redistribution to the UV is quite dramatic, even when subjected molecular absorption by O_2 and O_3. The UV reemission quite effectively raises the surficial fluences back to significant levels, even though the incident ionizing radiation has been attenuated to ridiculously small amounts in the thick atmospheres. For example, the fraction of incident X-rays and γ-rays reaching the surface on Earth (1024 g cm^{-2}) is 6×10^{-29} for the 1 MeV monoenergetic case, while including the UV redistribution to the biologically relevant 200–320 nm region, even in the presence of an ozone screen, raises this number to at least 2×10^{-3}.

The results depicted in Fig. 1.14 depend sensitively on the adopted upper limit of 320 nm for "biologically effective" UV radiation, but we feel that a value of 320 nm is quite reasonable. Figure 1.15 shows the strong dependence of the transmission on the adopted upper wavelength limit for "biological significance." For the case of O_3 absorption, the dependence is quite severe, so the transmission will depend on which specific biological process is of interest. It is well known that UV-B radiation around 320 nm has major effects

on contemporary organisms and ecosystems, and even wavelengths as large as 350 nm can have a variety of biological effects (e.g., Jagger 1985). For example the action spectrum for induction of squamous cell carcinoma in mice has a strong peak at 300 nm and is smaller by only an order of magnitude at 320 nm (Nilsson 1996, p. 88). Additionally, UV-B (280–315 nm by convention) can penetrate ocean surfaces to much larger depths than UV-C (100–280 nm). Although many DNA action spectra peak at 260 nm and have declined by a factor of 10–100 by 300–320 nm, the action spectrum for particular *mutations* do not show this universal behavior. As one of many well-known examples, the measured action spectrum for the UV-induced mutation to resistance to novobiocin in *Haemophilus influenzae* has a sharp peak around 330 nm and drops by two orders of magnitude below 280 nm and above 360 nm (Cabrera-Juarez and Setlow, 1976). A recent survey of the numerous effects of the longer-wavelength UV-B radiation on terrestrial organisms and ecosystems is given by Paul and Gwynn-Jones (2003).

1.3.5 Additional considerations

The Chapman solution is inaccurate for thin atmospheres and high energies

The problem of energy deposition in an exponential atmosphere for the case of pure absorption was solved by Chapman (1931). While our situation is more complicated, the photons are nevertheless depositing energy in the atmosphere, and we can compare our results to Chapman's solution, which is commonly used to estimate the effects of ionizing radiation (e.g., Gehrels et al. 2003). Assuming an exponential attenuation in an exponential atmosphere, Chapman showed that the energy deposition rate, q, as a function of altitude is (see Chamberlain 1978)

$$q(y) = q_{\max} \exp\left(1 - y - e^{-y}\right), \tag{1.33}$$

where $y = (z - z_{\max})/h$ is the dimensionless altitude, $z_{\max}$ is the altitude of maximum deposition, and h is the atmospheric scale height. This solution is based upon an exponentially increasing optical depth, so that the attenuation of the radiation (and hence the energy deposition) follows the profile of an exponential raised to an exponential. Additionally, the

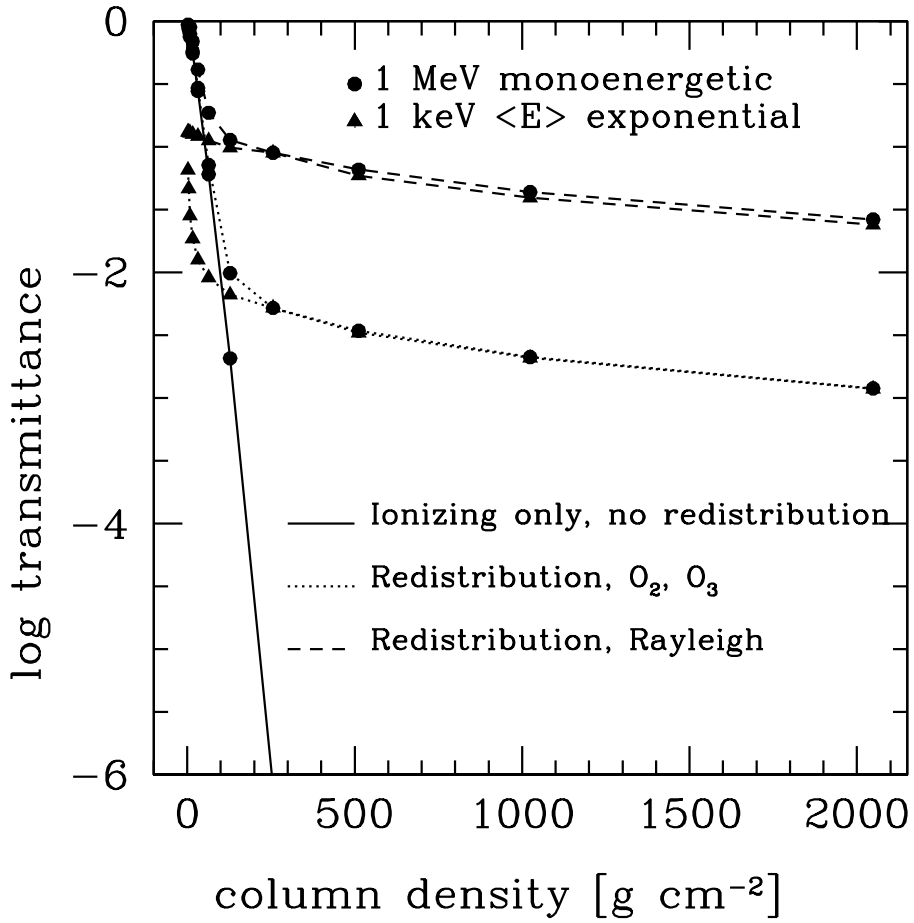

Figure 1.14: Fraction of the incident energy reaching the ground is shown both without and with the additional contribution of the redistributed UV for two simple models of UV redistribution for an atmosphere with a column density of 1024 g cm^{-2}. The no redistribution case for a 1 keV average energy exponential spectrum is not shown because the transmitted fraction is practically zero.

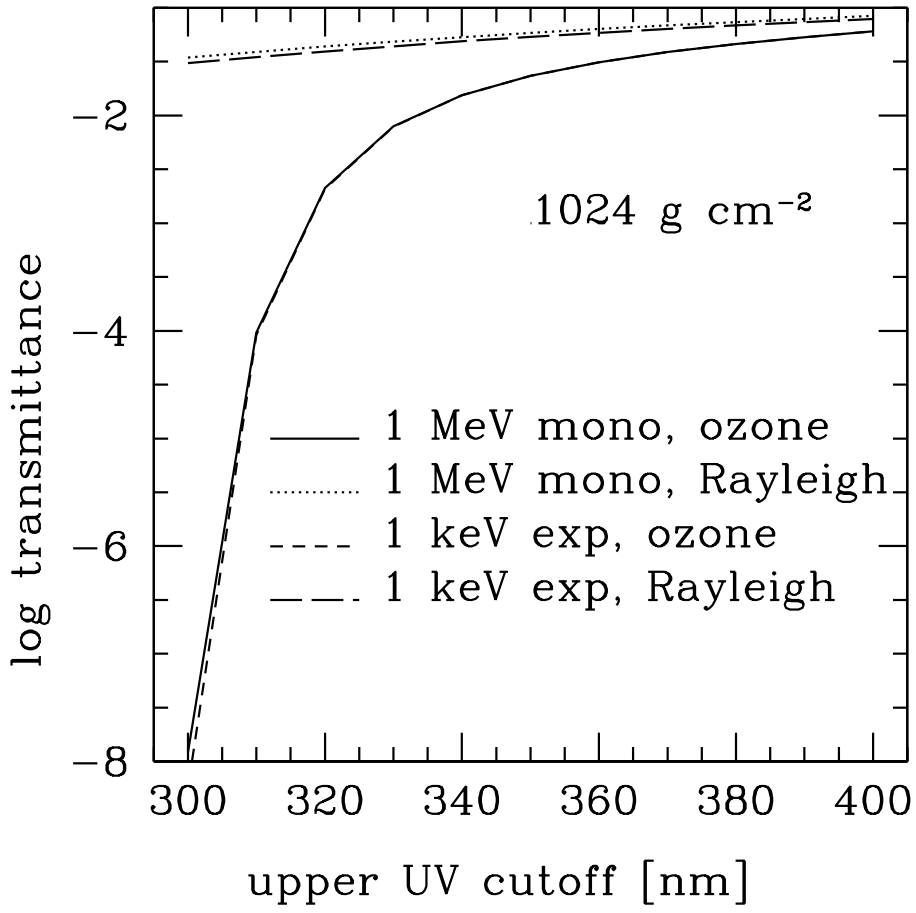

Figure 1.15: Fraction of biologically significant redistributed UV energy that is reaching the ground on Earth as a function of the upper cutoff for the biologically significant flux. The lower limit is taken to be 200 nm in all cases. The result is insensitive to the cutoff for the Rayleigh scattering case, but very sensitive in the O_3 case for cutoffs in the range 300–340 nm. The sharp falloff in the O_3 case for wavelengths shorter than 340 nm is due to the rapidly increasing O_3 cross section at smaller wavelengths (peaking around 260 nm). Significant biological effect occurs up to 350 nm in some organisms under UV irradiation. Our work assumes 320 nm for the cutoff.

altitude of maximum deposition in the Chapman solution scales logarithmically with the optical depth:

$$z_{\max} = h \log \tau. \tag{1.34}$$

Our Monte Carlo results, which take into account multiple scatterings, yield an energy deposition curve which is of the same shape as that which the Chapman solution (which assumes a monoenergetic incident spectrum) predicts, but with the entire curve shifted to lower altitudes due to the effects of multiple scattering. This is evident in Fig. 1.13. Also it can be seen that continuous spectra give different overall shapes, with our model flare spectrum depositing more energy higher in the atmosphere than a monoenergetic spectrum at the same average energy. In principle, the shape of the energy deposition curve for the continuous spectrum could be retrieved via the Chapman solution by summing appropriately weighted Chapman curves at each energy in the range of energies in the continuous spectrum.

In short, the general shape of the Chapman profile is accurate at one particular energy (and hence for our monoenergetic supernovae spectra), but it underestimates how far into the atmosphere the radiation will penetrate because of the neglect of multiple scattering. This effect is minor for the thickest atmospheres (column densities $\gtrsim$ 300 g cm^{-2}) but becomes significant for thinner atmospheres (column densities $\lesssim$ 300 g cm^{-2}).

To gauge the effect of multiple scatterings in our Monte Carlo model, we calculated (Fig. 1.16) the fraction of the atmosphere above the height of maximum energy deposition, which is a measure of how far the radiation has penetrated the atmosphere. The effects of lower deposition altitudes are more pronounced for thinner atmospheres and higher energies. More scatterings occur before the photons are photoabsorbed for higher incident energies, and each scattering has a longer mean free path in thinner atmospheres. In terms of the fraction of the atmospheric mass penetrated by the radiation, the full radiative transfer yields 10–50% greater penetration, depending on the thickness of the atmosphere and the energy of the incident radiation. At low energies the photoabsorption dominates, so the results approach the Chapman solution. The Chapman monoenergetic solution could be used to build up solutions for continous spectra, so it is not invalid for incident spectra such

as flares or gamma-ray bursts. The key quantity is the average energy of the spectrum and the thickness of the atmosphere. The most pathological situation for the Chapman solution is a high-energy radiation source (e.g., supernovae and gamma-ray bursts) incident on a thin atmosphere ($\lesssim$100 g cm^{-2}).

Surface energy fluences are not sensitive to the angle of incidence

We find that decreasing the angle of incidence can measurably decrease the surface fluence of the *original* incident radiation, with the effect becoming quite significant for the highest energies ($\gtrsim$ 1 MeV) and thickest atmospheres ($\gtrsim$ 500 g cm^{-2}). Though in our model we assume normal incidence for every photon, the surface of a real exoplanet subjected to a source at astronomical distances will observe a point source with varying zenith distances, depending on the viewing geometry. This effect means that we have calculated only an upper limit to the direct transmittance of the atmospheres to the incident *ionizing* radiation. We note that this ionizing radiation is already insignificant in a biological sense for column densities greater than about 100 g cm^{-2}. As found earlier, the primary contribution to the surface flux in thick atmospheres is the redistributed UV. Since the UV is primarily attenuated by molecular absorbers, atmospheres thick enough to deposit most of the incident energy above the absorbers will be indifferent to the angle of incidence of that radiation. Figure 1.17 illustrates the effect. In the thick atmospheres, we find that the angle of incidence has only a very small effect on the reemitted UV that reaches the surface in the biologically effective region of the spectrum; for thin atmospheres, the effect is negligible for both the incident radiation and the reemitted radiation because the optical depths are by definition small. We are therefore justified in neglecting the effects of the angle of incidence.

1.4 Relevance of results to astronomical sources

Our work is based on the fact that most planetary systems must be occasionally irradiated by bursts of X-ray and γ-ray photons from various astronomical events, a facet of planetary radiation environments that has been overlooked in the past. In order to place the above

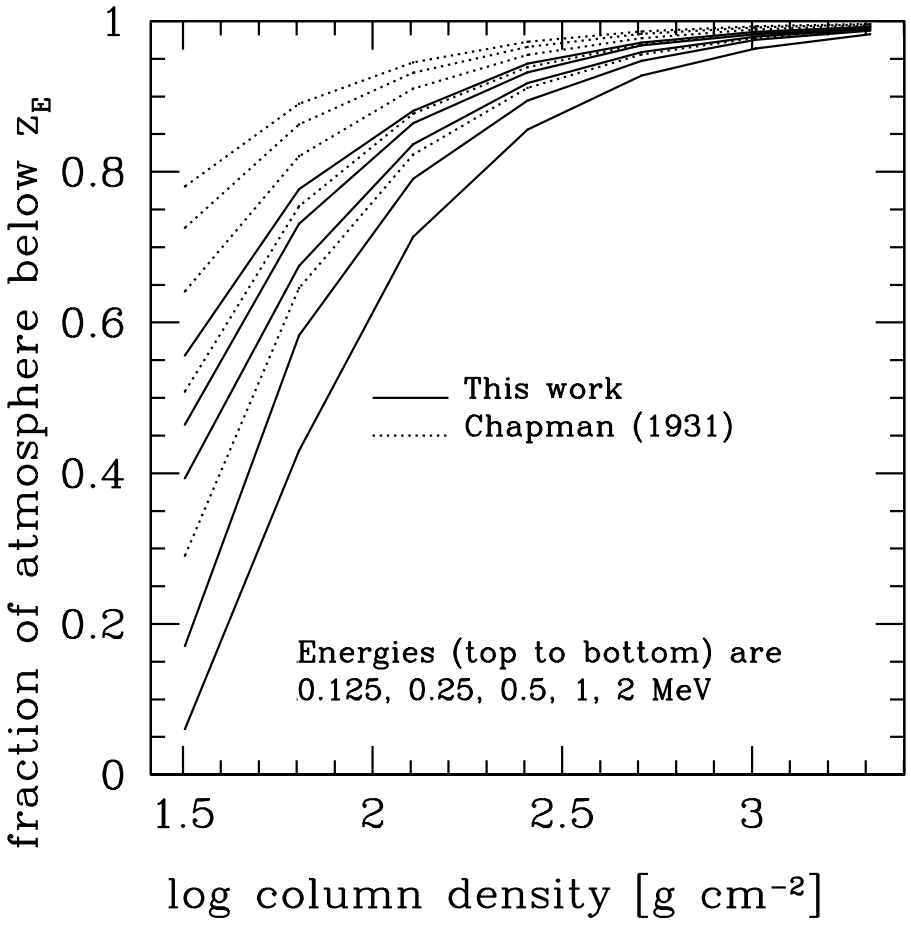

Figure 1.16: Comparison of the calculated location of peak energy deposition of monoenergetic radiation with that predicted by the Chapman solution. Results are presented in terms of the fraction of the atmosphere by mass penetrated by the energy deposited at the height of maximum energy deposition. Since the Chapman mechanism neglects subsequent scatterings, the altitudes of maximum energy depositions are higher than in our calculations. The effect is quite significant for the thin atmospheres with column densities $\lesssim 100$ g cm^{-2}.

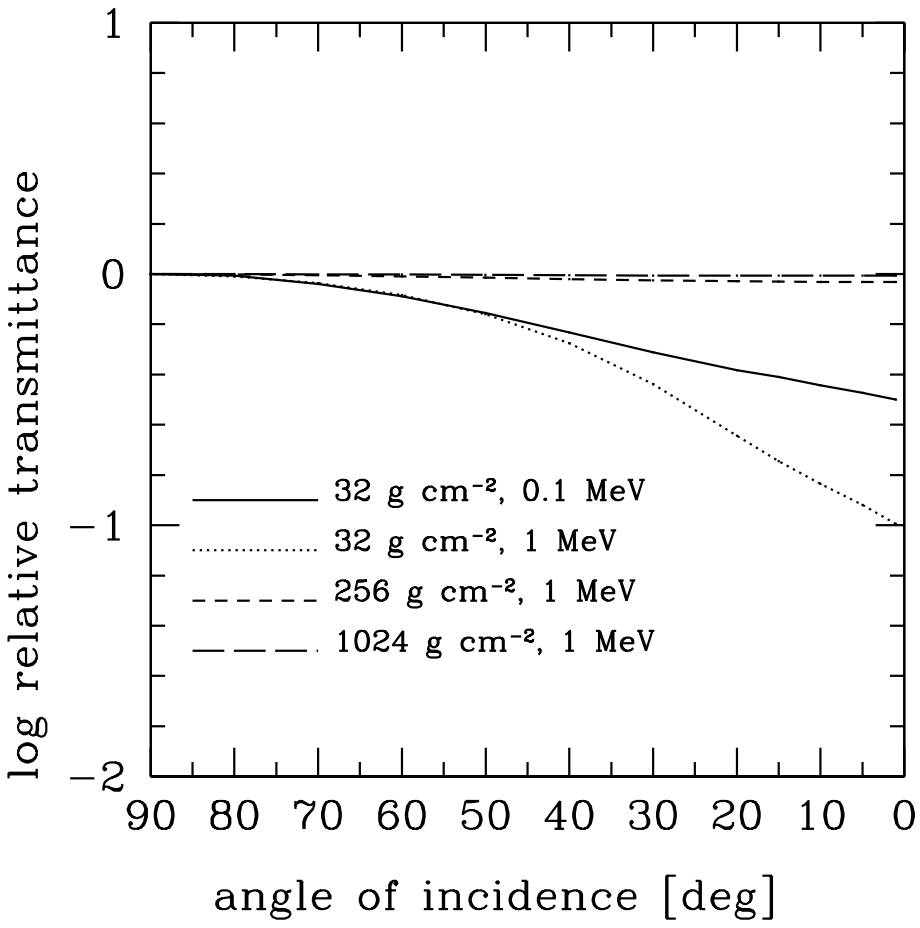

Figure 1.17: The effect of varying the angle of incidence. Plotted is the transmittance of the atmosphere as a function of angle of incidence relative to normal incidence. The curves include UV redistribution subjected to O_2/O_3 absorption in the transmittance (which raises the transmitted fractions above that of only the direct ionizing radiation). In the thick atmospheres, we find that the angle of incidence has only a very small effect on the reemitted UV that reaches the surface when redistribution is included; for thin atmospheres (and hence small optical depths), the effect is negligible for both the incident radiation and the redistributed radiation.

calculations in their proper context, we briefly summarize the major sources of such ionizing radiation, concentrating on the estimated frequencies and durations of the events.

1.4.1 Stellar flares

Surely the most frequent sources of stochastic irradiation by ionizing photons are flares from the parent star. For older solar-like stars the sun provides the best-studied example. Solar flares are associated with ionizing radiation from keV X-rays to GeV γ-rays. The time variation of flare output depends on wavelength region and varies from flare to flare, e.g., Fig. 10.11 in Foukal (1990), Fig. 6.7 in Lang (2000), and Fig. 9.2 in Golub and Pasachoff (1997), with the gradually declining flare phase lasting up to an hour or more. The radiative energy release in a single flare varies by orders of magnitude, with the strongest solar flares ever observed emitting a few times 10^{32} erg (e.g., the 4 Nov 2003 flare). This corresponds to a flux above the Earth's atmosphere of only 60 E_{32} erg cm^{-2} s^{-1}, where E_{32} is the energy in units of 10^{32} erg and we adopted an average duration of 10 min. This is consistent with the maximum observed soft X-ray peak fluxes (Fig. 1 in Zirin et al. 2000).

Given the small historical interval over which such observations are available, even in the visual part of the spectrum, and the rapidly decreasing frequency of higher-energy events, it is reasonable to assume that still higher-energy events do occur, even if they have not been detected. The frequency distribution of flare energies from EUV to hard X-rays, derived from several space missions, can be described by a fairly robust power law (Crosby et al. 1998; Aschwanden et al. 2000; Lin et al. 2001; Güdel et al. 2003, and references therein), with log-log slope about -1.6. Extrapolating these data to higher energies, we find that the frequency of flares of such large energy that 1% of the X-ray energy (using our result for an atmosphere of column density similar to the Earth's) exceeds the solar UV flux at 1 AU of about 1×10^4 erg cm^{-2} s^{-1} at the Earth's surface in the biologically active 200–320 nm region is about one per century. This frequency should be decreased if the steeper soft X-ray (0.1–0.8 nm) energy-frequency distribution recently found by Veronig et al. (2002) is correct.

That such flares do occur, even in old, weak-flaring stars like the sun, is supported

by Schaefer et al. (2000), who have identified nine cases of superflares with energy outputs of 10^{33}–10^{38} erg on otherwise normal F8–G8 main sequence stars. These flares cannot be attributed to binaries, rapid rotation, or youth, and therefore may be common in solar-type stars. Schaefer et al. (2000) additionally estimate a very uncertain recurrence time of 10^2–10^3 yr.

Intense flares are much more frequent in younger solar-mass stars, as evidenced by both coronal X-ray emission of solar analogues of different ages (Guinan and Ribas, 2002) and estimates of stellar wind momentum fluxes from solar-mass stars of different ages (Wood et al., 2002). It is also known that intense, although less frequent, flares occur in stars even more massive than the sun, such as the F star EUV flares observed by Mullan and Mathioudakis (2000).

Using the available data on solar-mass stars of various ages, we find that the frequency of flares energetic enough to yield, after redistribution, UV fluxes in excess of the stellar flux should be on the order of once per 1–1000 yr depending on stellar age for habitable zone planets with atmospheres as thick as that of the Earth orbiting solar-mass and higher-mass stars. The frequency will be larger for planets with smaller atmospheric column densities; the dependence of the fraction of flux redistributed from X-rays to UV as a function of planetary atmosphere column density is shown in Fig. 1.14. Although even small changes in the UV irradiance can have sizeable effects on the Earth's atmosphere (see Larkin et al. 2000), the brevity and large duty cycle of very energetic flares make their importance uncertain for solar-mass stars.

The situation is quite different for lower-mass, red main sequence stars of spectral type M. These stars are the most numerous stars in the Galaxy (see Chabrier 2003 and references therein), and calculations indicate that atmospheric circulation is sufficient for atmospheric retention and liquid water oceans in spite of synchronous rotation (Joshi et al., 1997; Joshi, 2003). The potential importance of these stars for exobiology was first clearly recognized and discussed in detail by Heath et al. (1999).

Very low-mass stars spend a significant fraction of their long lives in a state dominated by strong and frequent flare activity (e.g., Shakhovskaya 1995). Such stars, called

"flare stars," "emission line stars," or "UV Ceti stars" (after the prototype), are designated as spectral type dMe (see Gershberg et al. 1999 for an extensive database and bibliography).

These low mass stars are sources of frequent intense flares with energies as large as 10^{34}–10^{35} erg in ionizing radiation (Cully et al., 1993; Hawley and Pettersen, 1991) occurring roughly once per 100 hours of monitoring for some stars, with larger energies occurring at smaller rates. Figure 4 of Audard et al. (2000) shows that the rate of EUV flares with energies exceeding 10^{32} erg ranges from $\sim$ 0.1–100 per day, depending on the star's coronal X-ray luminosity (which is correlated with age). There are several examples of dMe stars with intense flares of energies exceeding 10^{34} erg in the blue and UV, as summarized by Liebert et al. (1999); see also Hawley and Pettersen (1991) and Pagano et al. (1997). Although these cases were not observed in the X-ray region, examples exist of comparable X-ray flares in other dMe stars (e.g., EV Lac, Favata et al. 2000). The larger and more frequent energy releases in very low mass star flares are accentuated by the proximity of conventional habitable zones: $\sim$ 0.05–0.15 AU for stars in the range of masses 0.1–0.4 $M_{\odot}$ (see Kasting et al. 1993). Since the habitable zone distance is partly determined by bolometric flux, habitable planets around these stars will be subjected to flare rates and fluxes many orders of magnitude larger than the Earth.

As a specific example, Cully et al. (1993) describe soft X-ray flares of energy above 10^{34} erg lasting over 2 hours for the dMe star AU Mic. This would give a flux above a habitable zone planet atmosphere of about 10^5 erg cm^{-2} s^{-1}. Using the results of §1.3 for the UV redistribution, and the relative UV fluxes expected in dM stars, we find that the redistributed flare energy would swamp the stellar photospheric UV by an order of magnitude for a habitable planet atmosphere as thick as Earths. Considering the flare energy-frequency scaling for about 20 dMe stars in the U and B photometric bands by Gershberg and Shakhovskaya (1983) and more recent studies of harder radiation flares summarized by Güdel et al. (2003), we estimate that the UV radiation environment of very low-mass stars should be completely dominated by redistributed flare energy. The flares occur roughly once per day, with about an order of magnitude variation in this rate. Even the steady coronal X-ray emission may be important for the most active of these low-mass

stars.

We expect biological activity and atmospheric chemistry to be strongly influenced by the exposure to such intensely fluctuating radiation environments, although the nature of the effects remains to be estimated. In particular, it is unknown whether such a mutationally rich environment would enhance or suppress the rate of evolution even in simple population genetics models.

1.4.2 Stellar explosions

Stellar explosions could also result in chemically and biologically significant fluxes and fluences of ionizing radiation, albeit with a much larger duty cycle than parent star flares. Supernove produce γ-ray emission associated with the radioactive decay of freshly synthesized elements, mainly production of ^{56}Ni that decays to ^{56}Co and then to ^{56}Fe. Monte Carlo calculations of γ-ray deposition (e.g., Höflich et al. 1998) estimate a Type Ia supernovae release of 6×10^{48} erg per Type Ia event (see also Karam 2002); Type II supernovae are much less important. Using an average Galactic rate of Type Ia supernovae of 3×10^{-14} yr^{-1} pc^{-3} (Barbon et al., 1999), the average time between Type Ia supernovae at distance $D_{\rm kpc}$ kiloparsecs is found to be $T = 8 \times 10^3 D_{\rm kpc}^{-3}$ yr. If 1% of the γ-rays are redistributed to UV by the mechanism discussed in the present work, we find that a biologically interesting fluence at the surface of a planet should occur once every 10^4 yr. However the associated flux would be swamped by the parent star UV flux for a habitable zone planet orbiting a solar-type parent star. The supernovae redistributed UV flux will only exceed the parent star flux for low-mass host stars which have a smaller fraction of their flux in the UV, or for moons of giant planets at larger distances from solar-like host stars. We emphasize that the integrated mutation rate due to SN explosions is negligible compared to the background mutation rate because of the small durations compared to the recurrence timescale. Biologically, such intermittent hypermutation events may be most important for partial sterilization of planets and consequent effect on niche structure.

The γ-rays from supernovae can affect the atmospheric chemistry of habitable planets of solar-type stars, independently of any UV redistribution, through the direct effects

of high-energy photons. The chemistry resulting from irradiation of a present-day Earth atmosphere was studied in detail by (Gehrels et al., 2003) using a single-scattering approximation for the radiative transfer. The more accurate transfer calculations in the present work agree fairly well with their results for energy deposition as a function of altitude in the thick-atmosphere, low-energy regime. However the expected rate of SN events near enough to significantly affect atmospheric chemistry is estimated to be only 1–2 per Gyr (Gehrels et al., 2003).

Supernova cosmic rays arriving later may be a more potent source of shower γ-rays and fast particles. From an evolutionary perspective, such events are especially interesting because diffusive propagation of cosmic rays implies long but uncertain exposure durations from 100 yr (Ruderman, 1974) to 10^4 yr (Shklovsky, 1969). The modulation of Galactic cosmic rays by the astrosphere as planetary systems pass through dense interstellar clouds (as suggested, for example, by Begelman and Rees 1976; Zank and Frisch 1999) may be more important than cosmic rays directly generated by the supernova itself. The statistics of fluctuations in astrospheric modulation of cosmic rays are modeled in detail in Smith and Scalo (2006).

Finally, we consider gamma-ray bursts as a potential source of intermittent ionizing radiation. Their energy output is so large that they could deliver a biologically important dose from essentially anywhere in the Galaxy, although the duration, ~ 10 sec on average, is so small that the main effects would be either partial sterilization of a planet or residual atmospheric chemistry perturbations. Recent evidence favors strong redshift evolution of the cosmic star-formation rate (e.g., Kewley et al. 2004 and references therein), which is needed to bring the observed gamma-ray burst rate to a Milky Way rate, so we use the "strong evolution" rates in Scalo and Wheeler (2002) to estimate the frequency of gamma-ray bursts at a given fluence. We find that the redistributed UV flux will only exceed the solar UV flux about once per 4×10^8 yr, with larger rates for lower-mass parent stars. For ozone depletion, the detailed study by Gehrels et al. (2003) of supernova direct gamma-ray irradiation requires an above-atmosphere fluence of $\sim 10^8$ erg cm^{-3}, giving a recurrence frequency of about 0.5 to 1 such events per Gyr, similar to but a little lower than was

found by Gehrels et al. (2003) for SN γ-rays. The numbers are similar because the larger energies of gamma-ray bursts are offset by the smaller rates per unit volume compared to supernovae.

We conclude that the most important source of ionizing radiation for both biological and chemical effects are flares from parent stars, especially for low-mass stars. Supernovae and γ-ray bursts, because of their large duty cycle, are probably only important if they induce partial extinction events, either directly through lethal dose exposure, or by atmospheric chemistry alterations (e.g., Melott et al. 2004). These events likely occur at a mean rate of one per 0.1 to 2 Gyr, depending on the mass of the parent star and the type of event involved. By contrast, the ionizing radiation environment of a habitable zone planet orbiting a low-mass star or a young solar-mass star probably involves a steady and frequent barrage of high-intensity flares with durations of minutes to hours occurring at rates of once per week to once per hour, depending on mass and age of parent star. The present work shows that a significant fraction of this radiation, rather than being absorbed high in the atmosphere, can reach the stratosphere or the surface in the form of redistributed UV radiation.

1.4.3 Energetic particles

Although we are only explicitly concerned with the effects of photons generated by astronomical events, high-energy particle emissions, mainly solar energetic particles (SEPs), solar chromospheric mass ejections (CMEs), and Galactic cosmic rays are also of interest, since their interaction with planetary atmospheres will result in the same kind of ultraviolet radiation through the generation of secondary electrons along the primary particle path. Some comparison of particles with photons is afforded by the recent summary of solar activity by Smith et al. (2003). Their Fig. 3 shows the flux of 1.8–3.8 MeV protons due to SEPs as a function of time during solar maximum and minimum. At solar maximum, the flux is of order 0.1 $(\mathrm{cm}^2\ \mathrm{s\ sr\ MeV})^{-1}$, with excursions up to two orders of magnitude larger and smaller. Since it is the total energy flux that matters for redistribution to ultraviolet radiation, we convert this to a total energy flux at the mean SEP energy to obtain 1×10^{-5}

erg cm^{-2} s^{-1}. Even allowing for a two order of magnitude enhancement, this flux is still small compared to a 10^{32}-erg solar flare at 1 AU, which is 10 erg cm^{-2} s^{-1}. The SEP flux is much more steady while the flare flux is only intermittent, so the fluence from SEPs is larger; however the redistributed UV flux from SEPs even at their peak is negligible. On the young sun or on more active, lower-luminosity stars, the average flare energy and frequency is much larger, and one might expect the energetic particle flux to keep in step (e.g., Wood et al. 2002 on astrospheric momentum flux variations). We arrive at similar conclusions by examining the data for CME $\sim$ 6-MeV protons from the 14 Jul 2000 Bastille day event (data from `http://soho.hascom.nasa.gov/hotshots` web site). The energy flux from Galactic cosmic rays is larger than that from solar cosmic rays, at least for older stars like our sun (see Smith et al. 2003), and may vary considerably as the sun travels through the Galaxy. Therefore we cannot rule out the importance of Galactic cosmic rays as a significant source of redistributed UV flux.

One type of solar particle that does seem important is the so-called "solar proton event," a short-duration SEP burst of $\gtrsim$ 10-MeV particles often associated with flares and presumably accelerated by coronal mass ejection shocks. The particle peak fluxes for the 35 most energetic of these events from 1973 to 2001 is given by El-Borie (2003). The average flux of particles with energies above 30 MeV is 0.2 erg cm^{-2} s^{-1}, while the largest is 1.6 erg cm^{-2} s^{-1}. This is a lower limit because the proton spectrum rises with decreasing energy down to at least 10 MeV, so these events rival the most energetic solar flares in energy flux. In fact Shea and Smart (1996) list the strongest solar proton event recorded as having a number fluence of 3.4×10^{10} cm^{-2} at 1 AU. If the event lasted an hour (typical for SEP bursts), the energy release at the sun would be 10 times that of the largest recorded solar flare.

For any energetic particle flux, whether Galactic or solar in origin, the resulting UV flux can be estimated by assuming most of the cosmic-ray energy is deposited in 35-eV secondary electrons that convert their kinetic energy into UV auroral radiation with the same efficiencies as found in the present paper for secondary electrons resulting from photon events.

1.5 Summary and Conclusions

The continuum UV emission from the sun would have been very intense during the Archean era before the development of the ozone layer. Furthermore, the sun was likely to have been much more active in the past when life first gained a foothold on Earth. Guinan and Ribas (2002) show that the coronal and X-ray to extreme UV emission of the young sun were 100–1000 times stronger than those of the present sun. Even now, solar flares are significant: they follow a power law fluence-per-interval relation that suggests that more powerful, but less frequent, flares are likely even for quiescent, aging solar type stars (Aschwanden et al., 2000). Mars may have once had a thick atmosphere that would still be subject to the strong redistribution of ionizing radiation into auroral UV in the manner we describe here, and it is now very susceptible to direct incident irradiation. Expanding our perspective to other stars hosting other planets, the case can easily be made that UV and ionizing radiation, including stochastic bursts of hard radiation, are the norm in our tumultuous Galaxy (Scalo et al., 2004).

To establish quantitatively the effects of ionizing radiation in terrestrial-like exoplanet atmospheres, we have used Monte Carlo models to propagate ionizing radiation through a suite of simple model atmospheres. We constrained the parameter space of the atmospheres by limiting the models to conditions that are consistent with "habitable" planets, in the sense that the atmosphere is thick enough to maintain liquid water on the surface, given enough ambient heating to keep the water in liquid form. We estimate the lower limit for atmospheric column depth for habitable planets to be about 30 g cm^{-2}. Above this limit, we characterize two types of atmospheres: "thin" and "thick."

Our results can be summarized as follows.

1. Thin atmospheres with column density less than about 100 g cm^{-2} will directly transmit a substantial portion of any incident γ-ray flux. Even for these thin atmospheres, incident X-rays will be blocked because of the high cross section for photoabsorption. Contemporary Mars represents an example of this sort of thin atmosphere.

2. For planets with relatively thin atmospheres, the ionizing radiation spectrum at the

surface from solar flares, supernovae, gamma-ray bursts or other sources of hard radiation should be relatively flat above 50–100 keV due to Comptonization, with a low-energy, photoabsorption cutoff.

3. We define thick atmospheres to be those with column density in excess of about 100 g cm^{-2}, in which both γ-rays and X-rays will be blocked. In this case, however, we show that, in the absence of UV blocking agents (O_3 or aerosols for instance), a substantial fraction of the incident energy will still arrive at the planetary surface as UV resulting from molecular excitation by secondary electrons produced by the Compton scattering of primary radiation and associated primary photoionization electrons. Typically 1–10% of the incident energy can reach the ground as this biologically-active "auroral" UV. This condition is typical of the Archean Earth where the only opacity to UV may be Rayleigh scattering.

4. A significant fraction of the incident energy may reach the surface even for contemporary Earth with its O_3 shield. We estimate than even today, a fraction of order 2×10^{-3} of incident hard flux will reach the surface of the Earth in the form of UV radiation in the 200–320 nm band, independent of the form of the incident ionizing radiation spectrum.

5. The spectrum of the redistributed UV radiation arriving at the planetary surface will depend on the rich and complex molecular emission line spectrum. We have considered relevant bands of N_2 to estimate that the net effect can be approximated by a continuous spectrum in which the energy flux is distributed approximately inversely with wavelength. We argue that essentially all molecules that might be substantially represented in the atmosphere of a habitable exoplanet would have electronic levels with similar spacings that would be excited with an efficiency comparable to N_2.

6. We show that the results are not substantially affected by thermalization of the incident radiation since the ionized fractions of the atmosphere are typically low, nor by quenching, i.e., collisional deexcitation of the molecules, at the typical low electron densities, nor by the angle of incidence.

7. Our results show that low altitude "secondary ionospheres" can be produced in thick atmospheres if the ionizing radiation source is a supernova or gamma-ray burst. In the case of stellar flares, the existing ionospheres of thick atmospheres will be further ionized by a substantial margin. Ionization fractions in all cases of irradiation that exceed the parent star continuum are comparable to or greater than the steady-state terrestrial ionospheres. This phenomenon could affect atmospheric chemistry and global climate, especially in the case of the more frequent stellar flares on low-mass stars.

8. We do not know if early Mars had a thick atmosphere and, if so, whether or not it contained UV blocking agents (Haberle et al., 1994b; Leblanc and Johnson, 2001). The present work suggests that, even if it did, its early evolution, when life might have been forming or expanding through evolutionary niches, would have been punctuated by bursts of reprocessed UV from stellar flares at relatively frequent intervals and again by more exotic but inevitable astronomical events at larger intervals.

Planets with thick atmospheres can be shielded from direct ionizing radiation and even from ordinary continuum UV if their atmospheres contain effective UV shields and still be subject to bursts of biologically significant UV. Smith et al. (2004a) estimate that steady-state solar UV could be exceeded by redistributed UV from intense solar flares roughly once per decade. The redistributed flare energy rapidly increases in importance for the very common lower mass stars that have less continuum UV flux and more intense and frequent flares (see Güdel et al. 2003; Andreeshchev et al. 2003.

The point of view that much of terrestrial and extraterrestrial life is driven by radiation sources was first outlined in the classic book by Shklovskii and Sagan (1966), but has lain substantially dormant since. Rothschild (1999) discusses a large number of possible relations between radiation and biological evolution. Significant aspects of evolution itself may be in response to changing radiation environments. Much DNA damage is either not repaired, leading to cell death, or is repaired precisely, in which case there is no mutation. In neither extreme is there evolution. On the contrary, a significant amount of current-day mutation is due to error-prone light-induced DNA damage repair of cyclobutane pyrimidine

dimers incurred by UV radiation (e.g., Alpen 1998; Jagger 1985; von Sonntag 1987). In addition, the mechanisms involved in the repair of DNA damage due to UV and ionizing radiation are often the same as those involved in gene transfer and meiosis (Michod and Wojciechowski 1994 and references therein). It is conceivable that early life had to learn the techniques of radiation repair for survival, but then adapted them to powerful modes of evolution, first lateral gene transfer and then sexual reproduction. In this context of the possible fundamental importance of UV damage and repair, it is then especially interesting that planets with thick atmospheres that will shield surficial life from direct ionizing radiation will nevertheless shower the surface with UV irradiation in response to the stochastic astronomical radiation environment from the host star and more distant, yet significant Galactic events.

Chapter 2

Solar X-ray Flare Hazards on the Surface of Mars

Chapter synopsis: The largest solar flares can deliver high enough X-ray doses through the Martian atmosphere to the surface to sterilize organisms with terrestrial-like radiation tolerances. This suggests that extant life would need to survive not only the low-level, background doses of particle radiation but extreme intermittent doses of photon radiation. Exposure is limited to the hemisphere facing the sun, but the duration of large solar storms can be longer than a Martian day, so global lethality could occur. Depending on the size of the largest solar flares, even bacteria could conceivably be sterilized. Organisms can be protected from X-rays by several cm of Martian soil—one more reason why extant Martian life would likely reside in a subsurface environment.

2.1 Introduction

Habitability for all types of life—from human to microbial—is a central problem for the next decades of Mars exploration. In particular, knowledge of surficial radiation doses from all possible sources is essential. Cordoba-Jabonero et al. (2003) have calculated in detail the transfer of ultraviolet (UV) radiation in the Martian atmosphere and folded the surface flux with a DNA action spectrum to obtain UV dose rates (see also Cockell et al., 2000;

Mancinelli and Klovstad, 2000). Schueger et al. (2003) treated the same problem experimentally, with the survival of spores of *Bacillus subtilis* in a Mars simulation chamber. Molina-Cuberos et al. (2001), Pavlov et al. (2002), and De Angelis et al. (2004) have estimated the fluxes of Galactic cosmic-ray particles on the present and ancient Martian surface and subsurface. Pavlov et al. find that the maximum dose rate due to Galactic cosmic rays is about 0.2 Gray yr^{-1}, using dosimetry units in which 1 Gray (Gy) $\equiv$ 100 rad and 1 rad $\equiv$ 100 erg g^{-1} absorbed. This dose rate occurs at a depth of about 25 g cm^{-2}. Measurements and detailed simulations of the cosmic-ray dose rate have been carried out by the Martian Radiative Environment Experiment (MARIE) on the Mars Odyssey Orbiter (Saganti et al., 2004), with measured and modeled surface values mostly around 0.06 Gy yr^{-1}. Integrated over a microorganism's generation time, the corresponding doses are smaller than the lethal dose for any terrestrial microorganism, but the whole-body human dose would be significant over decades, suggesting problems for manned Mars missions. The dose due to ionizing radiation is also of interest in the context of natural transfer of microorganisms between solar system bodies, in particular Mars and Earth (Mileikowsky et al., 2000).

X-rays from the most energetic solar flares are potentially important for Martian life, but have not yet been treated. The steady solar coronal X-ray, EUV, and FUV emission is currently fairly small (Güdel et al., 2003). In contrast, during a solar flare, the flux of ionizing photons can increase by orders of magnitude, and large dose rates are possible. Unlike on Earth, the Martian atmosphere is currently thin enough that a significant fraction of this radiation can arrive at the surface, where it may lead to genetic damage and mutations in terrestrial-like organisms. The fraction of energy absorbed in the atmosphere or reprocessed to UV (Smith et al., 2004a; Smith et al., 2004b) is minimal. Moreover, the X-ray flux from the flares of interest here are orders of magnitude larger than the Martian keV X-ray fluxes observed by the Chandra X-ray Observatory (Dennerl, 2002), which are probably generated in the Martian atmosphere by solar X-rays (Cravens and Maurelis, 2001) and the solar wind (Gunell et al., 2004).

The highly intermittent flares discussed here must be distinguished from other radiation sources (Galactic cosmic rays and solar UV) that have had approximately constant

intensities during Mars' recent history. In particular, the present UV flux on Mars' surface is very large (Cockell et al., 2000; Cordoba-Jabonero et al., 2003; Mancinelli and Klovstad, 2000), comparable to most estimates for the Archaean Earth (Cockell, 2002). The corresponding UV doses would be lethal to most terrestrial organisms. But the UV flux has changed only on the timescale of Mars' atmospheric loss (e.g. Chassefière and Leblanc, 2004), so it seems reasonable that organisms on Mars could have adapted. Laboratory directed evolution experiments involving bacteria exposed to various changing environments support the idea that organisms on Mars could have developed additional repair pathways, or more efficient use of existing repair pathways, to cope with the secularly increasing UV flux. The serial transfer experiments by Ewing (1995, 1997) involving exposure of wild-type *E. coli* strains to large UV, X-ray and gamma-ray fluxes clearly show bacteria increasing their radiation resistance in the presence of increasing and (normally) lethal intensities. The complexity of gene expression in response to UV irradiation (e.g. Quillardet et al., 2003) and the variety of UV repair pathways suggests the potential for great flexibility in resistance.

We therefore make the basic assumption that Martian organisms have developed enhanced UV resistance strategies, either by repair efficiency, ultraviolet transparency of the nucleic acids that make up its genome (assuming they are coding organisms based on nucleic acids), or habitat shielding (e.g. a very thin, ~ 100 μm, dust layer Cockell et al., 2000). Kolb et al. (1994) have pointed out the availability of base structures that are UV transparent, suggesting that the bases used by early terrestrial organisms were different that that of post-ozone organisms. Cockell and Airo (2002) argue, however, that this is unlikely because the lack of absorption longward of 230 nm must be accompanied by a reduction in electron transfer reactions, which are important for many cellular functions. Cockell and Airo (2002) suggest that the energetic benefits of charge transfer associated with delocalized pi-electron-containing base pairs outweighs the cost of strong UV absorption and concomitant damage. Whether or not this argument is valid, we do not assume UV transparency, only adaptation to the increasingly hostile UV environment, resulting in enhanced repair efficiency, as is observed in the laboratory.

Evolution of enhanced resistance to the X-ray flares discussed in the present work

would be difficult or impossible. The flare durations are very short (about an hour), and the times between exposures are orders of magnitude larger than organism generation times, so no adaptation could occur. Thus highly intermittent flare radiation can be lethal in a way that gradually increasing UV (or nearly constant cosmic-rays) cannot.

In this paper, we focus on the following question: at the Martian surface, for a strong solar X-ray flare of given total energy and spectrum, how does the biological dose compare to the lethal doses of various terrestrial organisms? We then extrapolate the recurrence frequency-energy release relation for solar flares to estimate the mean time between such lethal events for a variety of organisms. Finally, we contrast X-ray dose rates with that of cosmic rays and discuss shielding considerations.

2.2 Solar Flare Properties

2.2.1 Spectra

X-rays and γ-rays with energies between 10^{-1} and 10^{6} keV[1] comprise a significant fraction of solar flare photon emission (e.g. Haisch et al., 1991; Hudson, 1991; Kanbach et al., 1993; Ryan, 2000). Hard X-ray (hereafter HXR) spectra are often taken to peak around 10–25 keV (Crosby et al. 1993; but see Krucker and Lin 2002), but this is very uncertain because it is near the sensitivity cutoff of most instruments (RHESSI being a notable exception). Flare X-ray spectra are often fit by a single power law (Crosby et al., 1993; Bromund et al., 1995; Veronig et al., 2002) or two piecewise power laws (Krucker and Lin, 2002). The range of the estimated power-law spectral index (log-log slope) p is large for hard X-ray flares (Lee et al., 1993; Bromund et al., 1995; Qiu et al., 2004): most flares have a p between 2.5 and 6, with a median around 4 and little correlation with total X-ray output. Another study of a large number of flares in the 10 to 100 keV range using GOES data (Veronig et al., 2002) suggests that the typical slope may be flatter for these flares, although still with a very large spread. Using results from RHESSI, Battaglia et al. (2005) find that the non-thermal (HXR) emission spectral index may be correlated with total energy release,

[1] 1 Å= 12.4 keV

such that the larger flares have flatter (harder) spectra, but no such correlation was found in the thermal (soft X-ray) emission. If this correlation is real, then the large solar X-ray flares described here may deliver even larger doses than we estimate (see §2.4.2). Given the uncertainty described, we take the slope of the incident photon spectrum as a parameter (see §2.3), constrained by the observed distribution of p, and assume no correlation between spectral index and total energy output.

2.2.2 Durations

Solar flares have a complex temporal structure. The distribution of flare durations has been estimated using several datasets and characteristically fits a decreasing power law (Lee et al., 1993). Most HXR flares have short durations ($\lesssim$ 20 sec), with a loose correlation between duration and total energy release. We are only concerned with the rare, highest-fluence flares, however, with durations found by Crosby et al. (1993) for HXR and Veronig et al. (2002) for soft X-ray (SXR) flares of about 15 min, with the more energetic flares tending to last longer. The X-class data of Veronig et al. have a median duration three times longer than the B-class data (30 min and 10 min, respectively). Just as with spectral slope, the flare-to-flare variation in duration is large and difficult to characterize quantitatively. For example, some flares emit much of their energy as gamma rays over several hours (Ryan, 2000).

For our purposes, though, the duration is unimportant; the acute lethal dose is almost always independent of dose rate (Sparrow et al., 1967), and thus depends on fluence, not flux. Note that almost all flares have durations much smaller than a Martian day, suggesting that mutation and lethality could occur only on one hemisphere at a time. On the other hand, flare events clustered over many days are sometimes observed (e.g. the Halloween flares of Oct–Nov 2003; Woods et al. 2004), which could progressively irradiate the whole planet.

2.2.3 Energy Release

The total photon energy release in flares is difficult to estimate and varies by at least 10^8 from flare to flare, but a large number of studies using EUV, SXR, or HXR satellite events roughly agree that the differential distribution of flare energy releases dN/dW is a power law with index about -1.6 to -1.8 over at least six orders of magnitude in total energy release W (Hudson, 1991; Lee et al., 1993; Crosby et al., 1993; Bromund et al., 1995; Aschwanden et al., 2000; Lin et al., 2001; Güdel et al., 2003; Qiu et al., 2004), although a somewhat steeper index (-2.0) has been inferred from a very large sample of SXR flares (Veronig et al., 2002).

The largest X-ray release observed among contemporary solar flares is about 10^{31} to 10^{32} erg, which can be seen from the recurrence frequency-energy distribution ($\propto dN/dW$) given graphically in Aschwanden et al. (2000). Eleven large X-class flares occurred during the extraordinary solar outbursts between 18 October 2003 and 5 November 2003, with SXR releases in the GOES 1.0–8.0 Å (1.6–12 keV) band peaking at about 2×10^{31} erg for an effective duration of 30 min. Observations using the SORCE instrument's Total Irradiance Monitor yielded a total flare energy at all wavelengths for the somewhat weaker 28 October flare of 4.6×10^{32} erg (Woods et al., 2004). Radiation and charged particles from these flares compressed the Earth's Van Allen belt to within 20,000 km of the surface (Baker et al., 2004), temporarily damaged the orbiting Mars Odyssey communication instruments, and significantly reduced stratospheric ozone levels (Randall et al., 2005).

Based on astronomical observations, we believe it reasonable to infer that much more energetic solar flares have occurred in the past:

1. There is little doubt that solar-like stars can produce very energetic, and frequent, X-ray flares. Data presented by Audard et al. (2000) indicate SXR flares (0.01–10 keV) of energy greater than 3–5 $\times 10^{34}$ erg for the young, solar-like stars 47 Cas and EK Dra (age $\sim$ 100 Myr) and 2×10^{33} erg for an older, solar-like star κ Cet (age $\sim$ 1 Gyr), with frequencies of about *one per ten days* at these energies. Considering the short sampling period and the form of the derived frequency-energy release relation, more energetic flares seem likely, though less frequent.

2. Schaefer et al. (2000) have identified nine "superflares" with energy outputs of 10^{33} to 10^{38} erg on otherwise normal F8–G8 main sequence stars. Two of these stars were solar-like and produced X-ray flares with energies about 100–1000 times larger than the largest observed solar X-ray flare. These flares cannot be attributed to binaries, rapid rotation, or youth, and may in fact be common in solar-type stars, although cannibalization of giant planets has been suggested (Rubenstein and Schaefer, 2000).

3. Stothers (1980) interpreted NO_3^- abundance spikes in several Antarctic ice cores as due to flares with energies around 10^{32}–10^{33} erg with a recurrence timescale of $\sim 10^2$ yr, consistent with the extrapolation of the frequency-energy relation we adopt below in Eq. 2.6.

4. On lower mass dMe main-sequence stars, flares are more frequent, with photon releases exceeding 10^{34}–10^{35} erg observed, often serendipitously (Hawley and Pettersen, 1991; Pagano et al., 1997; Liebert et al., 1999; Favata et al., 2000; Christian et al., 2003). These energies are enormous, considering that the bolometric luminosities of these stars are much smaller than that of the sun.

Although flares of such large energy release have not been observed in the sun, these data for other stars strongly suggest that the maximum observed is limited only by duration of observation. We have found no compelling physical argument for an upper limit to flare energy releases below the levels discussed in this paper, but the slope of the empirical frequency-energy release relation suggests that some upper limit must exist to avoid energy divergence (Hudson, 1991). Given the above considerations, we expect the maximum flare release to be *at least* 10^{35} erg, and assume this to be true in what follows.

2.3 Radiative Transfer Method

We calculate in detail the transfer of the incident ionizing radiation through the Martian atmosphere using a previously developed Monte Carlo code (Smith et al., 2004b) that accurately treats Compton scattering and X-ray photoabsorption. We use the empirical approximation of Setlow and Pollard (1962) for the photoabsorption cross section for energies

greater than the K edge:

$$\sigma_{\rm pa} = 2.04 \times 10^{-30}(1 + 0.008Z) \left(\frac{Z}{E}\right)^3 \ {\rm cm}^2, \tag{2.1}$$

where E is the energy in units of 511 keV and Z is the atomic number of the target atom. Compton scattering cross sections are calculated using the full Klein-Nishina formula. We assume that the atmospheric gas density falls off exponentially with height, with a scale height of 11 km and a total column density of 16 or 22 g cm^{-2}, corresponding to rough limits set by the freezing and thawing of the polar ice caps. This model works well because the high-energy radiative processes involved here are relatively insensitive to the exact vertical distribution and composition of gas, instead depending mainly on the total column density and mean molecular weight.

Solar-flare-photon number spectra are assumed to be distributed as E^{-p}, with $2 < p < 6$ (see §2.2). For calculational purposes, the flare spectrum is assumed to extend from 10 keV to 511 keV. The 10-keV lower limit is taken because photons below this energy are nearly completely absorbed by the atmosphere and unimportant to the surficial dose, while the upper limit is set high enough that a negligible number of incident photons are at higher energies, even for the shallowest spectra (lowest p). Given a lower limit $E_{\rm min}$ and a specified normalization $N_{\rm tot}$, the differential number spectrum can be written (neglecting any upper cutoff for simplicity)

$$\frac{dN}{dE} = (p-1)\ N_{\rm tot}\ E_{\rm min}^{p-1}\ E^{-p}, \tag{2.2}$$

and the average energy in the spectrum is obtained by integrating between the minimum and maximum cutoff energies:

$$\langle E \rangle = \frac{1}{N_{\rm tot}} \int_{E_{\rm min}}^{E_{\rm max}} E \frac{dN}{dE}\ dE. \tag{2.3}$$

This is the spectrum that is propagated through the atmosphere using the Monte Carlo code. Note that henceforth the total energy release figures refer only to the energy between

10 and 511 keV.

After transport through the atmosphere, the photon fluence is converted to a biological dose by assuming that the surficial radiation is absorbed by pure water. Much of the damage by ionizing radiation is thought to be "indirect," involving chemical reactions initiated by energy deposited in the bulk cell water or first hydration layer rather than "direct" ionization of DNA (von Sonntag, 1987; Ward, 1999), although this terminology is now recognized as an oversimplification (Fielden and O'Neill, 1991). We then estimate the dose by integrating the surficial energy spectrum $E\ dN/dE$ over the energy-dependent opacity of water $\kappa_{\rm w}(E)$:

$$D = \int_{E_{\rm min}}^{E_{\rm max}} \kappa_{\rm w}(E)\ E\ \frac{dN}{dE}\ dE. \tag{2.4}$$

The water opacity in our code includes both Compton scattering and photoabsorption. It should also be noted that the biological quality factor and relative biological effectiveness (RBE) are both near unity for X-rays and γ-rays, so no adjustment is required to compare to empirical lethal doses, as in cosmic-ray studies.

Most of the uncertainty in our calculations is due to the fact that the total X-ray opacity of the Martian atmosphere depends sensitively on the uncertain energy spectrum of the flare photons, since the photoabsorption optical depth varies approximately as $\exp(-E^{-3})$. Given a particular flare spectrum, our results are accurate, but the spectral slopes vary greatly from flare to flare, even given the same total energy release (see §2.2). Thus we use the slope, p, as a free parameter that varies between 2 and 6 and present the results for a range in p. Later we integrate over an approximate representation of the observed frequency distribution of p for hard X-ray solar flares to derive appropriate average values for waiting times as a function of dose.

2.4 Results

2.4.1 Calculated Surficial X-Ray Spectra

The Martian atmosphere, though thin by terrestrial standards, significantly attenuates the incident flare radiation, but the high fluences associated with the most massive flares lead

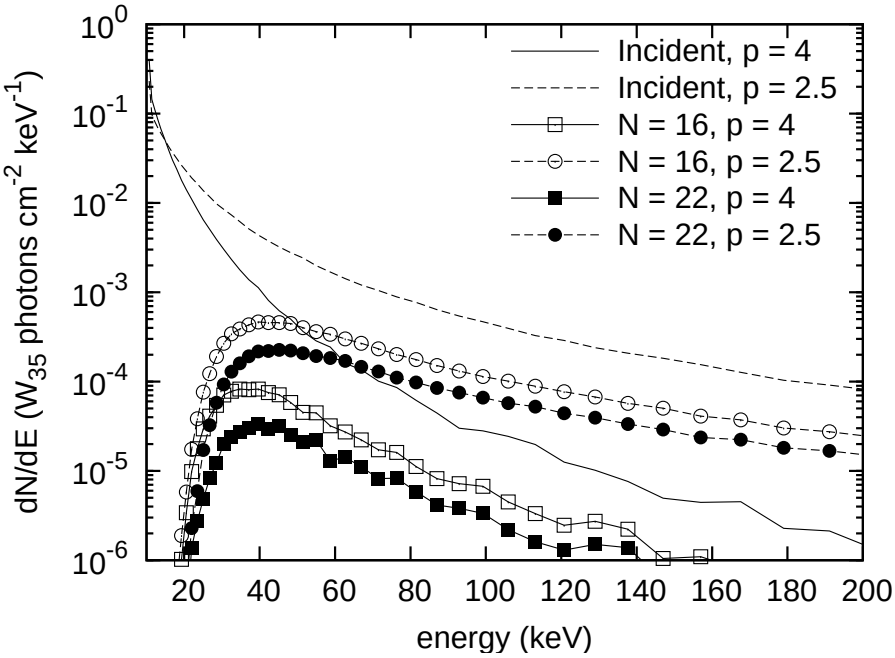

Figure 2.1: Surficial, reprocessed, X-ray flare spectra, assuming a parameterized, power-law model spectrum (see §2.3). Two incident spectra are shown, with power-law spectral indices of $p = 2.5$ and $p = 4$. For each of these spectra, associated surficial spectra are shown for two different column densities: 16 and 22 g cm^{-2}. Attenuation due to photoabsorption is most severe at low energies, leading to a sharp decline below about 20 keV in the flux per unit energy. Also, the original incident spectrum falls off at high energy, so the combined effect leads to a peak at intermediate energies (30–50 keV here).

to extreme irradiation of the surface nonetheless. We show in Fig. 2.1 the surficial fluence spectra from a 10^{35}-erg flare for two atmospheric column densities ($\Sigma = 16$ and $\Sigma = 22$ g cm^{-2}) and two spectral indices ($p = 4$ and $p = 2.5$), together with the above-atmosphere, incident spectra. The vertical axis scales linearly with flare energy release (we have used 10^{35} erg for this example). In general, for all column densities, spectra with lower mean energies (higher p) are attenuated more because of the rapidly rising (E^{-3}) photoabsorption opacity. This effect, combined with the falloff of the incident spectrum at high energies, together creates a peak in the surficial spectrum at moderate energies (30–50 keV here). Additionally, increasing the atmospheric column increases the attenuation at all energies, as one would expect.

2.4.2 Estimated Biological Doses

Ionizing radiation alters DNA through direct ionization and indirect chemical interactions involving diffusion of radical products of ionization and dissociation in the cytoplasm. Resulting biochemical effects include single- and double-strand breaks, base damage or abasic sites, multiply damaged sites, oxidized base clusters, and cross-linking within DNA or with proteins (Becker and Sevilla, 1993; Ward, 1999). An amazing suite of repair processes and associated enzymes repair the damage (Friedberg, 2003), but generally for each organism, above some critical amount of absorbed energy, fecundity greatly diminishes. Biological damage is quantified in terms of the amount of energy absorbed, or dose, typically in units of rads or Grays. The lethal dose is often defined as the dose that kills a particular fraction of a laboratory population. The dose for reducing the population by $1/e$ is denoted D_{37}, while the dose for reduction of the population by 90% is D_{90}.

The calculated X-ray doses in our situation are shown in Fig. 2.2 as a function of power-law index for two column densities: $\Sigma = 16$ g cm^{-2} and $\Sigma = 22$ g cm^{-2}. The calculation assumes a solar flare with a total X-ray release of 10^{35} erg (see §2.2). Again, for flares of different energy release, the dose simply scales proportionally. The doses for the shallowest spectra ($2 \leq p \leq 3$) are about two orders of magnitude higher than those for the steepest spectra ($5 \leq p \leq 6$), showing the tremendous sensitivity of the dose on the form of the incident spectrum. For comparison to the power-law spectra, we also show monoenergetic spectra with energies equal to the average energy in the power-law spectra for each spectral index. The dramatic decline in the dose with energy for the monoenergetic cases illustrates the importance of the high-energy tail in the power-law spectra and the inaccuracy of doing this calculation using a monoenergetic approximation.

The results shown in Fig. 2.2 can be confirmed by considering a 10^{35}-erg flare incident on the top of the atmosphere and subject to only absorption due to Compton scattering and photoabsorption. Strictly speaking, the Compton process is a scattering process, not absorption, but we will neglect photons that backscatter in the atmosphere and eventually reach the surface in order to get this estimate. This enables us to write an integral that approximates the total dose D in terms of the atmospheric optical depth

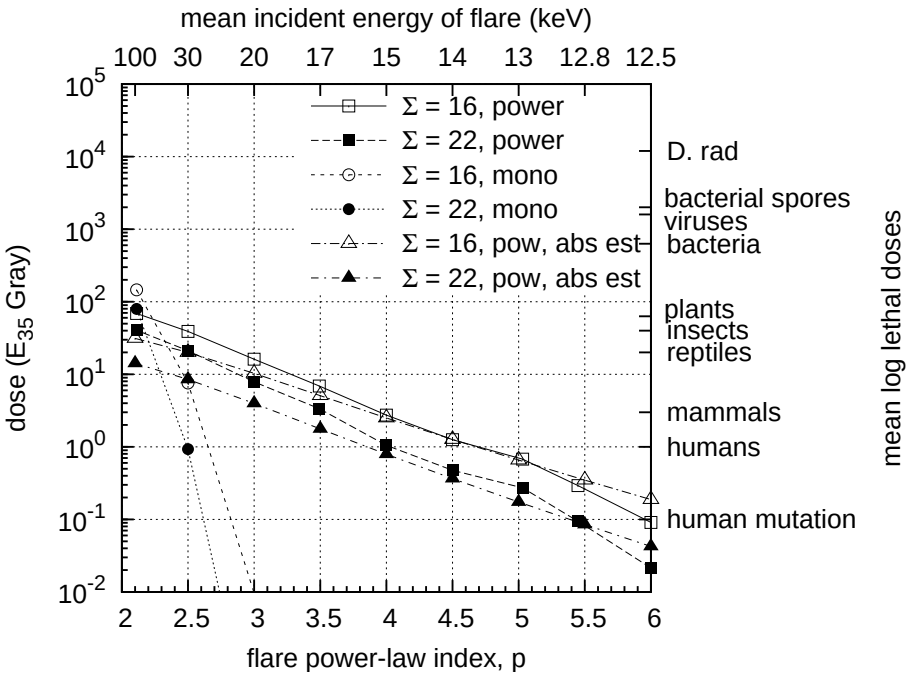

Figure 2.2: Surficial X-ray dose for a flare with 10^{35} erg total energy release versus spectral index. (Doses scale linearly with energy release.) Two column densities are used: 16 and 22 g cm^{-2}. Power-law flare spectra are denoted "power" in the legend. Monoenergetic incoming photons with energies equal to the mean incident flare energy are shown as "mono." This case demonstrates the inaccuracy of ignoring the full radiative transfer, since the curve decreases *much* more rapidly than the power-law cases. The final pair of curves (denoted "abs est") uses a power-law incident spectrum with the radiative transfer done using the analytic, absorption approximation discussed in §2.4.2. The general trend among all curves is that the dose decreases with increasing spectral index. This is because (as can be seen on the upper horizontal axis) the average energy of the flare spectrum decreases with increasing spectral index. The atmosphere is vastly more opaque to lower-energy X-rays, which dramatically affects the surficial dose. The right-hand vertical axis shows tick marks at the mean-log lethal dose of a few representative terrestrial organisms (see Table 1).

$\tau_{\rm a}(E)$ and the water opacity $\kappa_{\rm w}(E)$:

$$D = \int_{E_{\rm min}}^{E_{\rm max}} \kappa_{\rm w}(E)\ \exp[-\tau_{\rm a}(E)]\ E\ \frac{dN}{dE}\ dE, \tag{2.5}$$

where $N(E)$ is the incident number spectrum at the top of the atmosphere and $E_{\rm min}$ is the minimum energy considered in the Monte Carlo code. This integral can be evaluated numerically to confirm the results given in our Monte Carlo calculation; we have done this and present it as the final set of curves in Fig. 2.2 marked "abs est." The integral is very close to the full calculation at all energies, being only different by at most a factor of two, which suggests that backscattered radiation is only marginally important to the surficial doses. For the flattest spectra (p near 2), the code gives a higher (and more accurate) dose because it includes backscattered radiation. For steeper spectra, the difference between the above approximation and the code stems from the discrete number of bins in the surficial spectra in the code and the fact that the mean incident spectrum energy is very close to the lower cutoff energy, causing discretization errors in the output spectra when binning photon energies close to the cutoff. The integral above, being continuous, suffers no such errors, so is probably more accurate in this regime, where absorption dominates anyway.

The horizontal ticks along the right side of Fig. 2.2 show typical mean-log acute lethal doses for a variety of organisms. The most comprehensive compilation we know of (Sparrow et al., 1967) gives D_{90} for X-ray and γ-ray exposure of 79 organisms. We have expanded and supplemented this with more recent work, especially for microorganisms, including the review of virus lethal doses by Rohwer (1984), lethal doses in bacterial spores summarized by Russell (1982), studies of food pathogenic bacteria by Dion et al. (1994) and Farkas (1998), studies of Archaean hyperthermophiles by Kopylov et al. (1993) and DiRuggiero et al. (1997), mammalian studies presented in Fielden and O'Neill (1991), studies of mutations in human survivors of Hiroshima and Nagasaki (Turner, 1995, p. 398), the Chernobyl accident and Kazakhstan nuclear weapon tests (Dubrova, 2003), and inhabitants of the Kerala (India) radioactive hotspot (Forster et al., 2002). We find these results to be consistent with each other in cases we have checked.

Organism	Acute Lethal Dose (Gy)
mammals	1–10
higher plants	5–700
insects	1–2000
bacteria, protozoa, algae	30–15,000
viruses	150–20,000
bacterial spores	1,000–4,000

Table 2.1: Acute lethal dose ranges for representative organisms

Because of the large range of lethal doses found in nature we have chosen to represent various organisms in Fig. 2.2 by the average of the base-10 logarithm of the lower and upper limits found for that class. This is an appropriate choice because the available data from Sparrow et al. (1967) within each taxonomic class are distributed roughly uniformly in log lethal dose. Thus for mammals, with a range of 1–10 Gy, the number indicated on the log scale is 0.5. Table 1 lists the approximate lethal dose ranges for these organisms. Organisms with extremely large lethal doses are interesting for long-term survival prospects—e.g. adult Drosophilia at 1000 Gy, some Archaean hyperthermophiles at 2000–6000 Gy, *Rubrobacter radiotolerans* at 8000 Gy (Ferriera et al., 1999), *Deinococcus radiodurans* at 10,000 Gy (depending on cell phase; see Battista, 1997), and the virus-like proteinaceous infectious particle (prion) associated with scrapie at 20,000 Gy (Rohwer, 1984).

Even very low doses can be important. Doses for mutation and clustered DNA damage can be much smaller than the lethal dose. For example, in humans, the whole-body acute lethal dose is about 1–2 Gy, but mutations (Sparrow et al., 1972; Sankaranarayanan, 1982; Forster et al., 2002), chromosomal abnormalities in blood lymphocytes (Violet et al., 2005), and clustered DNA damage (Sutherland et al., 2000) occur at only around 0.01–0.2 Gy, and germ-line mutation doubling is believed to occur around 0.5 Gy (UNSCEAR 2001; Sankaranarayanan and Chakraborty 2000; but see Forster et al. 2002). So doses even smaller than the "humans" level in Fig. 2.2 should be considered hazardous for human exploration of Mars. We indicate this level at 10^{-1} Gy with the label "human mutation."

We have ignored the dependence of lethal dose on dose rate. Sparrow et al. (1967)

claim no evidence for a significant dependence in the literature they compiled, but it is undoubtedly true that at some level a dose rate dependence occurs, as has been observed in mammalian and other organisms. Since the duration of solar flares is random, it is difficult to convert received fluences into the fluxes needed for dose-rate calculations; hence we have ignored this and focused this work on time-integrated quantities.

Finally, recall the possible correlation between hard X-ray flux and spectral index found in the RHESSI data by Battaglia et al. (2005) mentioned in §2.2.1. If flares with a larger total energy release do indeed typically have flatter spectra, then they would have higher mean photon energies. The Martian atmosphere is more transparent to X-rays of higher energies, so this effect would boost the surficial doses received from larger flares. In this sense our results are an upper limit to the flare releases required to produce given doses.

2.4.3 Mean Times Between Lethal Events

The calculated surficial doses are very sensitive to the flare spectral index p, which varies greatly and unsystematically with other flare parameters, so a better way to determine the lethality risk is to integrate the frequency of events delivering a given dose for each p over the probability distribution of p values. We take this probability distribution to be the uniform distribution, which is roughly consistent with results shown in Lee et al. (1993), Bromund et al. (1995), Veronig et al. (2002), and Qiu et al. (2004) and other references given there. This procedure yields the total frequency of lethal events for an organism at the Martian surface due to all flares.

To estimate flare timescales as a function of release W, we normalize to one 10^{32}-erg solar flare per decade. Extrapolating the average HXR frequency-energy statistic dN/dW (see §2.2) gives the average time between events of energy release W_{32} (in units of 10^{32} erg) as $T(W) \simeq 10\, W_{32}^{q}$ yr, with q between about 1.6 and 1.8, and the mean time between events at least as large as W_{32} as

$$T(\geq W_{32}) = 10\,(q-1)\,W_{32}^{q-1}\mathrm{yr}. \tag{2.6}$$

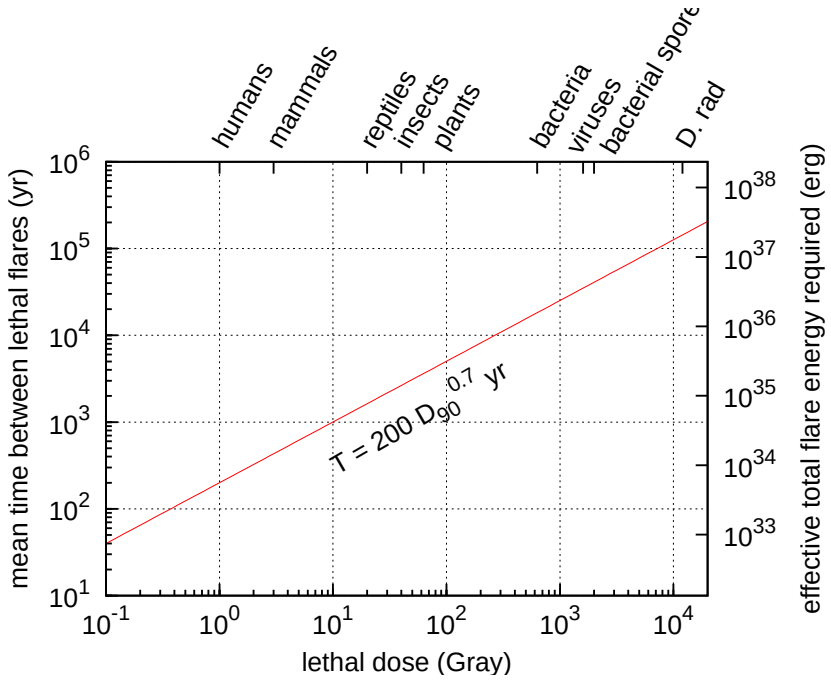

Figure 2.3: Mean time between flare events that deliver a given dose. The dose delivered depends on the spectral index, such that flares with larger spectral index must have a larger total energy to deliver a given dose (see Fig. 2.2). We have integrated over the distribution of spectral indices, and accounted for the dose dependence on this index, in order to find a mean time between events that deliver a given dose without specifying the spectral index (see §2.4.3). The upper horizontal axis shows the lethal doses of a variety of organisms for reference (see Table 1). As expected, the time between events increases as the dose necessary for lethality increases.

This agrees with the estimate of Hudson (1991) and is broadly consistent with the dozen or so 10^{31}–10^{32} erg events that have been observed since GOES soft X-ray monitoring began in 1976. Upper limits on proton fluences in lunar rocks, tree ring records of ^{14}C, and the requirement of finite energy suggest that the frequency-energy release relation dN/dW must steepen above some energy (Reedy et al., 1983; Hudson, 1991; Aschwanden, 1999), but the value of that energy is unknown.

Figure 2.3 graphically shows the mean time between lethal events for the same set of organisms given in Fig. 2.2 as a function of surficial dose, for an atmospheric column density Σ of 16 g cm^{-2}. To produce this plot, we use the mean of the empirical values of frequency-energy release slope, so $q = 1.7$ in Eq. 2.6. The right-hand side vertical axis

shows the corresponding flare energy releases W required for lethality. Again, this result is integrated over the spectral index distribution. Additionally, for a column density of 22 g cm^{-2}, the attenuation is roughly a factor of 2–3 higher (as can be see in Fig. 2.2), so the required lethal dose would be roughly a factor of 2–3 higher, implying a mean waiting time that is $2^{0.7}$–$3^{0.7} = 1.6$–2.2 times longer.

The mean time to lethality is strongly weighted toward the flattest ($p \sim 2$) flares. The atmosphere is more transparent to the flatter flares (because they have a higher average energy), so a lethal fluence at the surface requires less total energy release at the sun. Since flares with lower total energy release are much more common, chances are that the flare that finally delivers the lethal dose will have a smaller spectral index. We show this explicitly below.

To derive the equation for the mean time between flares of a given dose, as shown in Fig. 2.3, we first convert the waiting time distribution given in Eq. 2.6 back to the empirical flare energy release-mean frequency relation:

$$\overline{\nu}(W) = k_W W_{32}^{-q} \text{ yr}^{-1}, \tag{2.7}$$

where once again we use $q = 1.7$ and we estimate $k_W \sim 0.1$. The flares are roughly distributed uniformly by spectral index p, and since p ranges from 2 to 6, we can write the probability distribution function of p as $f(p) = 1/4$. The frequency distribution for the flares as a function of energy W and spectral index p is then

$$\overline{\nu}(W, p) = \overline{\nu}(W)\, f(p), \tag{2.8}$$

where we have assumed that W and p are uncorrelated.

To predict how often solar X-ray flares can deliver a particular lethal dose, we must transform this distribution to a function of dose D. This requires knowledge of the relation between total flare energy release and surficial dose for each spectral index p. In our case, this relation comes from our radiation transport code. An empirical fit to our calculations for a column density of 16 g cm^{-2} shows that the dose in Gray as a function of flare energy

is

$$D(W,p) = \frac{W_{32}}{k_D}\, e^{-p/p_0} \ \ \mathrm{Gy}, \tag{2.9}$$

with $k_D = 0.23$ and $p_0 = 0.53$. We can write the energy required to deliver a given dose by inverting this equation. Then, using the standard technique for transforming probability distribution functions, we have

$$\begin{aligned}
\overline{\nu}(D,p) &= \overline{\nu}[W(D,p),p] \left| \frac{\partial(W,p)}{\partial(D,p)} \right| && (2.10)\\
&= \overline{\nu}[W(D,p)] \left| \frac{dW}{dD} \right| f(p) && (2.11)\\
&= \frac{k_W k_D^{1-q}}{4} D^{-q} \exp[(1-q)p/p_0] \ \ \mathrm{yr}^{-1}. && (2.12)
\end{aligned}$$

Next, we would like to know how many flares of all spectral indices occur each year, but now the dose and spectral index are not independent, so we must integrate, instead of just scaling by 1/4:

$$\begin{aligned}
\overline{\nu}(D) &= \int_2^6 \overline{\nu}(D,p)\, dp && (2.13)\\
&= \frac{k_W k_D^{1-q} p_0}{4(q-1)} D^{-q} \left\{ \exp[2(1-q)/p_0] - \exp[6(1-q)/p_0] \right\} \ \mathrm{yr}^{-1}. && (2.14)
\end{aligned}$$

All flares that deliver doses above the lethal dose are most definitely lethal, so we must integrate the flare dose-mean frequency distribution above the lethal dose (we use D_{90} here) to find the total number of flares that occur on average per year that deliver at least the lethal dose:

$$\begin{aligned}
\overline{\nu}(\geq D_{90}) &= \int_{D_{90}}^{\infty} \overline{\nu}(D)\, dD && (2.15)\\
&= \frac{k_W k_D^{1-q} p_0}{4(q-1)^2} \left\{ \exp[2(1-q)/p_0] - \exp[6(1-q)/p_0] \right\} \ D_{90}^{1-q} \ \ \mathrm{yr}^{-1}. && (2.16)
\end{aligned}$$

Finally, to get the mean time between lethal events, simply take the inverse of this frequency: $\overline{T}(\geq D_{90}) = 1/\overline{\nu}(\geq D_{90})$. For the case discussed in this work, $k_W \sim 0.1$ and $q = 1.7$. Thus

the typical time between lethal flares as a function of lethal dose in Gray is

$$\overline{T}(\geq D_{90}) \simeq 200\ D_{90}^{0.7}\ \text{ yr.} \tag{2.17}$$

This time is much shorter than that yielded by an estimate using just a particular p value. For example, using $p = 4$ instead of integrating over the distribution of p would give about 3000 yr for the coefficient above instead of 200 yr. Properly treating the spectral indices as a distribution in the calculation is important. In fact, the true waiting times are probably a bit shorter than our estimate, since the distribution of spectral indices isn't exactly flat, but rather is peaked slightly at lower indices. In other words, the average flare spectrum may be somewhat harder than we take here.

Figure 2.3 indicates that a solar X-ray flare of 10^{38} erg would be needed to kill any organism as resistant as *D. rad*, bacterial spores, and the most resistant viruses (see Table 1) on the surface of Mars. Such flares would occur at least every $\sim$ 200 kyr if our extrapolation of the solar frequency-energy release scaling could be extended to these extreme energies. Since such energies have not been observed in the sun or other (non-binary) stars, we conclude that such extremely radiation-resistant microbial life on Mars may not be affected by solar flares. Bacteria and protists with the adopted mean log lethal dose require slightly less extreme flare energies and have corresponding times to lethality of about 20 kyr. Reptiles, insects, and plants require more reasonable flare energies, especially considering that many have lethal doses much less than the mean log (see Table 1 and Sparrow et al., 1967). Flares of only 10^{34}–10^{35} erg will result in mutations and lethality for mammals, reptiles, insects, and plants, and may occur every few hundred years. Similarly, a 10^{34}-erg flare, which can be lethal to humans, might occur every 200 yr on average.

Additionally, a correlation between hard X-ray flux and total flare energy release in which larger flares have harder (flatter) spectra (e.g. Battaglia et al., 2005) would decrease the time between lethal events. Larger flares would be more penetrating and would deliver higher doses than we have estimated, which would decrease the energy release needed for a given dose. Since less energetic flares are more common, lethality would occur more often.

2.4.4 Shielding and Dose Rate Considerations

Soil and CO_2 Ice Shielding

So far, we have ignored possible protection strategies, such as radiation shielding sources. As an illustrative example, we take the Mars Pathfinder rover soil sample data of Wänke et al. (2001) and calculate the opacity of this material to incoming flare spectra. Based on the composition of the soils in Table I of Wänke et al. (2001), we find that the samples have an effective atomic number of 15.2 (the Z that, when used in Eq. 2.1, yields the mean cross section of the soil obtained by element-by-element addition). The combined photoabsorption and Compton scattering opacity of this material can be calculated. We use the analytical approximation in Eq. 2.5 to calculate the transfer of the surficial radiation through the soil. Using an atmospheric column density of 16 g cm^{-2}, we find $1/e$ (i.e., optical depth unity) shielding columns for X-ray flares of spectral index $p = 2$ and $p = 6$ to be 7.7 g cm^{-2} and 3.6 g cm^{-2}, respectively. For an atmospheric column density of 22 g cm^{-2}, the same calculation gives only a slightly different result: 8.1 g cm^{-2} and 3.9 g cm^{-2}, respectively. With a typical density of terrestrial andesites of 2.7 g cm^{-3}, these soil columns suggest that around a few cm of regolith is enough to provide $1/e$ attenuation and that tens of cm will reduce the dose by 99% or more. For comparison, the possible ice layers found by Boynton et al. (2002) at 40–150 g cm^{-2} below the surface should be very well shielded.

CO_2 ice has an effective Z of 7.4, roughly half that of the soil, so $1/e$ shielding requires a slightly larger ice column. For an atmospheric column density of 16 g cm^{-2}, we find $1/e$ shielding columns of CO_2 ice for spectral indices $p = 2$ and $p = 6$ to be 8.2 g cm^{-2} and 4.6 g cm^{-2}, respectively. For a column density of 22 g cm^{-2}, we get 8.6 g cm^{-2} and 4.9 g cm^{-2}, respectively. Roughly three times the thickness of ice would be needed for the same $1/e$ shielding as corresponding soil columns due to the different densities. The difference is smaller than expected from the Z^3 dependence of the photoabsorption cross section because a large fraction of photons in the surficial spectrum, even for steep flare spectra, has energies high enough that the radiative transfer is dominated by Compton scattering, a process insensitive to elemental composition.

Altitude can change the atmospheric column density and have a measurable effect on the dose. The column density above Hellas Basin, the lowest topographical point on Mars, is roughly 8 to 14 g cm^{-2} larger (depending on season) than the average and consequently reduces the dose to a factor of about 1/7 to 1/3 of the dose at the mean surface level. This suggests that organisms in low areas would be better protected, but not completely safe.

Manned Mission Shielding

Astronaut protection is a critical issue for long-term, manned space missions. The total mass of a spacesuit depends mostly on the column density of the component material, so, given a fixed shielding requirement, the suit's mass will be minimized by maximizing the suit's opacity to incoming radiation. Typical next generation spacesuit designs provide only up to a few g cm^{-2} of mostly low-Z shielding material (see Ross et al., 1997, for a review). The lightweight and mostly low-Z suits are designed to provide efficient protection from incoming energetic particle radiation (such as cosmic rays). Charged particles lose more energy per unit column density traversed in materials with lower Z because the energy loss is roughly proportional to Z/A, where A is the mean atomic mass, and lighter elements maximize Z/A. Additionally, low-Z materials produce less secondary radiation (mostly neutrons) and lower absorbed doses when incident particles cause nuclear reactions in the shielding material (see, e.g., Schimmerling et al., 1996; Wilson et al., 2001).

X-ray radiation is most efficiently stopped by high-Z materials. Neglecting engineering considerations and particle radiation, the ideal shielding material for X-rays would maximize the quantity Z^3/A, because the photoabsorption opacity, which dominates at these energies, has roughly this dependence on Z and A, as can be seen in Eq. 2.1. Thus, heavier elements are favored for X-ray shielding, since atomic mass A increases much slower than Z^3 across the periodic table. Spacecraft and surface structures, such as "Marsbases," would probably contain a significant amount of high-Z material, and thus could provide adequate flare X-ray shielding if surrounding structures provide a shielding column of greater than tens of g cm^{-2} of $Z \gtrsim 10$ material. For example, polymers, water, and lower-Z metals, such as magnesium and aluminum, would be less desirable than titanium or steel alloys

(especially those high in molybdenum). Note that even a few g cm^{-2} of high-Z material is inadequate should a large solar X-ray flare occur during a spacewalk or "Marswalk." Balancing the two contrasting shielding requirements for particles and photons while minimizing the weight and rigidity of spacesuits may prove to be difficult.

All of these considerations also apply to moon missions and space missions elsewhere in the solar system, with doses being even higher outside of Mars' protective atmosphere and inversely proportional to the square of the distance to the sun.

X-ray Flares and Cosmic Rays: Dose Rate Differences

The mean times to lethality we give refer only to the surface of Mars on the hemisphere facing the sun for organisms with short generation times. Lethality from a solar flare contrasts with the situation for cosmic-ray exposure; the difference is one of acute versus extended weak exposure. Flares are intermittent bursts, and lethality will occur during the flare if the flare is sufficiently energetic. The organism lifetime does not affect lethality unless it is less than the mean flare duration (about 15 to 30 min for the flares considered here), and even most bacteria have longer generation times. For example, the average generation time for many *E. coli* strains is about an hour. Cosmic rays, however, cause damage over long periods of time from constant, relatively small, surficial fluxes. Organisms might be able to continuously repair the cosmic-ray damage (as on the present Earth), while the high dose rates of flare exposure may overwhelm genomic repair systems. The Saganti et al. (2004) and Pavlov et al. (2002) calculations cited in §2.1 give Galactic cosmic-ray dose rates of 0.06–0.2 Gy yr^{-1}. Taking the representative dose rate to be 0.1 Gy yr^{-1}, the time to accumulate a lethal dose from cosmic rays is longer than the lifetime of all but the most sensitive mammals and long-lived plants. Pavlov et al. (2002) also state that living organisms would survive cosmic-ray irradiation, and that only dormant organisms, with their inactive genomic repair systems, would be killed by the slowly accumulating damage. In contrast, solar flares have dose rates high enough to kill both living and dormant organisms.

2.5 Summary and Implications

Continuing astronomical observational programs are recording larger and larger X-ray flares from stars of solar mass and smaller. The most energetic flares observed on the sun are almost large enough to cause mutation and lethality in higher organisms on the surface of Mars, and extrapolation to higher energies implies greater, but less frequent, biological damage.

Using a previously developed Monte Carlo radiative transport code (Smith et al., 2004b), we have calculated the surficial X-ray spectra and corresponding biological doses due to solar flares with a range of spectral indices. We compared our results to the average lethal doses for a representative range of terrestrial organisms. We find that, if the sun has flares much larger in energy output than those observed (as supported by observations of other stars), organisms with a range of radiological tolerances, from mammals to plants, insects, and reptiles to even high-tolerance bacteria, spores, and viruses could be sterilized on the hemisphere of Mars facing the sun during the flare. Though a single flare leads to only partial sterilization, flares are often clustered in time, so it may be possible to irradiate the whole surface over the course of weeks during a period of extreme solar activity.

Estimates were given for the mean time between lethal events based on extrapolating the observed recurrence frequency-energy release distribution for solar flares. Precise results are difficult because of the random nature of flare occurrence and spectral indices, so we provide mean times between lethal flare events integrated over the spectral index distribution. In addition, the estimated mean times between flares of such energies are orders of magnitude less than the age of the solar system, so may have occurred 10^3–10^7 times for the period during which Mars has had its present thin atmosphere, depending on the maximum possible solar flare energy and required lethal dose.

Finally, we showed that a column thickness of $\sim$ 4–8 g cm^{-2} of Martian soil would be sufficient to provide $1/e$ attenuation of the surficial flare energy. The conflicting shielding requirements for particle radiation and the X-rays discussed here leads to a difficultly designing safe spacesuits for manned Mars or lunar exploration, but designing safe "Marsbases" and other ground structures should be easier.

Chapter 3

Risks due to X-ray Flares during Astronaut Extravehicular Activity

Chapter synopsis: X-rays from the largest solar flares pose a danger to astronauts on extravehicular activities, when spacesuits are their only radiation shielding. Large solar X-ray flares occur with little or no warning and deliver the full radiation dose in such a short time that escape is impractical. A relatively small, metallic shield affixed to a lunar rover, for example, could provide emergency protection.

3.1 Introduction

The risk for space travelers due to solar-produced radiation, as well as Galactic cosmic rays, has been studied extensively for nearly four decades, but the predictability and frequency of potentially lethal doses of high-energy solar radiation is still far from understood. A long series of studies suggest that the most energetic solar particle events (SPEs) (Reedy, 1996; Shea and Smart, 1990, 2000; Miroshnichenko, 2003; Reames, 1999) can produce lethal biological doses that require careful consideration of shielding requirements for spacecraft, lunar and Martian habitats, and spacesuits for extravehicular activities (EVAs), e.g., (Silberberg and Tsao, 1979; Silberberg et al., 1987; Dyer et al., 1996; Schimmerling et al., 1996; Badhwar, 1997; Cucinotta et al., 2001; Miroshnichenko, 2003; Cucinotta et al., 2004;

De Angelis et al., 2004; Getselev et al., 2004; Wilson et al., 2004; Cougnet et al., 2005; Johnson et al., 2005; O'Brien, 2005). The August 1972 SPE, often taken as the standard high-fluence event for protection studies, was not an isolated anomaly. The February 1956, November 1960, October 1989, and October-November 2003 events produced solar-particle fluxes sufficiently large that an astronaut on the moon protected by only a spacesuit would likely have perished, and many events approaching these fluences have been recorded (Shea and Smart, 2000; Miroshnichenko, 2003). The durations of these events (many hours, see Miroshnichenko 2003) are large enough that evacuation to shelter would prevent serious exposure to an astronaut on an EVA. Associated speed-of-light precursors (photon flares and CME eruptions), while not always available for the strongest SPEs (Reames, 1999), could allow further time for escape.

Given the computational difficulties of calculating the propagation of solar cosmic rays in the inner heliosphere and the resulting biological doses, it is surprising that the effects of ionizing photons, in particular X-rays from solar flares (Haisch et al., 1991; Hudson, 1991), have not been considered. It is easy to show that the fluence from the most energetic hard X-ray flares observed would result in an amount of energy absorbed per gram of tissue larger than the lethal dose for an unprotected human at 1 AU. Acute doses for various biological endpoints are well studied, especially because of their relevance to oncological research. The frequency of very energetic flares is similar to that of the most energetic SPEs; their durations are so small that evacuation is much more problematic; and there are no early and reliable precursors that can be used to predict their onset as in the case of SPEs. Furthermore, the shielding requirements are nontrivial and somewhat different from those for solar energetic particles (SEPs), requiring high-Z material, in contrast to the mostly low-Z material in current spacesuit designs. Bone surrounding blood-forming marrow might mitigate hematological effects, but risk of carcinogenesis remains significant. We calculate here the expected doses from energetic solar X-ray flares and use their observed frequency-fluence relation to estimate the probability per unit time of a hazardous flare exposure.

3.2 The Largest Solar Flares

Solar flare photons span energies between 10^{-1} and 10^{6} keV (Haisch et al., 1991; Hudson, 1991; Kanbach et al., 1993; Ryan, 2000). The spectrum of hard X-rays (HXRs) is often taken to peak at energies of 10–25 keV or higher (Crosby et al., 1993; Battaglia et al., 2005; Krucker and Lin, 2002) and are usually fit by a single power law of the form $F(E) \sim E^p$ (Crosby et al., 1993; Lee et al., 1993; Bromund et al., 1995; Veronig et al., 2002; Qiu et al., 2004). The range of the estimated power-law index (log-log slope) p is large for HXR flare spectra, with p between 2 and 6, the median around 3.5, and a small but significant correlation between p and total X-ray output as shown by RHESSI data (Battaglia et al., 2005).

X-class solar flares (the most energetic flares) have typical durations of about 5–30 min (Crosby et al., 1993; Veronig et al., 2002), with the more energetic flares tending to last longer. As with spectral slope, flare durations vary widely, but even with the longest of these durations the dose should be considered acute, in contrast to low-level, extended exposure to Galactic cosmic-rays. The acute lethal dose is almost always independent of dose rate (Sparrow et al., 1967), so we assume that the non-lethal acute dose depends on total fluence, not flux, and hence on the flare total energy release.

The total photon energy release W in flares is difficult to estimate and varies by at least a factor of 10^8, but a large number of studies using EUV, soft X-ray (SXR), and HXR satellite events roughly agree that the differential distribution of flare energy releases dN/dW is a power law with index about -1.6 to -1.8 over at least six orders of magnitude in total energy release W (Hudson, 1991; Lee et al., 1993; Crosby et al., 1993; Bromund et al., 1995; Aschwanden et al., 2000; Lin et al., 2001; Güdel et al., 2003; Qiu et al., 2004).

The largest X-ray releases observed among contemporary solar flares is $\sim 10^{32}$ erg (Hudson, 1991; Crosby et al., 1993). Eleven X-class flares occurred during the extraordinary solar outbursts between 18 October 2003 and 5 November 2003 (Gopalswamy et al., 2005), with SXR releases in the GOES 1–8 Å (2–10 keV) band peaking at 2×10^{31} erg for the largest bursts. Observations using the SORCE instrument's Total Irradiance Monitor yielded a total flare energy at all wavelengths for the 28 October flare of 4.6×10^{32} erg (Woods et al.,

2004). Radiation and charged particles from these flares compressed the Earth's Van Allen belt to within 20,000 km of the surface (Baker et al., 2004), damaged the orbiting Mars Odyssey communication instruments, and reduced polar ozone levels significantly (Randall et al., 2005).

Although most of our calculations are for a 10^{31}-erg flare, it seems likely that much more energetic flares than considered here have occurred. Such flares have been serendipitously discovered in other solar-like stars with otherwise normal characteristics (Schaefer et al., 2000). Upper limits on proton fluences inferred from cosmogenic isotopes in lunar samples (Reedy et al., 1983; Reedy, 1996), tree-ring records of ^{14}C (Lingenfelter and Hudson, 1980), and the statistics of impulsive nitrate events (McCracken et al., 2001) suggest that the frequency-fluence relation steepens for high-energy particle fluences above about 10^{10} cm^{-2}, probably due to streaming-limited fluxes associated with self-confinement by ion-wave interactions (Reames, 1999). In contrast, no such limit, empirical or theoretical, has been established for photon flares, other than an upper limit to avoid divergence of total energy (Hudson, 1991; Aschwanden, 1999).

We adopt a mean recurrence time for 10^{32}-erg flares of 10 yr, agreeing with the estimate of (Hudson, 1991) and broadly consistent with the dozen or so 10^{31}–10^{32} erg events that have been observed since GOES soft X-ray monitoring began in 1976. The average HXR frequency-energy release statistic dN/dW is taken as a power law in W, with log-log slope 1.7. Thus, we take the mean time between events of energy release W_{31} (in units of 10^{31} erg) as

$$T(W) = 0.2\, W_{31}^{1.7} \text{ yr}. \tag{3.1}$$

3.3 Methods

For our calculations, solar flare photon number spectra are assumed to be distributed as power laws, E^p, with $2 < p < 6$ (see above). The flare spectrum is assumed to extend from 10 keV to 511 keV. The 10-keV lower limit is taken to simulate the HXR flares, which often begin to flatten to a thermal form around this energy, while the upper limit is set high enough that a negligible number of incident photons are at higher energies, even for

the shallowest spectra (lowest p). Henceforth, total energy release quantities refer only to the energy between 10 and 511 keV.

We transport the incident ionizing radiation using a single-scattering approximation. The primary interaction processes at X-ray energies are photoelectric absorption and Compton scattering. The photoabsorption opacity is much larger, so the radiative transfer can be computed by employing an effective opacity, in which both Compton scattering and photoabsorption are treated as absorption processes. By including the Compton cross section in the opacity, we in effect assume that the material is optically thin to Compton scattering, such that at most a photon will scatter no more than once before exiting. Errors incurred by this approximation are negligible, as we have verified using Monte Carlo simulations (Smith et al., 2004b). The Compton-scattering coefficient was computed exactly using the Klein-Nishina formula, while the photoabsorption cross section was approximated using the emprical form of (Setlow and Pollard, 1962):

$$\sigma_p(E) = 2.4 \times 10^{-30}(1 + 0.008Z)\left(\frac{Z}{E}\right)^3 \text{ cm}^2, \tag{3.2}$$

where Z is the atomic number of the target nucleus and E is the energy of the incident photon in units of 511 keV. We found this form to be an excellent fit to cross-section data for light elements and for energies higher than the K edge. The K edges of carbon and aluminum are at (respectively) 284 and 1560 eV (Henke et al., 1993) and are well below our spectral cutoff energy of 10 keV, so our calculation is in the energy regime that is consistent with the cross-section fit. The effective opacity of the material is then

$$\kappa(E) = \frac{\sigma_p(E) + Z\sigma_c(E)}{Am_H}, \tag{3.3}$$

where A is the mean atomic mass in amu of the target material, m_H is the mass of a hydrogen atom, Z is its atomic number, and σ_c is the Compton cross section. The single-scattering approximation results in exponential attenuation of the incident fluence. In terms of the effective opacity κ and the areal density Σ (g cm^{-2}) of the shielding material, the

attenuated energy fluence F is

$$F(E, \Sigma) = E \frac{dN}{dE} \exp[-\kappa(E)\Sigma]. \tag{3.4}$$

After transport through the shielding material, the photon fluence is converted to a biological dose by assuming that the remaining radiation is absorbed by pure water. Much of the damage by ionizing radiation is thought to be "indirect," involving chemical reactions initiated by energy deposited in the bulk cell water or first hydration layer, rather than "direct" ionization of DNA (von Sonntag, 1987; Ward, 1999), although this terminology is now recognized as an oversimplification (Fielden and O'Neill, 1991). We then estimate the dose as a function of areal density by integrating the attenuated incident photon energy spectrum over the effective opacity of water $\kappa_w(E)$ (calculated using the single-scattering method above):

$$D(\Sigma) = \int_{10}^{511} \kappa_w(E)\ F(E, \Sigma)\ dE, \tag{3.5}$$

where the attenuated fluence F is given above, and the limits of integration are in keV.

3.4 Minimum Hazardous Dose

To estimate risks to humans exposed to solar-flare X-rays, critical levels of acute radiation exposure for various types of health outcomes (e.g. hematologic damage, organ failure, cancer, and lethality) are needed. Particularly useful is the minimum dose at which a given enhancement in occurrence of a disease relative to the average population occurs. We use dosimetry units for which 1 Gray = 100 rad = 10^4 erg g^{-1} absorbed. Since X-ray and higher-energy photons have small linear-energy transfer, dE/dx, their "quality factor" or "biological effectiveness" is very close to unity, independent of energy, so dose in Gy is approximately the dose in Sievert. The duration of exposures to flare X-rays of large fluence will be relatively short (10–60 minutes in most cases), so we restrict the discussion to evidence concerning acute human radiation-syndrome data.

At doses above about 0.5 Gy, summaries of a number of sources of data relevant

to acute radiation syndrome in humans are available (Alpen, 1998; Turner, 1995), as well as detailed specialized studies (Dickinson and Parker, 2002; Satoh et al., 1996; Dubrova et al., 1997; Dubrova, 2003). There is general agreement that severe damage, primarily hematologic and without assured recovery, occurs around 1 Gy. Estimates of the whole-body acute lethal dose vary from 2 to 5 Gy (UNSCEAR, 2001; Alpen, 1998; Turner, 1995). An upper limit to the radiation risk dose in an exposed individual is the ratio of the induced rate of mutations for low LET irradiation to the average spontaneous mutation rate per Gy over a large number of genes, recognizing that the mutation rate is highly variable among loci; this ratio is the mutation doubling dose. An estimate using 135 human genes for spontaneous rates and 35 mouse genes for induced rates (Sankaranarayanan and Chakraborty, 2000) gives a doubling dose of 0.8 Gy. This dose is for chronic irradiation, and a dose-rate reduction of a factor of three is usually assumed for acute doses, suggesting a doubling dose of 0.3 Gy for acute irradiation. However this estimate remains uncertain and subject to various definitions (Sankaranarayanan and Chakraborty, 2000; UNSCEAR, 2001).

Most work on X-ray and gamma-ray radiation risk to exposed individuals (not genetic disease endpoints) comes from studies of carcinogenesis. There is little doubt that the incidence of cancer due to radiation-induced genomic instability rises with acute dose above 0.2–0.3 Gy. Below this dose there is continued debate whether there is a "linear-no-threshold" relation between risk and ionizing-radiation dose, or whether doses below about 0.1 Gy result in "adaptive response" causing endogenous DNA damage prevention and immune simulation (Feinendegen, 2005). Alternatively, it is also likely that risk at low doses is larger than the linear-no-threshold extrapolation, even increasing with decreasing dose, because of bystander effects, as reviewed in (Hall, 2004). It is certain that mutations, often at significant loci (Sparrow et al., 1972; Sankaranarayanan, 1982; Forster et al., 2002), chromosomal abnormalities in blood lymphocytes (Violet et al., 2005), and clustered DNA damage (Sutherland et al., 2000) occur at much smaller doses in the range 0.01 to 0.1 Gy, but their impact on health risk has been difficult to assess because of the evidence for adaptive response at low doses. A compelling discussion by Brenner et al. (2003) argues that

there is good human-epidemiological evidence for increased cancer risk at an acute X-ray or gamma-ray dose of 0.05 Gy, and reasonable evidence for enhanced risk above 0.01 Gy, although the risk enhancement is in the 1–10% range.

Acute critical doses for significantly increased risk for other disease endpoints may also be of order 0.1 Gy or less, especially for hematological diseases. For example, the summary of delayed somatic effects due to acute doses by (Hanslmeier, 2002) indicates that gastrointestinal tract syndrome (leading to loss of digestion ability, bleeding ulcers, and diarrhea) sets in at 0.1 Gy for X-rays.

The risk of a particular genetic-disease endpoint per Gy of irradiation is more difficult to estimate, since the disease-specific induced mutation rate varies greatly and most models assume mutation-selection equilibrium. Inspection of risk estimates in humans and animal models for a number of genetic-disease classes that include 26 human disorders encompassing 135 genes (Sankaranarayanan and Chakraborty, 2000) indicates that risks for genetic-disease endpoints at 0.1 Gy due to acute X-ray doses are probably much smaller than the risks for somatic disease in an exposed individual discussed earlier.

Given that the linear increase of cancer risk with dose for acute doses above 0.1 Gy seems unequivocal, and that the threshold for delayed somatic-disease endpoints appears to also be about 0.1 Gy, we adopt this biological dose as an upper limit for significant risk increase due to X-rays, with the understanding that enhanced risk for several disease endpoints, but especially cancer (Brenner et al., 2003), may still be significant at lower doses. An important unresolved point is that adoption of a critical dose depends on the risk enhancement that one is willing to accept; our reading of the literature suggests a 10% enhancement in potentially fatal disease endpoints at 0.1 Gy, and less than 1% enhancement for genetic disease endpoints at this dose.

3.5 Results

We can now compare our adopted upper dose limit, 0.1 Gy, with that received behind polymer shielding, which is representative of current spacesuit design. We use pure carbon as a proxy for the mostly polymer construction of spacesuits because only the carbon atoms

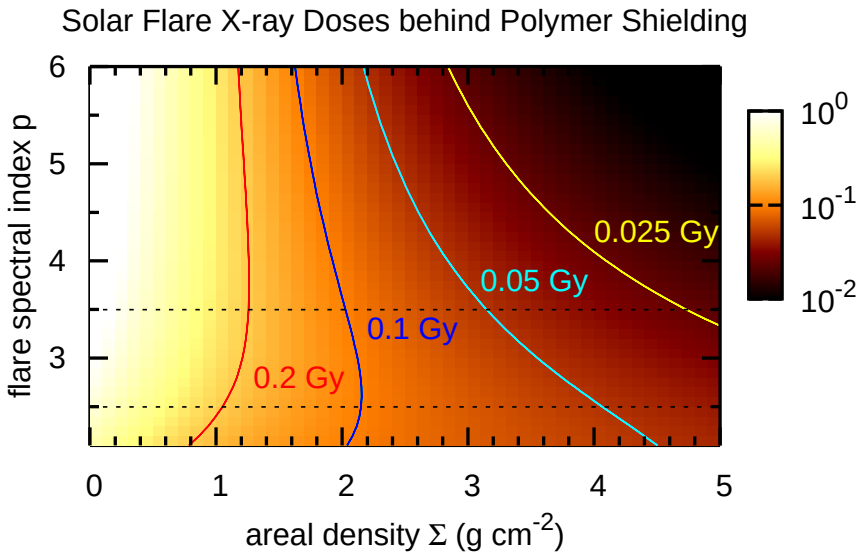

Figure 3.1: Acute biological doses behind polymer shielding (representative of current spacesuits) due to a 10^{31}-erg X-ray flare as a function of flare spectral index, p, and areal density, Σ. The dose is roughly independent of p for shields with areal densities smaller than about 2 g cm^{-2}. For larger shielding columns, the dose becomes sensitive to the spectral shape because more of the incident spectrum is attenuated, and hence reshaped, before being absorbed by the model water column. Areal densities of polymer in excess of 2 g cm^{-2} are needed to reduce the X-ray dose to below our adopted maximum acceptable acute dose of 0.1 Gy.

in polymers significantly absorb X-rays. The results, assuming a 10^{31}-erg solar flare, are shown in Fig. 3.1.

The typical areal densities of spacesuit components ($\sim$ 0.5–1.5 g cm^{-2}) provide little protection during a large solar flare. A relatively common, 10^{31}-erg flare would deliver over 0.2 Gy behind the current spacesuit—twice our adopted upper limit. A thicker spacesuit could reduce this dose to 1 Gy, but larger flares do occur, albeit less often. Bolstering spacesuits simply decreases the frequency of dangerous doses and does not eliminate the threat.

What is the likelihood of being exposed to doses above 0.1 Gy? If we use for simplicity a typical flare spectral index of 3.5, we find that the approximate dose behind polymer

shielding of areal density $\Sigma \gtrsim 0.3$ g cm^{-2} is

$$D(\Sigma, W) = 0.21\, W_{31} \Sigma^{-1.4} \text{ Gy}, \tag{3.6}$$

where W_{31} is the flare energy release in units of 10^{31} erg, and Σ is the areal density of the shielding material in g cm^{-2}. Using the flare energy-recurrence frequency relation given in the discussion of flare properties to eliminate W_{31}, the mean time between flares delivering *at least* a given dose $D_{0.1}$ behind a polymer shield of areal density Σ is

$$\tau(\geq D) = 0.08\, D_{0.1}^{0.7}\, \Sigma \text{ yr}. \tag{3.7}$$

If we then assume that time between flare events is typically much larger than the duration of exposure, and that flares occur at random, the probability of exposure to a dose of at least the critical dose is

$$P(D, \Sigma) = 1 \times 10^{-3} D_{0.1}^{-0.7} \Sigma^{-1} \tag{3.8}$$

per hour of EVA.

So in just 100 hours of EVA in the current spacesuit, an astronaut would accumulate a 10% risk of a dangerous exposure to solar flare X-rays.

3.6 X-rays Compared to Solar Energetic Particles

The present paper discusses only photons from flares, but the risk due to solar energetic-particle events (SEPs) is certainly not negligible, although we argue that the risk for EVAs is significantly smaller than estimated here for flares. The largest SEPs, such as the 14 July 2000, Feb 1956, and Aug 1972 events, had 1 AU fluences in the range 10^{10}–10^{11} cm^{-2} (Miroshnichenko, 2003), although per-particle energies were 100 times smaller than for Galactic cosmic rays. Silberberg and Tsao (1979) estimated the incidence of flares that produce SEPs with 1-AU doses greater than 1 Gy as about one per decade, similar to what we estimate for 10^{32}-erg photon flares that produce 2-Gy doses, as shown in the Fig. 1. A similar frequency for SPEs with fluences above 10^{10} cm^{-2} can be derived from the recorded

number of large events (Reedy, 1996; Shea and Smart, 1990; Miroshnichenko, 2003), nitrate ice core reconstruction covering several centuries (McCracken et al., 2001), and probability models (Feynman et al., 1993, 2002). In contrast, 10^{31}-erg X-ray flares that also require substantial shielding are about 50 times more frequent.

Spacesuits are the last line of defense until shelter is reached, so exposures during a flare will depend on the ratio of the time to reach shelter to the time to deliver the total fluence. Figure 3.2 shows that the doses behind aluminum shielding are significantly smaller than that received inside spacesuits, for the same areal density, because of the strong dependence of the photoabsorption cross section on atomic number of the target material. But X-ray flares leave only 10–30 min to reach shelter before the total fluence is delivered.

Hard X-ray flares are impulsive, with rise times of minutes or less. The time to withdraw to adequately shielded shelter is very small. A reliable energetic hard X-ray flare precursor signature occurring more than an hour before the flare maximum would be needed for this purpose. There are many signatures that have been proposed as flare precursors (Martin, 1980; Simnett, 1993, 1999), such as UV brightening, soft X-ray enhancements, microwave radio signatures, H-alpha filament disturbances, strong magnetic shear, sunspot motions, and the beginnings of chromospheric mass ejections (CMEs), whose onset is now known to slightly precede an associated flare on average. Most of these precursors are only observable for less than a few minutes before the onset of the flare, so do not give sufficient warning and would require elaborate monitoring systems. Some radio precursors, such as polarization signatures, are observed up to tens of minutes before a flare, but are not observed in the majority of flares. Similarly, for all precursor signatures there are flares seen without the precursor and observations of "precursors" that are not followed by a flare; no precursors are necessary and sufficient (Golub and Pasachoff, 1997). Even more seriously, none of these precursors are predictors of the energy release of the flare itself, so given the large frequency of flares that pose no biological hazard, use of these precursors would likely result in a large false-alarm rate.

Most probabilistic approaches for flare prediction are based on a combination of historical rate of flaring for a given sunspot classification group and additional information

such as shear, magnetic topology, and previous large-flare activity (Gallagher et al., 2002). A more recent Bayesian method relies only on flare-event statistics (Wheatland, 2005). These methods are most suited for probabilistic prediction of quantities like the number of flares of a certain class in a given year, but not for EVA hazard warnings. An example is that the Bayesian method would have predicted a 20% probability for an X-class flare on 4 Nov 2003, using data up to one day before, including a highly clustered series of strong and weak flares in the weak before, yet actually the most energetic flare in several decades was about to occur (Wheatland, 2005), a flare almost an order of magnitude more energetic than the model flare used in the calculations reported here. Such prediction algorithms might be useful for policies requiring no EVAs in windows of a week or so, when the probability of a large flare can be somewhat more accurately estimated, but this would greatly curtail manned exploration, depending on where the threshold for significance is placed and confidence in the prediction itself.

Because of diffusive propagation through the heliosphere, the first particles from SPEs arrive at 1 AU more than an hour after the initiating event (when one is observed) and take hours to reach hazardous fluences (Miroshnichenko, 2003, Fig. 2.7, 12.9) (Reames et al., 1997). This allows a simple and effective retreat strategy based on flare, CME, or even sunspot precursors (although not all energetic SPEs are associated with flares; (Reames, 1999)). Consequently, X-ray flares are more dangerous during EVAs.

3.7 Emergency Shielding

One simple protection solution would be to include a small (2–3 m^2) shield of high-Z material, such as aluminum, in EVA rover designs. Using the results in Fig. 3.2, an aluminum shield thick enough to protect against a 10^{31}-erg flare would have an areal density of at least 7 kg per square meter of shielding; for a 10^{32}-erg flare the mass requirement would be 70 kg m^{-2}. Additionally the shield would have to be articulated or detachable, in order to provide protection regardless of the sun's position in the sky.

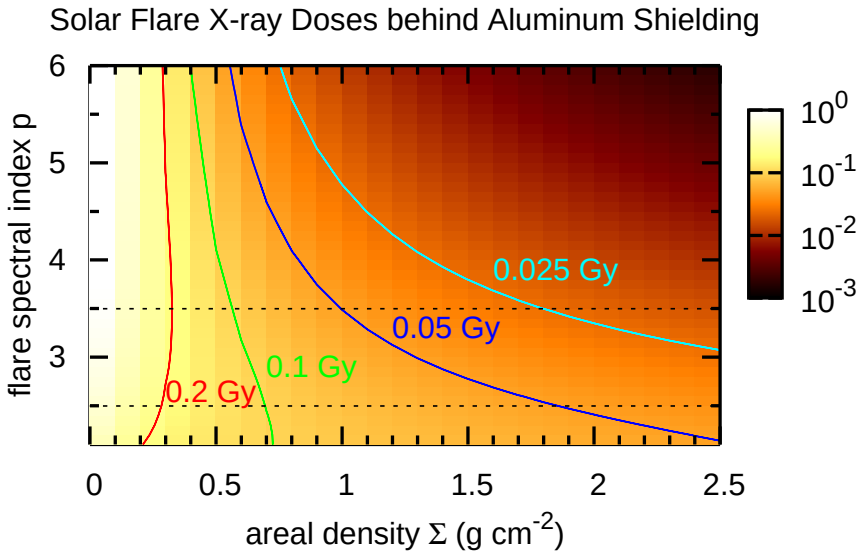

Figure 3.2: Acute biological doses behind aluminum shielding (representative of current possible radiation shelters) due to a 10^{31}-erg X-ray flare as a function of flare spectral index, p, and areal density, Σ. Aluminum has a higher atomic number than carbon (13 vs. 6) and absorbs X-rays much more efficiently. Only 2 g cm^{-2} of aluminum shielding would be required to reduce the dose to below 0.05 Gy for a 10^{31}-erg flare.

Chapter 4

Astrospheres, the Interstellar Environment, and Habitable Planets

Chapter synopsis: Only average ISM densities are required to elevate the Galactic cosmic-ray flux at the habitable zone to interstellar levels. The inclusion of gravitational effects on particle trajectories ("focussing") significantly enhances the ISM accretion flow and reduces astrosphere sizes. Charge exchange between stellar-wind ions and interstellar neutrals also has a measurable, albeit smaller, effect on the astrosphere size. Habitable zones around younger stars and lessr-massive stars are less often exposed to the raw ISM, a situation we call "descreening." Finally, the frequency of encounters with regions of the ISM dense enough to cause descreening is estimated.

4.1 Introduction

Planetary systems orbiting the Galaxy must pass through an ambient interstellar medium (ISM) containing irregular density and velocity structure on scales from 0.1 pc to 1000 pc, with densities spanning many orders of magnitude. That the interstellar medium (ISM) might influence the Earth's climate is an old idea, dating back to at least Shapley (1921)

and Hoyle and Lyttleton (1939), but the exact nature and magnitude of the effect is still not well known.

The sun is currently moving at 26 km s^{-1} (Witte, 2004) through the Local Interstellar Cloud, a 0.2-cm^{-3} cloudlet (Redfield and Linsky, 2000) within the Local Bubble, a very hot region of below-average density likely evacuated by the passing Scorpius-Centaurus OB cluster in the last 12 Myr (Maíz-Apellániz, 2001). In this environment, the solar wind meets the ISM flow at $\sim$ 100 AU from the sun (Stone et al., 2005), creating the cocoon-like heliosphere that presents a barrier to cosmic rays, gas, and dust originating in the ISM (Zank, 1999). In a few Myr, the sun will emerge from the Local Interstellar Cloud and the low-density Local Bubble environment and once again encounter a denser, more average, ISM. At that time the heliosphere will shrink, and fluxes of cosmic rays, neutral hydrogen, and dust will rise throughout the solar system.

Passage through a denser region of the ISM is accepted to cause increased fluxes of Galactic and anomalous cosmic rays, neutral hydrogen, and dust into the inner solar system (see, e.g., Zank and Frisch, 1999; Florinksi et al., 2003a; Pavlov et al., 2005a,b). Scherer et al. (2002) and Frisch (2006) review in detail the effects of enhanced cosmic-ray, hydrogen, and dust densities in the solar system. Even variations in the solar wind within a solar cycle cause a measurable change in background cosmic-ray flux (Smith et al., 2003) due to the varying modulation of Galactic cosmic rays.

Lunar soil samples show possible evidence of a such a past encounter with a dense region (Wimmer-Schweingruber and Boschler, 2000, 2001). Early calculations (Begelman and Rees, 1976; Talbot and Newman, 1977) of the frequency of encounters with denser regions of the ISM were extremely uncertain due to observational selection effects, and lack of knowledge about the three-dimensional structure of the ISM makes refining these early estimates difficult. An early rough estimate (Talbot and Newman, 1977) predicted at least one encounter with a cloud of density of at least 100 cm^{-3} per 30 Myr. Also, a random line of sight intersects either a cool, neutral-hydrogen cloud or a denser, molecular-cloud complex every $\sim$ 200 pc, so the solar system will encounter one of these regions every 20 Myr on average. Passage through a typical cloud of, say, 10 pc in diameter should take

about 1 Myr. Even denser regions would have larger effect but are rarer.

A summary of the most astrobiologically important implications follows:

1. Cosmic rays are one of the primary sources of ionization in the lower atmosphere (Usoskin et al., 2004), thus providing nucleation sites for cloud droplet formation and affecting the fraction of the Earth covered by clouds (e.g. Svensmark and Friis-Christensen 1997; Svensmark 2000; Marsh and Svensmark 2003; Christl et al. 2004; and see Carslaw et al. 2002 for a review), but this is a controversial point (Laut, 2003; Marsden and Lingenfelter, 2003; Pallé et al., 2004; Rahmstorf et al., 2004). If enhanced cosmic rays do cause increased, low-altitude, cloud cover, then passage through dense, interstellar regions is supposed to cool the Earth through the negative radiative forcing (Hartmann, 1993). Some have even attributed ice ages to such cosmic-ray enhancements (e.g. McCrea, 1975; Kirkby et al., 2004).

2. Even at their current low flux levels (due to the size of the current heliosphere), Galactic cosmic rays make a significant contribution to the surficial terrestrial ionizing radiation biological dose rate (25% excluding radon, UNSCEAR 2000; Turner 1995). One can easily demonstrate that ionizing radiation[1] can be an important mutational source compared to endogenous or "spontaneous" mutations due to copy errors or to exogenous non-radiative oxidative damage by noting that the phenotypic-mutation frequencies increase near locations of enhanced ionizing-radiation flux (e.g. Hiroshima, reactor leakage sites; see Straume et al. 2003).

3. Hydrogen and dust accretion can drive atmospheric chemistry in the upper atmosphere that catalyzes ozone destruction (McKay and Thomas, 1978; Lu and Sanche, 2001; Pavlov et al., 2005a). The resulting ozone loss may produce only a mild cooling and noctilucent clouds (McKay, 1985), or it may trigger ice ages and mass extinctions (McKay and Thomas, 1978; Yabushita and Allen, 1989; Yeghikyan and Fahr, 2004b; Pavlov et al., 2005b).

4. Accretion of additional gas and dust by the parent star could result in prolonged, enhanced, UV luminosity as the material transforms its kinetic energy into heat (Talbot and

[1]Photons and particles with energies above $\sim$ 10 eV.

Newman, 1977), perturbing Earth's atmospheric chemistry and increasing surficial mutation rates.

5. The proximity to the concentrated mass of a dense, interstellar cloud could perturb the Oort cloud and send a flurry of comets into the inner solar system (Hut and Tremaine, 1985), having unknown but potentially disastrous effects on Earth.

Understanding the nature of the ISM-Earth connection requires knowing how often we encounter clouds of a given density and how long traversing clouds typically takes. The most detailed calculation of the frequency of passage of planetary systems through clouds of various densities (Talbot and Newman, 1977) concentrated almost entirely on hydrogen accretion into the inner solar system and the sun, and did not study cosmic-ray flux changes, climatological changes, or the timing of the events. No further quantitative statistical work has been done in the intervening 25 years, even though there is little doubt that the ISM-heliosphere interaction could have profound climatic effects (e.g. Zank and Frisch, 1999). Other main-sequence stars most likely have "astrospheres" (see, e.g. Wood et al., 2002); if so, all planetary systems in the Galaxy will be subject to these effects.

We intend to show that encountering very dense, molecular clouds is not necessary for receiving close to the full interstellar Galactic cosmic-ray flux. The exponential nature of cosmic-ray modulation in the diffusion limit means that *the largest Galactic cosmic-ray flux variations occur when the heliosphere size is large and the local ISM density is small.* Note that we are referring only to the Galactic cosmic-ray flux; accretion of hydrogen and dust can continue to rise as the heliosphere shrinks, since the injection rate of that material into the solar system will scale with the local ISM density.

4.2 Cosmic-ray Transport Model: Convection-Diffusion

The standard kinetic equation for heliospheric cosmic-ray transport (Parker, 1965, Eq. 4) is

$$\frac{\partial F}{\partial t} + \underbrace{v_i \frac{\partial F}{\partial x_i}}_{\text{advection}} = -\underbrace{u_i \frac{\partial F}{\partial x_i}}_{\text{drift}} + \underbrace{\frac{\partial}{\partial x_i}\left(\kappa_{ij}\frac{\partial F}{\partial x_j}\right)}_{\text{spatial diffusion}} + \underbrace{\frac{1}{3}\frac{\partial v_i}{\partial x_i}\frac{\partial F}{\partial \ln p}}_{\text{adiabatic changes}} + \underbrace{Q(x_i,p,t)}_{\text{sources/sinks}}, \tag{4.1}$$

where $F = F(x_i, p, t)$ is the cosmic-ray distribution function. Here, v_i is the stellar wind velocity; u_i represents global, field-averaged drifts, such as gradient and curvature drift due to the averaged interplanetary magnetic field; κ_{ij} is the diffusion tensor, stemming from random particle drifts; and Q is a generic source and sink term for effects such as spallation or charge exchange. Writing F as a function of only the scalar momentum p is sometimes called the "quasi-isotropic" distribution function and is a good approximation when pitch-angle scattering is efficient (Gombosi, 1998; Jokipii, 1999). Furthermore, this simplification allows us to write the equations henceforth as a function of kinetic energy K without loss of generality.

We assume steady state and spherical symmetry, dropping $\partial F/\partial t$ and keeping only an r dependence. Following Cravens (1997) and Gombosi (1998, Eq. 13.1), we also neglect drift and sources and sinks, so that the equation reduces to

$$r^2 v \frac{\partial F}{\partial r} + \frac{\partial (r^2 v)}{\partial r} C F = \frac{\partial}{\partial r}\left(r^2 \kappa \frac{\partial F}{\partial r} \right), \tag{4.2}$$

where

$$C \equiv -\frac{1}{3} \frac{\partial \ln F}{\partial \ln p} \tag{4.3}$$

is the Compton-Getting coefficient and usually ranges between 0 and 1.5, depending on p (Gombosi, 1998); we will take $C = 1$ here for simplicity. The resulting equation is the well-known convection-diffusion solution of Parker (1963):

$$\frac{1}{r^2} \frac{\partial}{\partial r}(r^2 v F) = \frac{1}{r^2} \frac{\partial}{\partial r}\left(r^2 \kappa \frac{\partial F}{\partial r} \right), \tag{4.4}$$

where r is the distance from the star and κ is the isotropic radial-diffusion coefficient. The convection-diffusion solution represents a balance between the outward advection of the cosmic-ray guiding centers by the solar wind and the inward random motions due to pitch-angle scattering in the irregular interplanetary magnetic field. This can be integrated twice

for a given energy K to yield

$$F(r,K) = F(D,K)\ \exp\left[-\int_r^D \frac{v}{\kappa(K)}\,dr'\right], \tag{4.5}$$

where $F(D,K)$ is the interstellar cosmic-ray density and D is the "modulation distance"—a distance larger than r at which F is equal to the interstellar value. The exponential term is usually called the "modulation parameter."

In terms of the field-oriented diffusion coefficients, the radial coefficient κ is

$$\kappa = \kappa_\parallel \cos^2\psi + \kappa_\perp \sin^2\psi, \tag{4.6}$$

with ψ the angle between the radial direction and the average interplanetary magnetic field direction, and $\kappa_\parallel$ and $\kappa_\perp$ are the diffusion coefficients parallel and perpendicular to the local, mean magnetic field, respectively. Since ψ approaches 90° for $r \gtrsim 10$AU, the typical assumption is that $\kappa \sim \kappa_\perp$ in the outer heliosphere (but see Parhi et al., 2003). We assume for simplicity that central stars in other habitable planetary systems have winds and interplanetary magnetic fields wound in spirals that are named after Parker's alien counterpart, in which case the same approximation holds. The reverse situation occurs in the inner heliosphere where the field is more radial. For example, Giacalone and Jokipii (1999) estimate $\kappa_\perp/\kappa_\parallel \sim 0.02$–$0.04$ at 1 AU, and Parhi et al. (2003) suggest the ratio is smaller.

In the quasi-linear theory of MHD wave-particle interactions, pitch-angle scattering is most efficient when the waves and particles are in resonance, such that the particle gyroradius is equal to the wavelength of the perturbed waveform (Berezinskii et al., 1990). The pitch-angle scattering coefficient in this case is roughly (Cravens, 1997; Kulsrud and Pearce, 1969)

$$D_{\mu\mu} \sim \Omega \frac{\langle \delta B^2 \rangle}{B^2}, \tag{4.7}$$

where Ω is the gyrofrequency and $\langle \delta B^2 \rangle$ is the mean-square field fluctuation (proportional to the power spectrum). Averaging $D_{\mu\mu}$ over pitch angle produces an approximate perpen-

dicular diffusion coefficient:

$$\kappa_\perp \simeq \frac{1}{2} r_g^2 \langle D_{\mu\mu} \rangle, \tag{4.8}$$

where r_g is the gyroradius (see Cravens, 1997; Kulsrud and Pearce, 1969, for details). This is a standard estimate for resonant-gyrofrequency cosmic-ray scattering (e.g. Cesarsky, 1980). Cravens (1997) estimates for the solar system

$$\kappa \sim \kappa_\perp \sim 10^{21} \beta(K) \text{ cm}^2\text{s}^{-1} \tag{4.9}$$

at 1 AU, where $\beta \equiv v/c$, and c is the speed of light, or in terms of kinetic energy

$$\beta(K) = \frac{(K^2/m^2 + 2K/m)^{1/2}}{1 + K/m}, \tag{4.10}$$

and m is the rest mass energy of the cosmic-ray particle (typically 938 MeV). For example, a 10-MeV proton has a β equal to 0.145, while a 1-GeV proton has a β of 0.875.

The cosmic-ray perpendicular diffusive skin depth $\lambda_\perp$ can be defined as $\lambda_\perp \equiv 3\kappa_\perp/\beta c$. For extremely relativistic cosmic-rays, $\beta \simeq 1$, and using a solar wind speed v equal to 400 km s^{-1} and Eq. 4.9, the skin depth is

$$\lambda_\perp \sim 6 \text{ AU}. \tag{4.11}$$

The modulation formula for cosmic rays in the solar system is then

$$F(r, K) = F(D, K) \exp\left[-\frac{D - r}{\lambda_\perp \beta(K)}\right]. \tag{4.12}$$

Thus the spatial scale of modulation in the solar system for the highest-energy cosmic-rays is about 6 AU, with lower-energy particles having smaller skin depths due to the β dependence. Surprisingly, and perhaps somewhat coincidentally, this is not too different from the results of much more sophisticated models (e.g. Parhi et al., 2003), though it captures none of the radial dependence of κ in those models. For our purposes, however, we simply want an estimate of the integrated cosmic-ray flux in a planetary system, so this

approximation is adequate and amenable to simulations of passages through the general ISM in which the cosmic-ray flux must be solved for millions of time steps. A detailed transport model would be prohibitive for such a study.

The appropriate choice of the effective modulation distance D is very uncertain, and so henceforth we take $D = r_a$, where r_a is the size of the astrosphere. We take the interstellar cosmic-ray spectrum $F(D, K)$ from Eq. 3 of Mori (1997), which is a fit to a compilation of recent estimates. Mori gives the Galactic cosmic-ray flux F in units of cm^{-2} s^{-1} as

$$F(D,K) = 4\pi \begin{cases} 1.67 p^{-2.7} \left[1 + \left(\frac{2.5 \text{ GeV c}^{-1}}{p}\right)^2\right]^{-1/2} & : \quad E \leq 100 \text{ GeV} \\ 6.65 \times 10^{-6} \left(\frac{E}{100 \text{ GeV}}\right)^{-2.75} & : \quad E > 100 \text{ GeV} \end{cases}, \tag{4.13}$$

where $p = (K^2 + 2Km)^{1/2}$ and $E = K + m$.

In order to fit measured modulated cosmic-ray spectra (e.g. Ip and Axford, 1985; Webber, 1998; Parhi et al., 2003) more closely, we use a larger radial diffusion coefficient than Cravens (1997) derived and add an additional energy dependence:

$$\kappa(K, \lambda) = 5 \times 10^{23} \, \lambda_\perp \, \beta(K) \, (1 + K/3.3 \text{ GeV}) \text{ cm}^2 \text{ s}^{-1}, \tag{4.14}$$

where $\lambda_\perp$ is the skin depth of the cosmic rays in AU and is typically between 0.05 and 0.2 AU (Parhi et al., 2003). The impact of varying λ is discussed in §4.4.1.

The fraction of the total cosmic-ray flux reaching a given radius from a star can be computed by integrating the modulated flux and dividing by the integrated interstellar flux:

$$f_{\text{CR}}(r) = \frac{\int_0^\infty F(r, K) \, dK}{\int_0^\infty F(D, K) \, dK}. \tag{4.15}$$

We then use a Simpson's rule numerical integrator to calculate the integrated cosmic-ray flux from this formula.

4.3 Astrosphere Models and Methods

4.3.1 Ram-pressure Balance Model

Probably the simplest model for a stellar wind-ISM interaction is that of the collision of two supersonic fluids with a negligibly thin, subsonic boundary layer in between. Parker (1963) showed that the location of the termination shock of the solar wind given by the shock-jump conditions was roughly where the ram pressure of the outflowing solar wind balanced the pressure of the counterstreaming ISM:

$$\left(\frac{r_s}{r_0}\right)^2 = \frac{\rho_0 v_0^2}{P_{\rm ISM}} g(\gamma), \tag{4.16}$$

where r_s is the shock distance, r_0 is a reference distance, ρ_0 is the solar-wind density at r_0, v_0 is the solar-wind velocity at r_0, $P_{\rm ISM}$ is the pressure of the ISM (including ram, thermal, and magnetic pressures),

$$g(\gamma) = \frac{2}{\gamma+1}\left[\frac{(\gamma+1)^2}{4\gamma}\right]^{\gamma/(\gamma-1)}, \tag{4.17}$$

and γ is the adiabatic index of the stellar wind (see Lee, 1997, Eq. 24). For a fully ionized gas, $\gamma = 5/3$, and $g = 0.88$. We will adopt this value of g in the pressure-balance expressions below.

When the ISM is streaming supersonically and superalfvenically past the stellar system, its ram pressure dominates $P_{\rm ISM}$, such that $P_{\rm ISM} \simeq \rho_{\rm ISM} V^2$, where $\rho_{\rm ISM}$ is the total ISM density and V is the relative velocity between the star and the ISM. Taking the size of the astrosphere r_a to be the distance from the sun to the termination shock,

$$\frac{r_a}{r_0} \simeq \left(g\frac{n_0}{N}\right)^{1/2} \frac{v_0}{V}, \tag{4.18}$$

where n and N will henceforth refer to the number density of the solar wind and ISM, respectively. Thermal pressure would be important (for the solar velocity with respect to the local standard of rest) for ISM densities below about 0.1 cm^{-3}, where temperatures

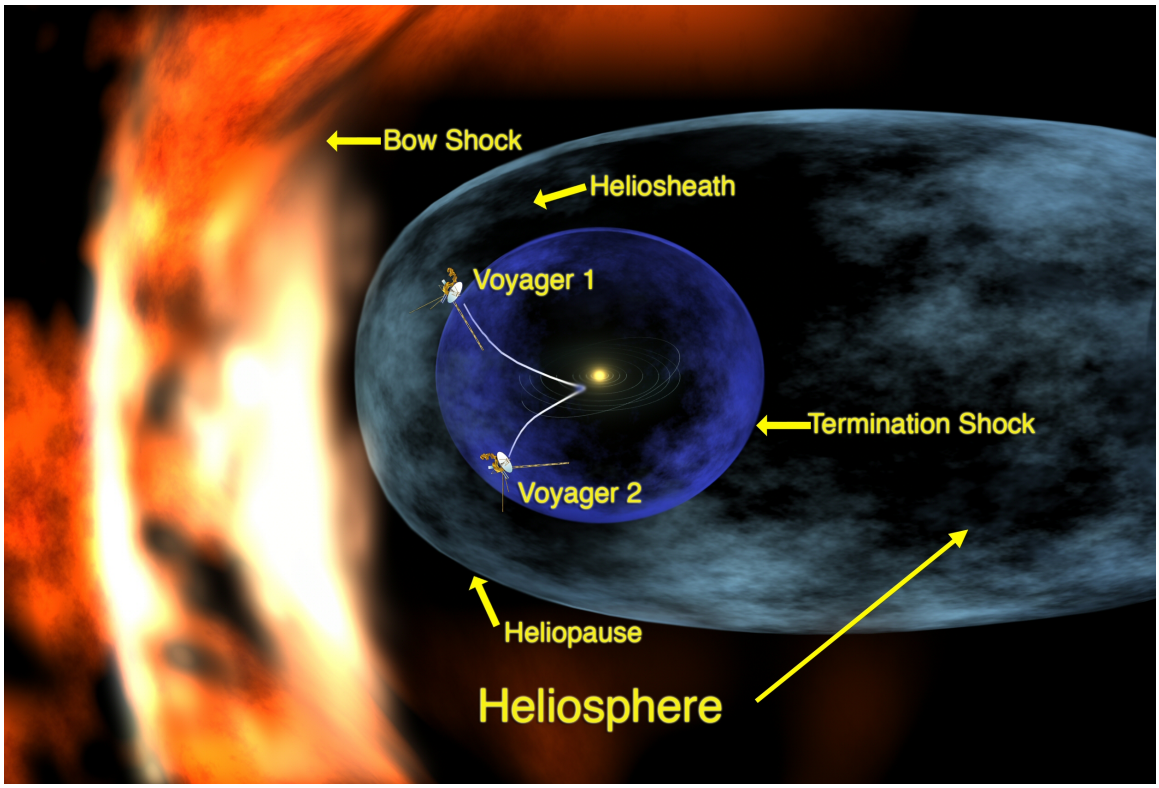

Figure 4.1: Cartoon of the heliosphere. The solar wind flows out from the sun, joins the ISM at the heliopause, and flows around the heliosphere out to into the tail. Since both fluids are moving supersonically, they each undergo a shock transition before meeting at the heliopause. Image source: NASA.

are high, but we are interested in the high densities where the shrunken astrosphere could lead to enhanced cosmic-ray and hydrogen fluxes to habitable planets, and these regions are typically cold compared to stellar velocities. For thermal pressure to compare to ram pressure, the following inequality must be satisfied:

$$T \gtrsim 3000 \left(\frac{V}{10 \text{ km s}^{-1}} \right)^2 \text{ K}, \tag{4.19}$$

where V is the star-ISM relative velocity. For the sun, $V = 26$ km s^{-1}, so we would need to enter a region with a temperature in excess of 20,000 K for the thermal pressure to compare to the ram pressure in determining the heliosphere size, and these regions usually have densities well below the regimes we are considering here.

Magnetic pressure is likely to be more important, although without a detailed MHD simulation of the entire ISM structure spanning orders of magnitude in scale, we can make only a rough estimate of the effect. Zeeman observations (Crutcher, 1999; Bourke et al., 2001) can be expressed in the form of an upper limit to a B-density relation:

$$B(N) = \begin{cases} 3 \ \mu\text{G} & : \quad N < 10 \text{ cm}^{-3} \\ 3 \ \left(\frac{N}{10 \text{ cm}^{-3}} \right)^{1/2} \ \mu\text{G} & : \quad N \geq 10 \text{ cm}^{-3} \end{cases} . \tag{4.20}$$

At densities below 10 cm^{-3} this simply gives a constant pressure $B^2/8\pi$ equal to 4×10^{-13} dyne cm^{-2}. Since the ram pressure is $2 \times 10^{-12} \ NV_{10}^2$ dyne cm^{-2}, the magnetic field isn't competitive with ram pressure until densities below 0.2 cm^{-3} (e.g. in the Local Interstellar Cloud; Florinski et al. 2004 have suggested that the magnetic field is anomalously large here). At higher densities, the square-root scaling gives a pressure that is proportional to the density, similar to the ram pressure. In this case the coefficient of the magnetic pressure acts to effectively increase the ISM-star velocity in the ram pressure, but the effect is small, even after multiplying by a small factor (Crutcher, 1999) to statistically account for the fact that only the line-of-sight component of B is detected by the Zeeman effect. This is because typical star-ISM velocities exceed the root-mean-square turbulent velocity in the ISM, which is in rough equipartition with the magnetic field. Given these considerations, we neglect the

magnetic field for simplicity, with the understanding that we somewhat overestimate the size of the heliosphere at low densities, and that in more realistic ISM models the magnetic field will undergo sizeable fluctuations, often uncorrelated with density, which will lead to episodes of magnetically controlled astrosphere sizes.

Using pressure balance to obtain the heliosphere size is a standard procedure (see Holzer, 1989) that agrees fairly well in the apex direction with more detailed models (e.g. Isenberg, 1986; Pauls et al., 1995; Fahr et al., 2000). This procedure may overestimate the astrosphere size relative to detailed multifluid or kinetic theory multidimensional models because of neglect of charge exchange of interstellar neutrals, which removes momentum from the solar wind (see Isenberg, 1986; Pauls et al., 1995; Zank and Frisch, 1999; Fahr et al., 2000; Wood et al., 2002; Florinski et al., 2004). We address the effects of charge exchange with another simple model in §4.3.2.

4.3.2 Charge-exchange Model

Introduction

When the local interstellar medium has a much larger density of neutral hydrogen than today, charge exchange can significantly modify the dynamics of the heliosphere-ISM interaction. To a good approximation, charge exchange simply swaps the identities of ions and neutrals. The process is sketched in Fig. 4.2, with the distance from the sun increasing rightward and time increasing downward. In the case of the heliosphere, a neutral hydrogen atom from the ISM flows inward with velocity equal to the sun-ISM relative velocity V toward an outwardly moving proton moving at the solar-wind speed v (the top step in the figure). Next, charge exchange swaps the charges of the proton and neutral but has no effect on the momenta (middle step). Finally, the inward moving ion feels Lorentz forces from the moving solar magnetic field and is accelerated up to the wind velocity (bottom step)

The net result is that an outflowing solar-wind proton becomes an outflowing neutral traveling at solar-wind velocity v, while an inflowing neutral becomes at outflowing proton also moving with the wind velocity. Since the original net momentum of the two particles

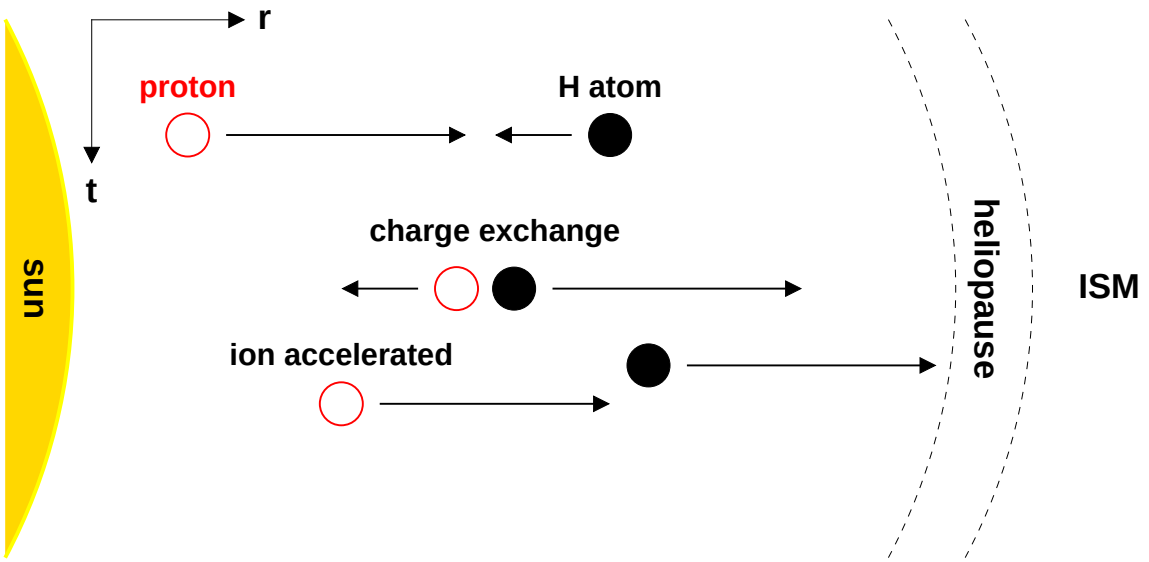

Figure 4.2: Cartoon of the charge exchange process. The outflowing solar proton and inflowing interstellar neutral essentially exchange identities, producing an inflowing ion and outflowing neutral. We assume here that the inwardly moving ion is immediately picked up by the solar wind, thus returning that ion to the outflow but removing momentum from the solar wind.

was roughly $m_p(v-V)$ and the final momentum is $2m_pv$, the rest of the solar wind must have given $m_p(v+V)$ in momentum to the two particles, where m_p is the mass of a proton. Since the original solar proton was (eventually) replaced by a proton with an identical velocity, we can say that the entire solar wind has lost $m_p(v+V)$ in momentum. To summarize, charge exchange has no effect on the local ion density, but does act to slow the wind velocity through momentum removal.

The charge-exchange cross section is (Fite 1965)

$$\sigma(v) = [2.1 \times 10^{-7} - 9.2 \times 10^{-9} \log \Delta v]^2 \text{ cm}^2, \tag{4.21}$$

where Δv is the relative velocity between the incident particles in cm s^{-1}. In this simple case, the flows start out highly supersonic, and, though we may suspect them to be ultimately slowed to subsonic speeds, we will for simplicity take both the solar protons and the interstellar hydrogen to be cold, with $T \sim 0$, so that thermal effects can be ignored in the basic equations. This is equivalent to assuming that the spread in velocities about the

bulk velocity is much smaller than the bulk velocity, so that to a good approximation each collision will occur with a relative velocity equal to the difference in bulk velocities of the solar wind and the ISM ($\Delta v = v + V$ in our notation).

The post-charge-exchange neutrals can be neglected with little loss of accuracy because the fast neutrals are moving at the same velocity as the solar wind and, in the limit of zero velocity dispersion, do not collide. The only particles with a relative velocity to the fast neutrals would be interstellar ions, which we will assume do not penetrate the heliosphere. Consequently, we expect the bulk flow of the ISM neutrals to be steady, but decrease in density as it penetrates into the heliosphere. Please note that this is the case simply because we are ignoring the fast, outwardly moving neutrals created through charge exchange that would normally serve to replenish interstellar neutrals, albeit at a different point in velocity space.

Representing the roughly spherical heliosphere embedded in a linear flow, our model consists of a spherically symmetric ion wind and a one-dimensional, linear neutral flow. For this model, the relevant continuity equations (CEs) are:

$$-\frac{d}{dr}(NV) = -nN\sigma(v+V), \tag{4.22}$$

$$\frac{1}{r^2}\frac{d}{dr}(r^2 nv) = 0, \tag{4.23}$$

where N is the interstellar (slow) neutral density and n is the total ion density. Additionally, we have a momentum equation (ME) for the ions only:

$$nv\frac{dv}{dr} = -nN\sigma(v+V)^2. \tag{4.24}$$

The charge-exchange sink term on the right-hand side of the neutral CE does not appear in the ion equation because of our assumption of immediate pick up of slow ions by the solar wind. This implies that no loss of ions occurs from the solar wind. Thus the only source of ions is photoionization.

Because of the weak interaction between the stellar-wind ions and the interstellar

neutrals, a kinetic-theory model would be more appropriate; but solving a kinetic model would involve knowing the particle distribution functions, which are uncertain for the sun and purely speculative for other stars. Additionally, we are interested in gross properties, such as the bulk velocity and density profile, that determine the astrosphere size. Thus, we approach the problem with phenomenological macroscopic equations. Solving multifluid equations like this is common among models of the heliosphere (see Zank, 1999), and they reproduce the macroscopic properties of the heliosphere quite well.

Limiting Cases

If we assume, for now, that $v \gg V$, then we can coax some analytic results from this model. In reality, v will not remain large compared to V as the wind slows, but the assumption would be satisfactory if the wind-deceleration rate is roughly constant for most of the distance across the heliosphere before spiking over a short distance near the heliopause, much like the energy-loss profile of a charged particle slowing through ionization losses (Longair, 1992). The solar wind has a very flat velocity profile out to the termination shock (Smith et al., 2003), but charge exchange plays only a minor role in the dynamics of the current heliosphere.

The ion CE in this limit yields

$$nv = \frac{n_0 v_0 r_0^2}{r^2}, \tag{4.25}$$

where n_0 and v_0 are the reference ion densities and velocities, respectively, taken at r_0. The neutral CE simplifies to

$$\frac{d \ln N}{dr} = nv \frac{\sigma}{V}(1+\epsilon), \tag{4.26}$$

where $\epsilon \equiv V/v$ and $\epsilon \ll 1$. Approximating ϵ and σ to be constant, N is

$$\begin{aligned} N(r) &= N_\infty \exp \int_r^\infty \frac{n_0 v_0 r_0^2 \sigma (1+\epsilon)}{V r'^2} dr' && (4.27) \\ &\simeq N_\infty \exp(-\lambda_{\mathrm{I}}/r), && (4.28) \end{aligned}$$

where $\lambda_{\rm I} \equiv n_0 \sigma r_0^2 (v_0/V + 1)$. For illustration, in the current heliosphere, $\lambda_{\rm I,\odot} = 4$ AU. Since the heliopause is over 100 AU away from the sun (Stone et al., 2005), this would imply that the current heliosphere filters interstellar neutrals very efficiently, and that large increases in the neutral flux reaching Earth might occur if the heliosphere were to shrink by even a small margin. If photoionization were included, this characteristic scale for neutrals should decrease, while the inclusion of the fast neutral atoms produced through charge exchange would tend to increase this number. This basic scale would be different for other stars only if the basic properties of the wind were different. For example, if the wind density at 1 AU were larger for that star than for the sun, then $\lambda_{\rm I}$ would be proportionately larger.

We can now solve for the ion velocity profile $v(r)$ by using the approximate $N(r)$ solution in a similarly approximated ion ME:

$$\frac{d \ln v}{dr} = -\sigma N(r) (1+\epsilon)^2, \tag{4.29}$$

where ϵ is defined as before. Integrating,

$$\begin{aligned} v(r) &= v_0 \exp \int_r^{r_0} \sigma N(r') (1+\epsilon)^2 dr' && (4.30) \\ &\simeq v_0 \exp \left[\frac{1}{\lambda_{\rm W}} \int_r^{r_0} \exp(-\lambda_{\rm I}/r') dr' \right] && (4.31) \\ &\simeq v_0 \exp \left\{ -\frac{1}{\lambda_{\rm W}} \left[r_0 e^{-\lambda_{\rm I}/r_0} - r e^{-\lambda_{\rm I}/r} - \lambda_{\rm I} \, {\rm E}_1(\lambda_{\rm I}/r_0) + \lambda_{\rm I} \, {\rm E}_1(\lambda_{\rm I}/r) \right] \right\}, && (4.32) \end{aligned}$$

where $r_0 \leq r$ and $\lambda_{\rm W} \equiv 1/\sigma N_\infty (1+\epsilon)^2$, and the exponential integral ${\rm E}_1(x)$ is defined as is usual (Abramowitz and Stegun, 1972):

$${\rm E}_1(x) \equiv \int_1^\infty \frac{e^{-xt}}{t} \, dt. \tag{4.33}$$

Again for illustration, the heliospheric value of $\lambda_{\rm W}$ is about 300 AU, so the solar wind should slow very little as it crosses the heliosphere, just as is observed (e.g. Smith et al., 2003). It is now apparent that $\lambda_{\rm W}$ is the mean free path of solar-wind ions subject to charge exchange in the inflowing ISM, while $\lambda_{\rm I}$ is the mean free path for ISM neutrals in

the outflowing solar wind. The expression for $\lambda_{\rm I}$ does not look like the standard form of a mean free path because the solar-wind density is not constant but declines with radius. In a sense, $\lambda_{\rm I}$ is an effective mean free path, representing an integrated scattering probability per unit distance.

If $r \gg \lambda_{\rm I}$ for any r of interest, then the exponential inside the integral can be expanded to yield the limit

$$\begin{aligned} v(r) &\simeq v_0 \exp\left[\frac{1}{\lambda_{\rm W}}\int_r^{r_0}(1-\lambda_{\rm I}/r')dr'\right] && (4.34)\\ &\simeq v_0 \exp\left[\frac{1}{\lambda_{\rm W}}(r_0 - r - \lambda_{\rm I}\ln r_0 + \lambda_{\rm I}\ln r)\right] && (4.35)\\ &\simeq v_0 \exp\left[\frac{1}{\lambda_{\rm W}}(r_0 - r)\right]\left(\frac{r}{r_0}\right)^{\lambda_{\rm I}/\lambda_{\rm W}}. && (4.36)\end{aligned}$$

This limit can be obtained less easily by employing a first-order, series expansion of $\mathrm{E}_1(x)$:

$$\mathrm{E}_1(x) \simeq -\gamma - \ln x + x, \tag{4.37}$$

where $\gamma = 0.57721\cdots$ is Euler's constant, but the result is the same.

For the current heliosphere[2], $\lambda_{\rm I}/\lambda_{\rm W} \sim 10^{-2}$, and to a very good approximation

$$\begin{aligned} v(r) &\simeq v_0 e^{(r_0-r)/\lambda_{\rm W}} && (4.38)\\ &\simeq v_0\left[1 + \frac{r_0 - r}{\lambda_{\rm W}}\right]. && (4.39)\end{aligned}$$

The wind velocity linearly declines with radius on a scale of about 300 AU, which is larger than the current heliosphere size. In such situations, the size of the astrosphere is likely determined not by charge-exchange interactions, but by MHD and kinetic interactions between the stellar and interstellar ions and magnetic fields, with charge exchange a modifying that basic interaction.

During a giant molecular cloud (GMC) encounter, $\lambda_{\rm W}$ might be 0.3 AU or less,

[2]Note that satisfying the limit $r_0 \gg \lambda_{\rm I}$ would require a different reference point than 1 AU for the current conditions.

making $\lambda_{\rm I}/\lambda_{\rm W} \sim 10$ and the wind velocity has a more complicated decline:

$$v(r) \simeq v_0 e^{(r_0-r)/\lambda_{\rm W}} \left(\frac{r}{r_0}\right)^{\lambda_{\rm I}/\lambda_{\rm W}} . \tag{4.40}$$

Now enough neutrals are accreting to devastate the wind. This case deviates the most from the approximation that $v \gg V$, since v will likely decline so much before any shock that the $1+\epsilon$ factor will become important and hasten the wind's demise. Thus this situation is more accurately handled by numerical integration of the continuity and momentum equations.

If $r \ll \lambda_{\rm I}$ for any r of interest, then an asymptotic expansion of E_1 is more useful:

$$\mathrm{E}_1(x) \simeq \frac{e^{-x}}{x}\left(1+\frac{1}{x}\right). \tag{4.41}$$

Rewriting v:

$$\begin{aligned} v(r) &\simeq v_0 \exp\left\{-\frac{1}{\lambda_{\rm W}}\left[(r^2/\lambda_{\rm I})e^{-\lambda_{\rm I}/r} - (r_0^2/\lambda_{\rm I})e^{-\lambda_{\rm I}/r_0}\right]\right\} & (4.42)\\ &\simeq v_0 \exp\left(-\frac{r^2}{\lambda_{\rm I}\lambda_{\rm W}}e^{-\lambda_{\rm I}/r}\right) & (4.43)\\ &\simeq v_0 \exp\left(-\frac{N_\infty V r^2}{n_0 v_0 r_0^2}e^{-\lambda_{\rm I}/r}\right). & (4.44) \end{aligned}$$

Rewriting $\lambda_{\rm I}\lambda_{\rm W}$ in terms of the wind and ISM parameters makes it clear that the ratio of the momentum fluxes of the ISM flow and stellar wind $N_\infty V/n_0 v_0$ determines the magnitude of the effect on the wind velocity. When the neutral density is high enough for all $r < r_a$ that the exponential is important, the wind velocity follows a complex profile that turns over from a $1-e^{-\lambda_{\rm I}/r}$ behavior at small r to e^{-r^2} behavior at large r.

To determine the size of the astrosphere in the pure charge-exchange case, we choose an ionization fraction $f_{\rm ion}$ for the local ISM using the following formula:

$$f_{\rm ion}(N) = \begin{cases} 0.5 & : \quad N < 3 \text{ cm}^{-3} \\ 10^{-4} & : \quad 3 \le N < 100 \text{ cm}^{-3} \\ 10^{-7} & : \quad N \ge 100 \text{ cm}^{-3} \end{cases} . \tag{4.45}$$

We then assume that the ions provide a confining ram pressure and thus set a maximum astrosphere size. The astrosphere size is then the smaller of (1) the radius, $r_{\rm ce}$, where charge exchange slows the wind to a standstill, or (2) the radius at which the ram pressures balance. The ram-pressure balance model of §4.3.1 serves as an upper limit, and the expression

$$r_{\rm ce} = \left(\frac{n_0 v_0}{N_\infty V} \right)^{1/2} r_0 \tag{4.46}$$

sets the lower limit. In intermediate-density situations, charge exchange is not effective enough to stop the wind before a shock would occur at the location of ram-pressure balance between the ions.

4.3.3 Gravitational Focussing

Gravitational focussing of particle trajectories strongly affects the density of the ISM surrounding heliosphere when the astrosphere size becomes comparable to the scale of the star's gravitational influence. This was first pointed out by Fahr (1968) for the case of collisionless orbits of protons in the inner solar system and then later first applied in the present context by Begelman and Rees (1976). If the ISM is moving relative to the star at velocity V, then this "gravitational radius" is $b = 2GM/V^2$, or

$$b = 18 \left(\frac{M}{M_\odot} \right) \left(\frac{V}{10 \text{ km s}^{-1}} \right)^{-2} \text{ AU}. \tag{4.47}$$

For reference, the Sun's present speed relative to the local ISM is estimated to be 26 km s^{-1} (Witte, 2004). Previous work has either neglected gravitational focussing or included its effect on the star-ISM velocity but only in the fluid limit (e.g. Talbot et al., 1976; Talbot and Newman, 1977). We assume that the ISM flow onto the astrosphere interface is collisionless rather than fluid-like, since the typical mean free path in neutral gas ($\sim 10^{15}/N$ cm for neutral-neutral collisions, where N is the local ISM number density) is larger than the astrosphere size in most cases of interest. The situation is marginal at low densities, but at the largest densities of interest, where gravitational focussing dominates the accretion, we show below that the astrosphere size decreases with density faster than does the interstellar

mean free path, so the collisionless case is appropriate.[3]

A complete solution to stellar accretion in the collisionless limit was derived by Danby and Camm (1957). The infall density can be expressed as an integral that must be evaluated numerically in the general case; but we are interested in interactions with cool, neutral material, and the thermal-velocity dispersion of the gas is negligible compared to the star-ISM velocity V. In the case of a cold gas, Danby and Camm find that the ISM density in the apex direction is enhanced by a factor

$$\eta(M, r, V) = \frac{(q^2 + 2p^2)}{2p(q^2 + p^2)^{1/2}}, \tag{4.48}$$

where $p \equiv V/\sigma$, $q^2 \equiv 2GM/\sigma^2 r$, and σ is the thermal-velocity dispersion of the gas. The ram pressure on the astrosphere will then be this density multiplied by

$$V'^2 = V^2 + \frac{2GM}{r}, \tag{4.49}$$

where the second term on the right accounts for gravitational acceleration.

Finally, the ram-pressure balance including gravitational focussing and any stellar-mass dependence is

$$n_0 v_0^2 \left(\frac{r_a}{r_0}\right)^{-2} g\,\xi(M, t) = N \left(V^2 + \frac{2GM}{r_a}\right) \eta(M, r_a, V). \tag{4.50}$$

This equation yields a quartic polynomial for the astrosphere size r_a.

High-density Limit

As planetary systems traverse dense clouds, the gravity of the central star will accelerate the accretion flow and enhance the density, having a doubly significant effect on the interstellar ram pressure. The minimum cloud density N_f for focussing to dominate can be obtained from the condition $b > r_a$, where b is the gravitational radius and r_a is the pressure-balance

[3] If the inflowing dense gas is mostly photoionized by the star, as found by Yeghikyan and Fahr (2004a), then the appropriate cross section is larger and the fluid limit would apply, but only for solar-mass stars, since lower mass stars have much lower ionizing fluxes.

astrosphere size neglecting focussing. This gives

$$N_f = 35\ \xi(M,t)\ \left(\frac{V}{10\ \mathrm{km\ s^{-1}}}\right)^2\ \left(\frac{M}{M_\odot}\right)^{-2}\ \mathrm{cm^{-3}}. \tag{4.51}$$

Thus in dense molecular clouds ($N \sim 10^2$–10^3 or larger; e.g. Larson 1981; Scalo 1985) the accretion flow will be dominated by gravitational focussing except possibly for the very least-massive stars.

Assuming that gravitational focussing dominates, the enhanced density at the apex of the astrosphere is

$$N \simeq \frac{N_\infty}{2V}\left(\frac{2GM}{r}\right)^{1/2}, \tag{4.52}$$

where N_∞ is the ISM density unperturbed by the star's gravity. The incoming velocity (much larger than the star-gas velocity V in this limit) is $V' \simeq (2GM/r)^{1/2}$. Expressed in terms of the gravitational radius b, we get

$$N \simeq \frac{N_\infty}{2}\left(\frac{b}{r}\right)^{1/2} \tag{4.53}$$

and

$$V' \simeq V\left(\frac{b}{r}\right)^{1/2}, \tag{4.54}$$

where $b/r \gg 1$ in the gravitational-focussing limit. Equating NV'^2 to the stellar-wind ram pressure then allows a simple solution for the astrosphere size of a planetary system whose flow outside the astrosphere is dominated by gravitational focussing. The result is

$$\frac{r_a}{r_0} = 4\left[\frac{N_\infty}{\xi(M,t)n_0}\right]^{-2}\left(\frac{V}{v}\right)^{-4}\left(\frac{r_0}{b}\right)^3, \tag{4.55}$$

or, substituting for b,

$$\frac{r_a}{r_0} = \frac{v^4\, r_0^3}{2\,G^3M^3}\ V^2\ \left[\frac{N_\infty}{\xi(M,t)\,n_0}\right]^{-2}. \tag{4.56}$$

Notice that in this gravitational-focussing limit the astrosphere size *increases* with increasing stellar velocity V. This unexpected behavior occurs because the slower the star is moving, the stronger is the effect of focussing, so that the ram pressure in this case scales

like V^{-4}. Additionally, since the astrosphere size varies as N_∞^{-2} in this limit, while the mean free path of the incoming gas to particle-particle collisions still scales linearly with N_∞^{-1}, the astrosphere size is decreasing faster (due to focussing) than the mean free path is as the star velocity decreases, and the validity of the collisionless approximation, as measured by the ratio of mean free path to heliosphere size, *increases* with increasing density.

By the definition of habitable distance (neglecting albedo variations),

$$r_h = r_E \left(\frac{L}{L_\odot}\right)^{1/2}, \tag{4.57}$$

where $L_\odot$ is the bolometric luminosity of the sun and r_E is the sun-Earth distance (1 AU). Although no single power law can accurately represent the mass-luminosity relation for low-mass stars (see below), an adequate relation for our purposes is $L/L_\odot = (M/M_\odot)^\alpha$, with $\alpha \sim 2$–3 for masses between 0.1 and 1 $M_\odot$, based on masses from suitable binary systems (see Henry et al., 1999; Delfosse et al., 2000), Hipparcos distances, and empirical bolometric corrections. The habitable-zone distance is then $r_h = r_E\ (M/M_\odot)^{\alpha/2}$. Taking the average number density of the solar wind at 1 AU, ρ_E, to be 7 cm^{-3} and evaluating numerical factors:

$$\frac{r_a}{r_h} = 8.9 \times 10^4\ \frac{V_{10}^2\ [\xi(M,t)]^2}{N_\infty^2} \left(\frac{M}{M_\odot}\right)^{-3-\alpha/2}. \tag{4.58}$$

This result will be useful when we estimate the minimum ISM density needed to descreen a habitable planetary system.

Analytic Estimate

Exposure to the full interstellar cosmic-ray spectrum (ignoring magnetospheric screening) will occur before the astropause has crossed inside the habitable zone ($r_a < r_h$; see §4.4.1), but this crossing represents the most conservative condition for descreening and is probably the most relevant for accretion of interstellar material. The minimum ISM density for this descreening condition to hold is

$$N_d > 300\ V_{10}\ \xi \left(\frac{M}{M_\odot}\right)^{-(3+\alpha/2)/2} \text{cm}^{-3}, \tag{4.59}$$

where the numerical coefficient is approximate because the star-gas relative velocity will vary from star to star by factors of a few. For $\alpha = 2.5$, the exponent of M is -2.1, so a star with $M = 0.5\,M_\odot$ (early M star) will require an ISM density 4 times larger than the Earth for complete descreening to occur, while a $0.1\,M_\odot$ star will require a density about 120 times larger.

This result is easily understood as a combination of several effects. First, the smaller stellar mass produces less gravitational focussing, reducing the exterior ram pressure and increasing the astrosphere size compared to larger masses. Second, the habitable-zone distance decreases with decreasing stellar mass, forcing the astrosphere to shrink to smaller distances for descreening of habitable planets to occur. Third, considering that the stellar-mass scaling factor $\xi(M)$ at a given age may increase with decreasing mass, similar to general stellar activity, only strengthens the conclusion. Finally, for cosmic-ray screening, cosmic rays must scatter to smaller radii at a given astrosphere size for lower-mass stars.

Numerical Calculation of Focussing Enhancement

Following the notation of the previous sections, the full polynomial equation for the astrosphere size can be derived in the collisionless limit by equating the wind ram pressure with the ISM ram pressure, using the Danby and Camm (1957) gravitational focussing solution for the density at the astrospheric apex point and the velocity as modified by gravitational focussing (Eq. 4.49). The result is

$$r_a^4 + 2\,b\,r_a^3 + \frac{5}{4}\,b^2 r_a^2 + \frac{1}{4}\,b^3 r_a - \frac{p^2}{N^2\,V^4} r_E^4 = 0, \tag{4.60}$$

where b is the gravitational radius as defined earlier, $p \equiv \xi n_E v^2$, V is the relative star-ISM velocity, and r_a is the astrosphere size. To calculate the astrosphere size for an arbitrary planetary system without regard to special limits or approximations, we solved this equation by first making the substitution $r_a = u - b/2$. This results in the depressed quartic equation:

$$u^4 - \frac{b^2}{4} u^2 - \frac{p^2}{N^2\,V^4} r_E^4 = 0. \tag{4.61}$$

We used the standard quadratic formula to solve for u^2 and took the positive, real root as the astrosphere size:

$$r_a = \left[\frac{b^2}{8} + \frac{1}{8}\left(b^4 + \frac{64p^2}{N^2\,V^4} r_E^4\right)^{1/2}\right]^{1/2} - \frac{b}{2}. \tag{4.62}$$

This equation takes the place of the simple $r_a \propto N^{-1/2}V^{-1}$ in the pure ram-pressure models, and one can see this basic dependence buried in the denominator of the second term inside the parenthesis in Eq. 4.62.

Combining Focussing and Charge Exchange

To include focussing in the the charge-exchange model, we modified the density at the outer boundary of the astrosphere r_a to be $N_\infty \eta(M, r_a, V)$. Since the focussing factor depends on r_a, this required iteration to converge on a solution. This is not a self-consistent approach, since it ignores the potentially significant change of the neutral density inside the astrosphere, but accounting for that effect would turn the problem into one of solving the dynamical equations, rather than a purely analytical one. And despite this approximate nature of this approach, the basic effect is still captured.

4.3.4 Comparison

Figure 4.3 shows the dependence of the astrosphere size in our two simple models on the external ISM density N_∞. The difference in the ionization fractions as the N increases is relatively unimportant, since at densities above 3 cm^{-3}, where the ionization fraction decreases to 10^{-4}, charge exchange slowing of the wind is already the primary determiner of the heliosphere size. The case without charge exchange assumes that the entire ISM density is available to provide ram pressure but still probably overestimates the size of the astrosphere, since no slowing of the stellar wind occurs. Gravitational focussing enhances the density and velocity of the ISM flow and compresses the astrosphere to smaller sizes than a pure ram-pressure estimation produces. The difference in astrosphere size with and without focussing is over an order of magnitude at $N = 1000$ cm^{-3}. The effect of charge

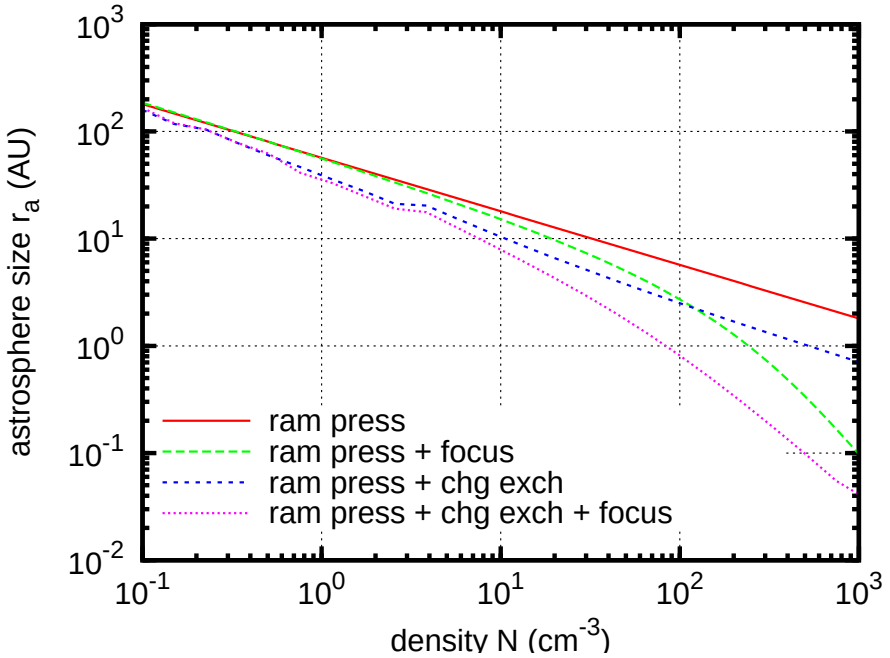

Figure 4.3: Dependence of the astrosphere size on local ISM density for the various models. The curves are, from top to bottom in the legend, a pure ram-pressure balance model, a ram-pressure model with gravitational focussing included, a ram-pressure model with charge exchange included, and a ram-pressure model with both charge exchange and gravitational focussing. The difference between the cases with and without gravitational focussing grows large as N increases, while charge exchange has only a factor of 2–3 effect on r_a at all densities.

exchange is never that severe, however. Even at high densities, the astrosphere is only a factor of 2–3 smaller when including charge exchange.

Given the small effect of charge exchange here, and the fact that we cannot include both focussing and charge exchange self-consistently, we choose to ignore the effect of charge exchange in many of the results that follow.

4.4 Results

4.4.1 Habitable zones can receive nearly the full interstellar cosmic-ray flux at average ISM densities

Under the convection-diffusion solution, the Galactic cosmic-ray flux at a given energy is exponentially modulated, so, when the astrosphere size gets to be comparable to the scale of modulation, the flux has already reached a large fraction of the interstellar value ($1/e$ in fact). Any further decrease in astrosphere size will produce progressively smaller cosmic-ray flux increases, so the flux is "saturated." This, most importantly, means that a habitable planetary system is effectively already unprotected by its astrosphere at ISM densities lower than what is required to compress the astrosphere inside the habitable zone. The effect for the heliosphere is shown in Fig. 4.4. Depending on the diffusion coefficient chosen, the Earth can be exposed to more than $1/e$ of the interstellar cosmic-ray flux at densities of just 0.2–2 cm^{-3}. This is quite close to the average density of the ISM of about 1 cm^{-3}, contrasting sharply with the requirement that the Earth be completely outside the heliosphere, which would require densities in excess of $\sim$ 100–300 cm^{-3} (see Fig. 4.3). If one includes the charge exchange and gravitational focussing in the astrosphere model, the densities required to saturate the cosmic-ray flux decrease significantly, from a factor of two at $1/e$ of the interstellar flux to 4–5 at 90% of interstellar. Figure 4.5 shows the case including charge exchange and focussing.

We therefore suggest that the Earth quite frequently receives Galactic cosmic-ray fluxes very near to that of the interstellar value. And, while dense molecular clouds will still greatly enhance interstellar gas and dust accretion, such rare events are not needed to cause a significant enhancement in the Galactic cosmic-ray flux.

Compared to other disk stars, the sun is moving slowly relative to the ISM (Rocha-Pinto et al., 2004; Witte, 2004), so the densities required to saturate the cosmic-ray flux are somewhat high. Higher velocities give the ISM a larger ram pressure in the star's rest frame and compress the astrosphere.[4] Figure 4.6 illustrates the effect. Interestingly, the

[4]Assuming that gravitational focussing can be neglected. This is discussed in §4.4.2.

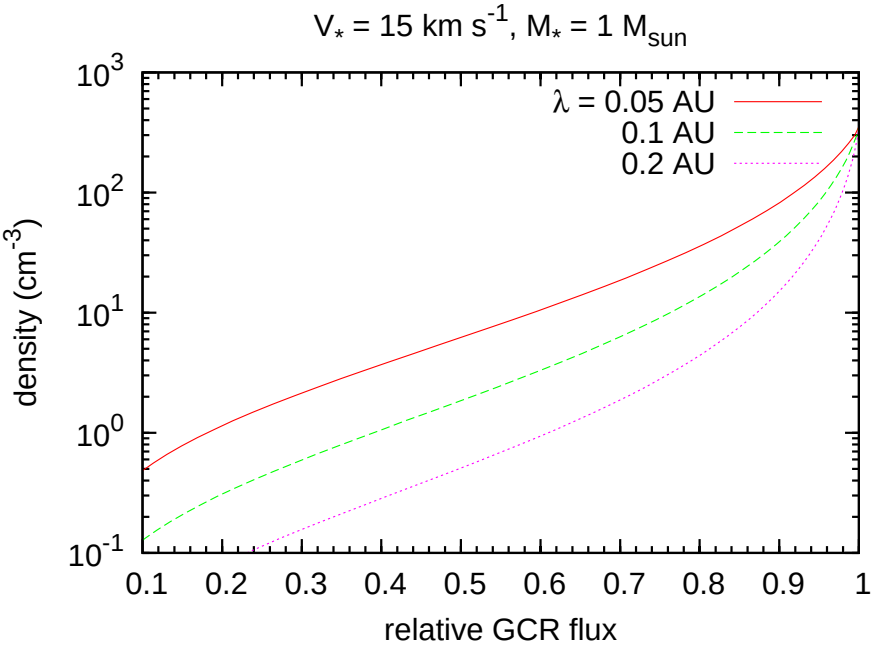

Figure 4.4: Fraction of the interstellar integrated cosmic-ray flux received at 1 AU as a function of interstellar density for three different diffusive skin depths. Pure ram-pressure balanced is assumed. The skin depth has a significant effect on the flux received, but in all cases densities near the average ISM density will raise the flux to above $1/e$ of the interstellar value.

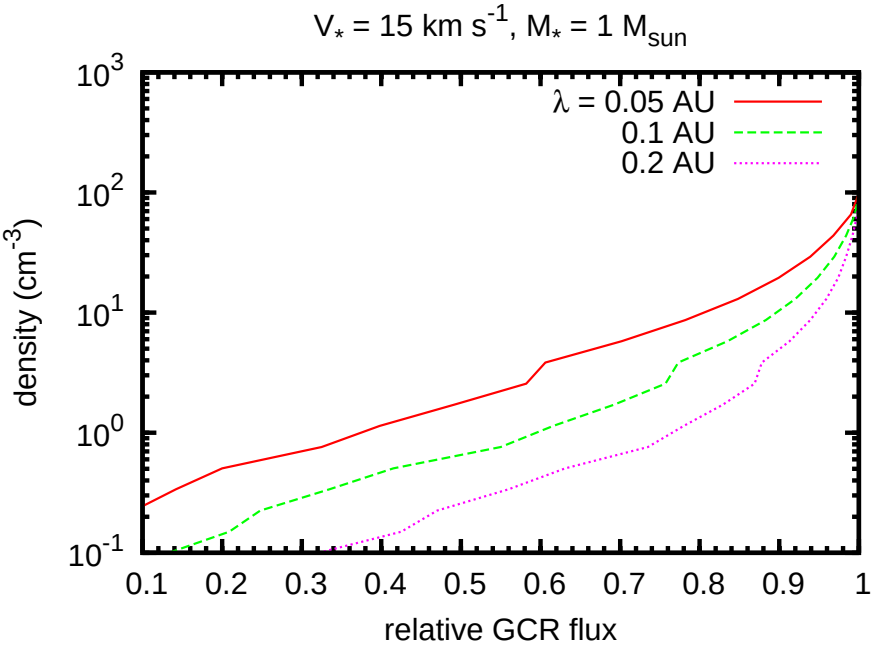

Figure 4.5: Fraction of the interstellar integrated cosmic-ray flux received at 1 AU as a function of interstellar density for three different diffusive skin depths for a ram-pressure balance model including both charge exchange and gravitational focussing. The smaller astrospheres produced by charge exchange and gravitational focussing mean that the flux of cosmic rays received at a given density goes up. Here, a density of only 0.1–1 cm^{-3} will produce fluxes of $1/e$ of the interstellar value. This is roughly half of that predicted by a ram-pressure model without these effects. In order to get 90% of the interstellar flux, this model requires a density of 5–20 cm^{-3}, in contrast to the 20–100 cm^{-3} in the case without charge exchange and focussing.

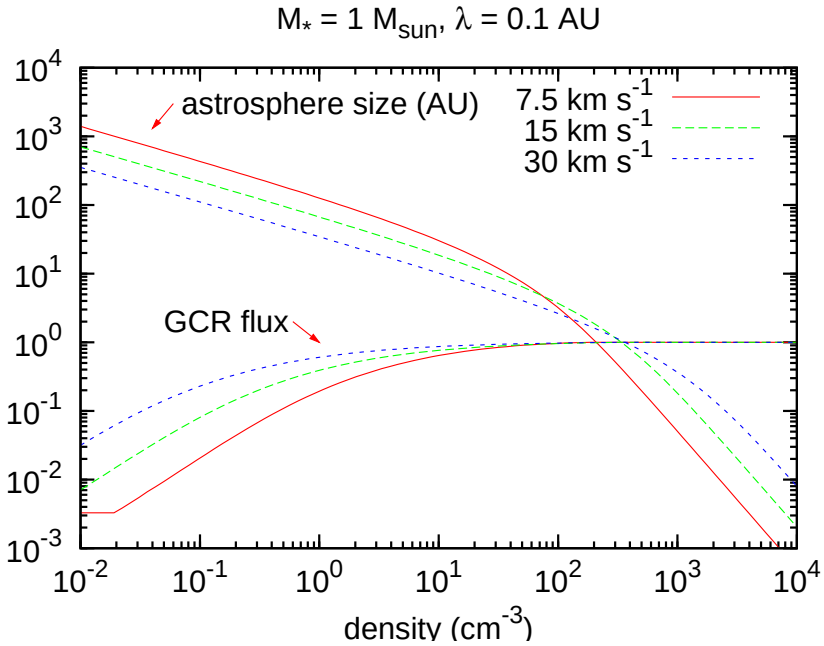

Figure 4.6: Dependence of the astrosphere size and normalized cosmic-ray flux on the relative velocity between the star and the ISM for a ram-pressure model with gravitational focussing included. Interestingly, the effect reverses once the gravity of the star becomes important, at which time a larger star-ISM relative velocity will actually produce a *larger* astrosphere. At the densities where focussing is important, the cosmic-ray flux is already close to the interstellar value, so focussing cannot enhance it further.

effect reverses once the gravity of the star becomes important, but this has no effect on the cosmic-ray flux. Velocity has a clear influence on the cosmic-ray flux normalized to the interstellar value when the astrosphere size is large, but the flux quickly saturates and, once gravitational focussing takes over, the habitable zone is already receiving nearly the full interstellar flux, and focussing has no further effect.

The perpendicular diffusive skin depth $\lambda_\perp$ of cosmic rays in the solar system is very uncertain (Parhi et al., 2003). We examined the effect of a range of skin depths on the integrated, modulated cosmic-ray flux normalized to the interstellar value. We have no reason to believe that astrospheres around other stars would have the same statistical characteristics as the heliosphere, so λ is essentially a free parameter, within a reasonable range. We varied λ between 0.05 and 0.2 AU, representing the range of supposed values for the solar system (Parhi et al., 2003). The results are shown in Fig. 4.7. As expected,

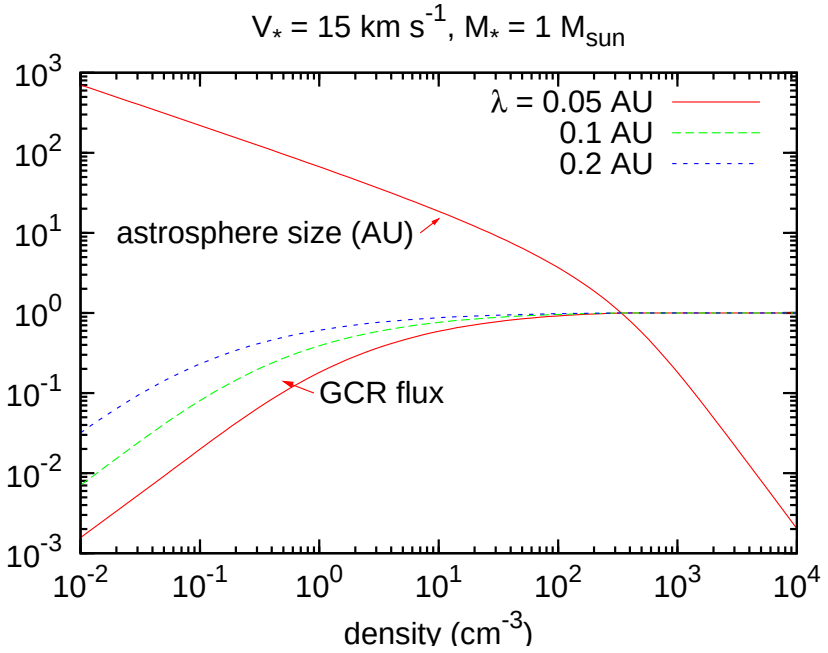

Figure 4.7: Dependence of the normalized cosmic-ray flux on the skin depth chosen for the transport equation for a ram-pressure model with gravitational focussing included. Smaller skin depths imply more frequent scattering in order to reach a given distance from the star, so we expect the flux to be lower with smaller skin depths. For low ISM densities ($\lesssim 0.1$ cm^{-3}), the flux is about an order of magnitude lower if the skin depth is 0.05 AU instead of 0.2 AU. The astrosphere size is shown for reference, but the skin depth has no effect on it in our models.

smaller λ yields a lower modulated cosmic-ray flux. Under the convection-diffusion model, this represents the cosmic rays having to scatter a greater number of times in order to reach a given distance from the star. We neglect any effect of cosmic rays on the astrosphere size, so no effect is expected, but the astrosphere size is shown in the figure for reference. Most importantly, the density required to raise the Galactic cosmic-ray flux to within $1/e$ of the interstellar value decreases by about an order of magnitude, depending on the choice of λ.

4.4.2 Gravitational focussing and charge exchange enhances the accretion flow at high ISM densities

We have already seen in Fig. 4.3 that in absolute terms focussing and charge exchange measurably shrink the astrosphere beyond what a simple ram-pressure model would predict.

But what about the astrosphere size normalized by the habitable-zone distance, r_h? This quantity gives a better idea of what densities are required to expose a habitable planet to the raw ISM accretion flow, while r_a in terms of AU is more useful when comparing cosmic-ray fluxes, since the cosmic-ray diffusive skin depth is assumed not to be a function of the habitable-zone distance.

The quantity r_a/r_h as a function of local ISM density is shown for three representative stellar masses (0.1, 0.5, and 1 $M_\odot$) in Fig. 4.8. In this figure, charge exchange is ignored for simplicity, since it has a much smaller effect overall than focussing. It is evident in Fig. 4.8 that the astrosphere is much further away in terms of the habitable-zone distance r_h for systems with lower-mass parent stars. The transition into the gravitationally dominated regime is located, for each of the three model planetary systems, by the knee in the curves as the ISM density increases. This knee occurs for lower ISM densities for systems with more-massive parent stars, since the effect of the star's gravity on the pressure balance grows at a given ISM density as mass increases. Figure 4.8 shows clearly that an M star must encounter a very high density interstellar region in order to compress its astrosphere significantly, and therefore full exposures to the Galactic cosmic-ray and accretion flux will be rarer than for a solar-type star. This occurs because the probability distribution of interstellar cloud densities declines rapidly with increasing density.

Henceforth, we will call the situation in which $r_a < r_h$ "descreening." A more quantitative calculation of the effect of focussing on the critical descreening density is obtained by solving for the density at which the astrosphere apex distance shrinks to the habitable-zone distance r_h, and then relating r_h to the stellar mass. From Eq. 4.60 the critical descreening density is

$$N_d = \frac{p\, r_E^2}{V^2} \left(r_h^4 + 2\, b\, r_h^3 + \frac{5}{4}\, b^2 r_h^2 + \frac{1}{4}\, b^3 r_h \right)^{-1/2} . \tag{4.63}$$

The habitable-zone distance depends on the luminosity of the parent star, $r_h \sim L^{1/2}$ in Earth-Sun units (again ignoring variations in albedo). Because the primary (approximately constant) quantity that governs the evolution of the star is its mass, it is traditional to parameterize L in terms of stellar mass M. We used the data for stellar masses and luminosities for stars less massive than 1 $M_\odot$ given in Hillenbrand and White (2004) and

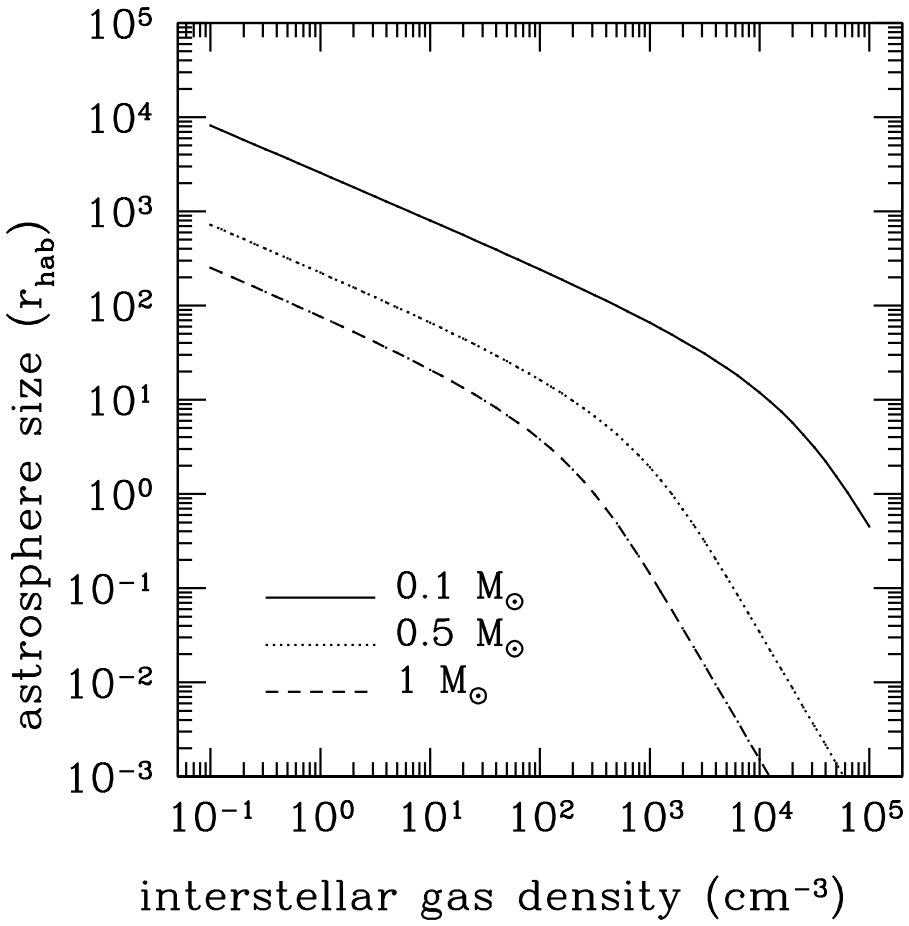

Figure 4.8: Astrosphere size, in units of liquid-water habitable-zone distance (defined here as the distance receiving the same bolometric stellar flux as Earth), as a function of ambient interstellar gas density for stars of three different masses. A ram-pressure model with gravitational focussing is used; charge exchange is ignored. The regime in which the inflowing interstellar ram pressure is dominated by gravitational focussing is at densities higher than the "knee" in each curve.

fit the following polynomial to it:

$$\log L = 4.10 \log^3 M + 8.16 \log^2 M + 7.11 \log M + 0.065, \tag{4.64}$$

where L and M are in solar units. The slope of this log-log relation varies from about 2 at the smallest masses to about 3 from 0.5 to 1 $M_\odot$. This allows us to calculate the critical descreening density (Eq. 4.63) in terms of the parent-star mass. The result is plotted for two different assumptions for the factor ξ (which parameterizes any variation in astrosphere density or velocity as a function of stellar mass) in Fig. 4.9, for an assumed star-ISM velocity of 15 km s^{-1}.

A planetary system orbiting a star of mass 1 $M_\odot$ will be exposed to the raw ISM if it encounters a region of density greater than a few times $10^2\, V_{10}$ cm^{-3}, which are quite common in the solar neighborhood, both in mostly atomic and mostly molecular form. On the other hand a system orbiting a star of mass 0.2 $M_\odot$ must pass within a region of density in excess of $10^4\, V_{10}$ cm^{-3} to suffer such an exposure, even if we assume no dependence of wind speed or density on mass, and such dense regions will be rarely encountered because their volume-filling factor is so small.

4.4.3 Younger stars and less massive stars are better buffered from descreening

Stars of different spectral types and ages presumably have winds analogous to the solar wind. Little information is available for other stars except for the variation of momentum flux with age for several solar-type stars (Wood et al., 2002). In the absence of charge exchange, which is discussed in §4.3.2, we take the wind speed to be independent of distance from the star, as is roughly the case for the solar wind (e.g. Whang et al., 2003), and equal to 400 km s^{-1}. For simplicity, we neglect the fast solar wind and assume that the mass and age variations can be expressed as a mass- and age-dependent scaling function $\xi(M, t)$ for the ram pressure in Eq. 4.50. We expect $\xi(M, t)$ to increase with decreasing mass and age, as inferred from the general activity level of main-sequence stars, but lacking any information on its functional

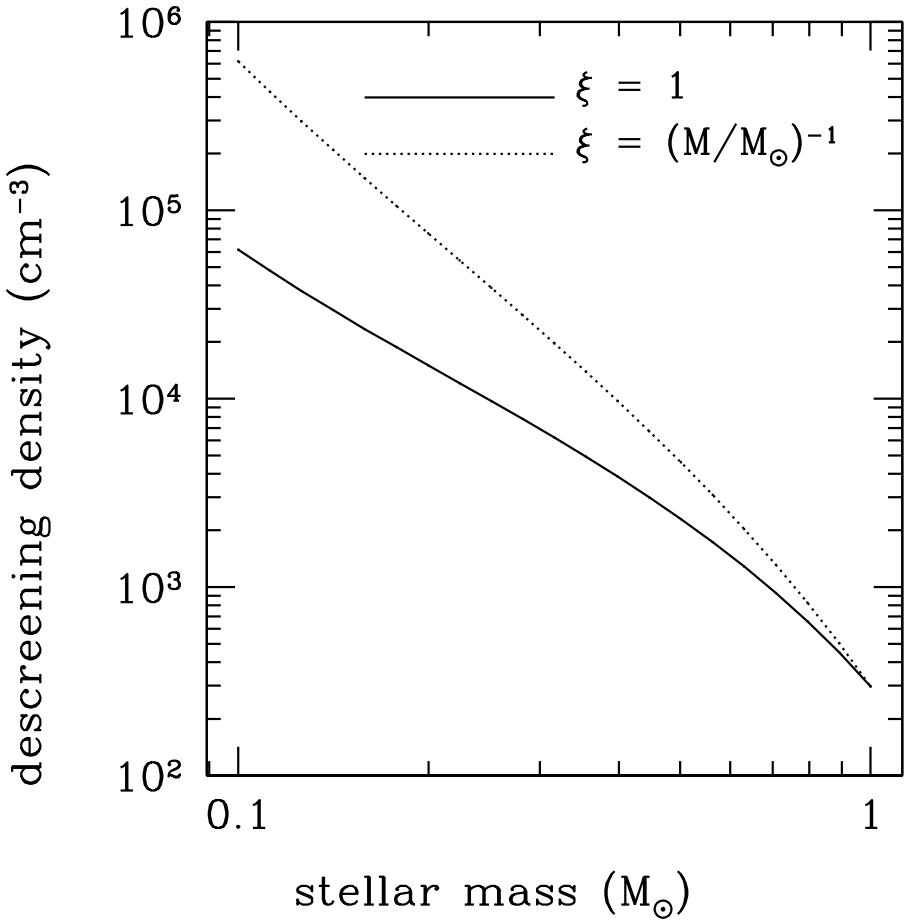

Figure 4.9: Critical interstellar density for descreening, defined as an event during which the astrosphere size is equal to the conventional liquid-water habitable-zone distance, as a function of parent-star mass. The solid line is for no mass dependence of the stellar-wind parameters; the dashed line is for astrosphere momentum flux (parameterized by the factor ξ) increasing with decreasing mass (see text). Comparison with Fig. 4.8 shows that descreening densities are at or larger than the density above which gravitational focussing dominates.

form, we keep it a parameter.

The mass of the sun is not normally included in heliosphere models. The reason is simple: the heliosphere is not small enough for gravitational focussing to have a large effect. When the sun encounters dense regions of the ISM, however, the heliosphere can shrink to sizes small enough that the sun's gravity begins to pull excess interstellar material in, effectively increasing the interstellar ram pressure and further shrinking the heliosphere. Figure 4.10 shows the result of varying the mass of the central star. The astrosphere size is significantly changed at high densities where focussing dominates, but the cosmic-ray flux is unaffected, since it has already saturated by those densities. This effect also means that habitable planets around stars of different masses will have different astrosphere sizes in otherwise identical interstellar regions. The lowest-mass stars, such as M stars, will tend to have larger astrospheres, and habitable planets orbiting M stars will be the most protected from climatic, radiobiological, and meteorological effects of interstellar gas and dust and, to a lesser extent, cosmic rays.

The age of a star can also affect the astrospheric dynamics. If younger stars have stronger winds, then ξ should increase with decreasing age t. The effect for a younger star would be identical to that of a less-massive star and would depend on the chosen functional form of $\xi(t)$.

4.5 Frequency of Descreening Encounters

Saturating the cosmic-ray flux is extremely easy, since it requires only average ISM densities, so we need only estimate how often densities large enough to descreen an astrosphere are encountered in the ISM. For any reasonable characterization of the ISM, the frequency of encounters of a test object with a cloud of a given density decreases with increasing density. Unfortunately this statement is difficult to quantify because interstellar densities are normally very poorly determined. The densities are almost always derived from the observed column density of some tracer (e.g. dust, or a molecule like CO), a conversion factor from tracer to total column density, and then a conversion to density by dividing the column density by a characteristic size of the region of interest. This latter step is

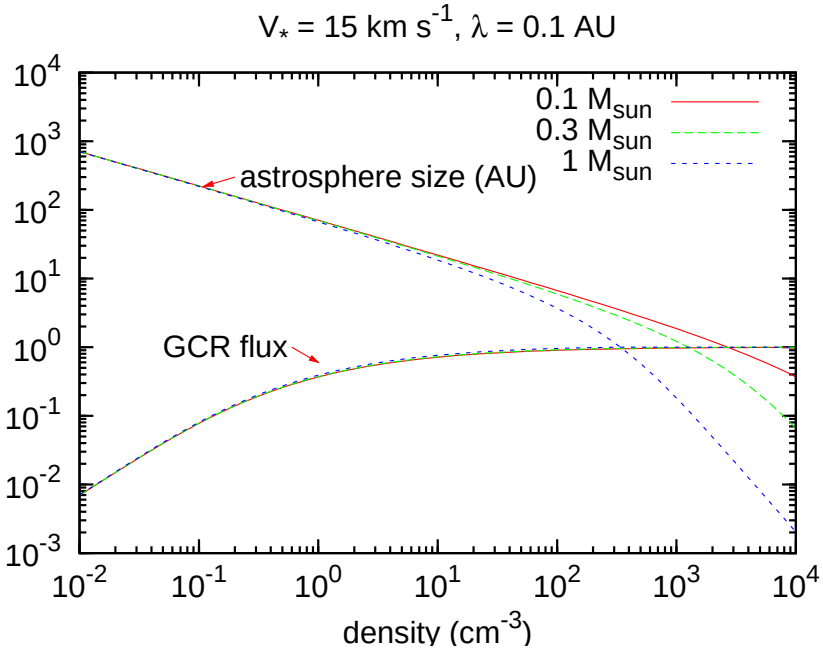

Figure 4.10: Dependence of the astrosphere size and normalized cosmic-ray flux on the mass of the central star using a ram-pressure balance model with gravitational focussing included. The astrosphere size is unaffected until the gravitational focussing by the star becomes important. For ISM densities above this turnover, lower-mass stars will have significantly larger astrospheres.

especially uncertain because the apparent size is determined by the sensitivity limit of the observations (column density normally decreases outward on average) and by the adopted distance to the region. However we can use the approach of Talbot and Newman (1977) as applied to various catalogues of regions identified as discrete "clouds" in different surveys in order to see that, even given these uncertainties and selection effects, the frequency of occurrence of dense ISM regions must decrease rapidly with increasing density.

Talbot and Newman (1977) used the Lynds (1962) catalogue of about 1800 "dark clouds," [5] for which Lynds provided "opacity classes" and angular areas. Grouping these clouds into bins of a given column density range using the opacities, and using the mean size $R(n)$ for each group, gives the number of clouds with density in each density range. Plotted as a histogram, this gives the number of clouds per unit volume of space per unit density range, denoted $n_{\rm cl}(n)$, where n is the internal particle density. If $l(n)$ is the average number of clouds encountered of density $(n, n+dn)$ per unit line-of-sight distance, then $n_{\rm cl}(n) = [\pi R(n)^2\ l(n)]^{-1}$. Since the frequency of encounters is proportional to $l(n)^{-1}$, this gives a frequency $\nu \propto R(n)^2\ n_{\rm cl}(n)$.

We reexamined the cloud property table given by Talbot and Newman (1977), but we use only the data for the three highest opacity classes.[6] Using the derived average densities in each class, we find the distribution $n_{\rm cl}(n) \propto n^{-1.8}$ and $R(n) \propto n^{-0.8}$, giving a cumulative frequency of encounters $\nu(>n) \propto n^{-2.4}$. This agrees with the exponent of -2.3 obtained using directly the $l(>n)$ values in their table, or the scaling of their quantity N_e which is the number of expected encounters by the sun over 4.6 Gyr.

This result is very uncertain because the Lynds cloud sample, besides its small size, suffers from a number of selection effects:

1. Clouds with angular sizes less than about 2–5 arcmin cannot be detected on Palomar Schmidt plates because the number of background stars is too small. This corresponds to a minimum detectable cloud size that increases with distance. Since smaller clouds tend

[5] That is, regions on photographic plates that appear darker than the surrounding area because of reduction in the number of visible stars by dust extinction.

[6] The points for "Standard cloud," actually derived from reddening statistics, "CO" and "HI" are ill-defined averages for entire surveys, and the lower opacity class extinction clouds suffer from selection effects as explained below and as can be seen in Fig. 1 of Talbot and Newman.

to be denser, the density probability distribution is probably too flat because of this effect.

2. Column-density detection is somewhat restrictive, because regions with extinction less than about one magnitude cannot be detected as a decrease in background star density, while at extinctions above about 5–6 magnitudes clouds look black independent of their extinction. The latter effect causes the catalogue to lump clouds of densities above the saturation threshold into the bin of highest column density, again making the apparent probability distribution of cloud densities appear too flat.

3. The increasing number of foreground stars makes it progressively more difficult to detect clouds further than several hundred parsecs. This effect produces an underestimate of the extinction to distant, large, and usually lower-density, clouds.

4. Nearby clouds likely obscure more distant clouds, so that some small clouds located in front of larger clouds are not detected, and so on (Scalo and Lazarian, 1996).

5. Distances to individual clouds detected in extinction are very uncertain. A way around this would be to examine only clouds in nearby complexes, like Taurus, which are all at about the same distance, but then the number of clouds would be small for statistical purposes (Scalo, 1985). Talbot and Newman (1977) assumed they were all at the same distance.

For these reasons we have also derived the *relative* frequency of encounters with regions above a given density using the FCRAO Outer Galaxy Survey of carbon monoxide emission, which gives data for over 10,000 clouds (Heyer et al., 2001). This survey is subject to selection effects analogous to 1 (angular resolution limit) and 2 (CO can only be excited above a density of about 100 cm^{-3} but the [^{12}CO] line saturates at large column densities; also there is a sensitivity threshold on column density) above. The CO sample does not suffer from uncertainties 3–5 above because the clouds are detected using a spectral line, and the velocity information not only separates clouds along the same line of sight but allows distance estimates based on a kinematic model (rotation curve) for the Galaxy. We used the cloud properties from this survey (available electronically) to construct a density probability distribution $n_{\mathrm{cl}}(n)$, but chose to include only clouds with distances less than 5 kpc, since a plot of the number of clouds vs. distance indicated that incompleteness becomes serious

beyond this point. We note that the clouds were identified by decomposition of larger structures, so the catalogue does not contain larger, and on average less dense, regions within which the catalogued clouds were contained (Heyer, private communication). This should not affect our results much because these larger regions have average densities that are mostly below the critical descreening density for any but the most massive parent stars considered here. Following Heyer et al., we take the calculated CO luminosity $L_{\rm CO}$ to be proportional to the mass of the cloud and then divide by the size cubed in order to estimate the average internal density. Following this procedure, we find that $n_{\rm cl}(n)$ declines rapidly with density. If a power law is fit to the histogram, excluding the highest and lowest bins, the cumulative probability distribution function at the high-density end (2×10^3 to 2×10^4 cm^{-3}) has a power-law slope of about -3, similar to the result found for the Lynds clouds. We also find the $R(n) \propto n^{-1}$ for this sample; this result is in part a reflection of the same selection effect as for the Lynds cloud sample, since the surveys tend to be restricted in column density, yielding such a correlation. Nevertheless we adopt it as an average correlation. This gives a density dependence of the cumulative encounter rate of n^{-4}, compared to $n^{-2.4}$ from Talbot and Newman. We also performed the same calculation but assuming all the clouds are at the same distance, to mimic the selection effect due to the unknown distances in Talbot and Newman's calculation, and find that $n_{\rm cl}(> n)$ becomes basically flat, but the distortion should be less severe for Talbot and Newman because the range in distances is smaller.

We can also estimate the *absolute* frequency of descreening events for solar-mass stars from the Heyer et al. (2001) CO cloud catalogue and compare to Talbot and Newman (1977) result for extinction clouds. For the 7900 CO clouds within 5 kpc, we estimate a volume surveyed of 0.86 kpc^3, assuming the clouds are distributed in a uniform disk with a half-thickness of 50 pc, which is close to most estimates for the scale height of the CO distribution perpendicular to the plane of the Galaxy. This yields the total cloud space density $n_{\rm cl}$. Most of these clouds are at average internal densities above 300 cm^{-3} (the number declines rapidly below this density, suggesting selection effects), which is roughly the estimated descreening density for the solar system (Fig. 4.9). The frequency of encounters

is approximately $\nu = \pi \langle R^2 \rangle \, n_{\rm cl} \, \bar{v}$, where $\bar{v}$ is the mean star-cloud velocity (see Talbot and Newman, 1977).[7] We find a mean-square cloud radius $\langle R^2 \rangle = 1.2$ pc^2. Adopting a mean star-cloud velocity of 20 km s^{-1} gives a descreening frequency of 0.7 Gyr^{-1}. This is about six times smaller than obtained from including only the Lynds class 3–6 clouds from Talbot and Newman (1977, Table 1). Since we found that placing the Heyer et al. clouds all at the same distance significantly flattens the $n_{\rm cl}$ distribution, the assumption of a single distance could be part of the discrepancy. A major difference arises from the fact that the mean square sizes in the Lynds sample are much larger than found for the Heyer et al. sample. Such differences are perhaps expected because of the different selection criteria and selection effects (see Heyer et al. 2001 for discussion in the CO sample), and the different distances to which the surveys extend, but this expectation gives us no basis to decide which is the more realistic estimate. The difference should probably be considered a reflection of the inherent uncertainty involved in estimating the descreening frequency. Both results are lower limits because of the resolution effect discussed earlier, by which smaller, denser clouds are missed at larger distances, but we do not know the size of the corresponding correction factor.

Given these considerations, we think that the descreening frequency for the sun cannot be estimated to better than an order of magnitude, but probably lies between 1 and 10 Gyr^{-1}. Since the critical descreening density scales approximately as M^{-2} (eq. 10), and $n_{\rm cl}(> n)$ decreases rapidly with n, we see that the descreening frequency declines extremely rapidly with decreasing stellar mass. Using the dark cloud $n_{\rm cl}(> n)$ power-law slopes found above, we get a mass dependence of M^5, while the CO cloud slopes yield M^8.

It should be pointed out that these results only apply to relatively dense clouds that can be seen in extinction or CO, and we do not know how the frequency scales with density for smaller densities. In addition, our estimated rates for dense regions are probably

[7] Our frequency estimates assume a random distribution of clouds, but are not much changed by the fact that these clouds, as well as those in Lynds (1962) sample, are actually clustered into larger structures. The *mean* encounter frequency is roughly the volume filling fraction of the clouds divided by their radius, and neither of these quantities is affected by clustering as long as the clouds do not overlap. The time series of encounters will be radically different in the clustered case, with long periods without descreening punctuated by clusters of frequent descreenings, but the *average* rate of encounters is similar if taken over a sufficiently long time interval (~ 1 Gyr here). For recent history, however, this clustering effect would be important. We discuss the details of the time history during intrusion into a large complex using hydrodynamic simulations in a separate publication.

underestimates, since both the Lynds and Heyer et al. (2001) cloud catalogues select against dense clouds because of resolution effects, as discussed above.

Since we showed earlier that an M-star planet must encounter a region of density $\sim 2 \times 10^3$ (for M0, $\sim 0.5 M_\odot$) to 3×10^4 (for M9, $\sim 0.1 M_\odot$) cm^{-3} for descreening, while a solar-type star requires only ~ 300 cm^{-3}, the frequency estimates given above imply that descreening will occur 10^2 to 10^9 times less frequently for M-star planets (i.e., never). Even for somewhat higher mass stars, the frequency of descreening is apparently such a strongly decreasing function of density that, given the crude estimate of 1–10 descreening encounters per Gyr for the Earth, even stars of spectral types late G and early K should be relatively immune from descreening.

Bibliography

Abramowitz, M., Stegun, I.A., Eds., 1972. Handbook of Mathematical Functions (Dover: NY).

Adami, C., Ofria, C., Collier, T.C., 2000. Evolution of biological complexity. Proc. Natl. Acad. Sci. 97, 4463–4468.

Alpen, E. L., 1998. Radiation Biophysics. Academic Press, San Diego.

Andreeshchev, A., Scalo, J., Smith, D.S., 2003. Very low-mass M stars as sites for habitability and evolution: The radiation environment. Astrobiology, submitted .

Aschwanden, M.J., in The Many Faces of the Sun: A Summary of the Results from NASA's Solar Maximum Mission, K. T. Strong, J. L. R. Saba, B. M. Haisch, J. T. Schmelz, Eds. (Springer, NY, 1999), pp. 273-300.

Aschwanden, M. J., Tarbell, T. D., Nightingale, R. W., Schrijver, C. J., Title, A., Kankelborg, C. C., Martens, P., Warren, H. P., Jun. 2000. Time variability of the "quiet" Sun observed with TRACE. II. Physical parameters, temperature evolution, and energetics of extreme-ultraviolet nanoflares. Astrophys. J. 535, 1047–1065.

Audard, M., Güdel, M., Drake, J. J., Kashyap, V. L., 2000. Extreme-ultraviolet flare activity in late-type stars. Astrophys. J. 541, 396–409.

Badhwar, G.D., in Shielding Strategies for Human Space Exploration, J. W. Wilson, J. Miller, A. Konradi, F. A. Cucinotta, Eds., NASA Conf. Pub. 3360 (1997), pp. 17-29.

Baker, D.N., Kanekal, S.G., Li, X., Monk, S.P., Goldstein, J., Burch, J.L., 2004. An extreme distortion of the Van Allen belt arising from the "Halloween" solar storm in 2003. Nature. 432, 878–881.

Band, D., Matteson, J., Ford, L., Schaefer, B., Palmer, D., Teegarden, B., Cline, T., Briggs, M., Paciesas, W., Pendleton, G., Fishman, G., Kouveliotou, C., Meegan, C., Wilson, R., Lestrade, P., 1993. BATSE observations of gamma-ray burst spectra. I—Spectral diversity. Astrophys. J. 413, 281–292.

Banks, P.M., Kockarts, G., 1973. Aeronomy: Part A. Academic Press, NY.

Barbon, R., Buondi, V., Cappellaro, E., Turatto, M., 1999. The Asiago Supernova Catalogue—10 years after. Astron. Astrophys. Supp. 139, 531–536.

Battaglia, M., Grigis, P.C., Benz, A.O., 2005. Size dependence of solar X-ray flare properties. Astron. Astrophys. 439, 737–747.

Battista, J.R., 1997. Against all odds: the survival strategies of *Deinococcus radiodurans*. Ann. Rev. Microbiology. 51, 203–224.

Becker, D., Sevilla, M.D., 1993. The chemical consequences of radiation damage to DNA. Adv. Radiation Biol. 17, 121–180.

Begelman, M. C., Rees, M. J., 1976. Can cosmic clouds cause climatic catastrophes. Nature 261, 298–299.

Berezinskii, V.S., Bulanov, S.V., Dogiel, V.A., Ginzburg, V.L., Ptuskin, V.S., 1990. Astrophysics of cosmic rays (North-Holland).

Birk, G.T., Lesch, H. and Konz, C., 2004. Solar wind induced magnetic field around the unmagnetized Earth. Astron. Astrophys., 420. L15–L18.

Bond, I.A., Udalski, A., Jaroszynski, M. and 29 others, 2004. OGLE 2003-BLG-235/MOA 2004-BLG-53: A planetary microlensing event. Astrophys. J. Lett., 606. L155–L158.

Bourke, T.L., Myers, P.C., Robinson, G., and Hyland, A.R., 2001. New OH Zeeman measurements of magnetic field strengths in molecular clouds. Astrophys. J., 554. 916–932.

Boynton, W.V., Feldman, W.C., Squyres, S.W., and 22 others, 2002. Distribution of hydrogen in the near surface of Mars: Evidence for subsurface ice deposits. Science. 297, 81–85.

Brasseur, G.P., Orlando, J.J., Tyndall, G.S., 1999. Atmospheric Chemistry and Global Change. Oxford Univ. Press, NY.

Brenner, D.J. et al., Pub. Natl. Acad. Sci. U.S.A. 100, 13761 (2003).

Bromund, K.R., McTiernan, J.M., and Kane, S.R., 1995. Statistical studies of ISEE 3/ICE observations of impulsive hard x-ray solar flares. Astrophys. J. 455, 733–745.

Brown, R.T., 1973. Ionospheric effects of cosmic gamma-ray bursts. Nature 246, 83–84.

Burger, R.A. and Hattingh, M. (1998) Toward a realistic diffusion tensor for Galactic cosmic rays. Astrophys. J., 505. 244–251.

Butler, P., Vogt, S.S., Marcy, G.W., Fischer, D.A., Wright, J.T., Henry, G.W., Laughlin, G., and Lissauer, J. (2004) A Neptune-mass planet orbiting the nearby M dwarf GJ 436. Astrophys. J., in press. (http://arxiv.org/astro-ph/0408587)

Bzowski, M., Fahr, H.J., and Rucinski, D. (1996) Interplanetary neutral particle fluxes influencing the Earth's atmosphere and the terrestrial environment. Icarus, 124. 209–219.

Cabrera-Juarez, E., Setlow, J.K., 1976. Mutation of *Haemophilus inluenzae* transforming DNA *in vitro* with near-ultraviolet radiation: Action spectrum. Mutation Res. 35, 199–206.

Carr, M.H., 1999. Retention of an Atmosphere on Early Mars. J. Geophys. Res., 104, 21,897–21,909.

Carslaw, K.S., Harrison, R.G., and Kirkby, J. (2002) Cosmic rays, clouds, and climate. Science, 298. 1732–1737.

Cesarsky, C.J., 1980. Cosmic-ray confinement in the Galaxy. Ann. Rev. Astron. Astrophys. 18, 289–319.

Chabrier, G., 2003. Galactic stellar and substellar initial mass function. Pub. Astron. Soc. Pac. 115, 763–795.

Chabrier, G. and Baraffe, I., 2000. Theory of low-mass stars and substellar objects. Ann. Rev. Astron. Astrophys., 38. 337–377.

Chamberlain, J., 1961. Physics of Aurora and Airglow. Acad. Press, NY.

Chamberlain, J.W., 1978. Theory of planetary atmospheres: An introduction to their physics and chemistry. Academic Press, NY.

Champion, K.S.W., Cole, A.E., Kantor, A.J., 1985. Standard and reference atmospheres. In: Jursa, A.S. (Ed.), Handbook of Geophysics and the Space Environment. Air Force Geophysics Lab, Springfield, VA.

Chapman, S., 1931. The absorption and dissociative or ionizing effect of monochromatic radiation in an atmosphere on a rotating Earth. Proceedings of the Physical Society 43, 26–45.

Chassefière, E., Leblanc, F., 2004. Mars atmospheric escape and evolution: Interaction with the solar wind. Plan. Sp. Sci.. 52, 1039–1058.

Chesson, P., Huntly, N., 1997. The roles of harsh and fluctuating conditions in the dynamics of ecological communities. Amer. Natur. 150, 519–553.

Christian, D. J., Mathioudakis, M., Jevremovic, Dupuis, J., Vennes, S., Kawka, A., 2003. The extreme-ultraviolet continuum of a strong stellar flare. Astrophys. J. Lett.. 593, L105–L108.

Christl, M., Mangini, A., Holzkämper, Spötl, C., 2004. Evidence for a link between the flux of galactic cosmic rays and Earth's climate during the past 200,000 years. J. Atmos. Solar-Terr. Phys., 66. 313–322.

Cockell, C.S., 2002. Photobiological uncertainties inthe Archaean and post-Archaean world. Intl. J. Astrobiol. 1, 31–38.

Cockell, C.S. and Airo, A., 2002. On the plausibility of a UV transparent biochemistry. Origin Life Evol. Biosphere. 32, 255–274.

Cockell, C.S., Catling, D.C., Davis, W.L., Snook, K., Kepner, R.L., Lee, P., and McKay, C.P., 2000. The ultraviolet environment of Mars: Biological implications past, present, and future. Icarus. 146, 343–359.

Cordoba-Jabonero, C., Lara, L.M., Mancho, A.M., Márquez, A., Rodrigo, R., 2003. Solar ultraviolet transfer in the Martian atmosphere: Biological and geological implications. Plan. Sp. Sci. 51, 399–410.

C. Cougnet et al., Earth, Moon, and Planets. 92, 279 (2005).

Cravens, T.E., 1997. Physics of Solar System Plasmas. Cambridge Univ. Press, NY.

Cravens, T.E., Maurelis, A.N., 2001. X-ray emission from scattering and fluorescence of solar x-rays at Venus and Mars. Geophys. Res. Lett. 28, 3043–3046.

Crisp, D., 2000. Ionosphere. In: Cox, A.N. (Ed.), Allen's Astrophysical Quantities. Springer, NY, pp. 271–272.

Crosby, N.B., Aschwanden, M.J., Dennis, B.R., 1993. Frequency distributions and correlations of solar X-ray flare parameters. Solar Physics 143, 275–299.

Crosby, N.B., Siegmund, O.H.W., Vedder, P.W., Vallerga, J.V., 1993. Extreme Ultraviolet Explorer deep survey observations of a large flare on AU Microscopii. Astrophys. J. Lett. 414, L49–L52.

Crosby, N., Vilmer, N., Lund, N., Sunyaev, R., 1998. Deka-keV X-ray observations of solar bursts with WATCH/GRANAT: Frequency distributions of burst parameters. Astron. Astrophys. 334, 299–313.

Crutcher, R.M., 1999. Magnetic fields in molecular clouds: observations confront theory. Astrophys. J., 520. 706–713.

Crutzen, P.J., Isaksen, I.S.A., and Reid, G.C., 1975. Solar proton events: stratospheric sources of nitric oxide. Science, 189. 457–458.

Cucinotta, F.A., et al., 2001. Radiat. Res. 156, 682.

Cucinotta, F.A., et al, 2004. Adv. Sp. Res. 34, 1383.

Cully, S.L., Siegmund, O.H.W., Vedder, P.W., Vallerga, J.V., 1993. Extreme Ultraviolet Explorer deep survey observations of a large flare on AU Microscopii. Astrophys. J. Lett. 414, L49–L52.

Danby, J.M.A. and Camm, G.L., 1957. Statistical dynamics and accretion. Mon. Not. Roy. Astron. Soc., 117. 50–71.

De Angelis, G., Clowdsley, M.S., Singleterry, R.C., Wilson, J.W., 2004. Mars radiation environment model with visualization. Adv. Space Res. 34, 1328–1332.

Dehnen, W. and Binney, J.J., 1998. Local stellar kinematics from HIPPARCOS data. Mon. Not. Roy. Astron. Soc., 298. 387–394.

Delfosse, X., Forveille, T., Segransan, D., Beuzit, J.-L., Udry, S., Perrier, C., and Mayor, M., 2000. Accurate masses of very low mass stars. IV. Improved mass-luminosity relations. Astron. Astrophys. 364, 217–224.

Dennerl, K., 2002. Discovery of X-rays from Mars with Chandra. Astron. Astrophys. 394, 1119–1128.

De Visser, J.A.G.M., Hermisson, J., Wagner, G.P., Ancel Meyers, L. and 15 others, 2003. Evolution and the detection of genetic robustness. Evolution, 57. 1959–1972.

Dickinson, H.O., Parker, L., 2002. Int. J. Cancer. 99, 436.

Dion, P., Charbonneau, R., and Thibault, C., 1994. Effect of ionizing dose rate on the radioresistance of some food pathogenic bacteria. Can. J. Microbiol. 40, 369–374.

DiRuggiero, J., Santangelo, N., Nackerdien, Z., Ravel, J., and Robb, F.T., 1997. Repair of extensive ionizing-radiation DNA damage at 95 C in the hyperthermophilic archaeon *Pyrococcus furiosus*. J. Bacteriology. 179, 4643–4645.

Dole, S.H., 1964. Habitable Planets for Man, Blaisdell, New York.

Dubrova, Y.E., 2003. Long-term genetic effects of radiation exposure. Mutation Res. 544, 433–439.

Dubrova, Y.E., et al., 1997. Mutat. Res. 381, 267.

Dyer, C.S., et al., 1996. Adv. Space Res. 17, (2)53.

Edgar, B.C., Miles, W.T., Green, A.E.S., 1973. Energy deposition of protons in molecular nitrogen and applications to proton auroral phenomena. J. Geophys. Res. 78, 6595–6606.

El-Borie, M.A., 2003. Major solar-energetic particle fluxes: I. Comparison with the associated ground level enhancements of cosmic rays. Astroparticle Phys. 19, 549–558.

Elena, S.F. and Lenski, R.E., 2003. Evolution experiments with microorganisms: The dynamics and genetic bases of adaptation. Nature Rev. Gen., 4. 457–469.

Endl, M., Cochran, W.D., Tull, R.G., and MacQueen, P., 2003. A dedicated M swarf planet search using the Hobby-Eberly Telescope. Astrophys. J., 126. 3099–3107.

Evans, D., 1974. Precipitating electron fluxes formed by a magnetic field aligned potential difference. J. Geophys. Res. 79, 2853.

Ewing, D., 1995. Evolution of radiation resistance in *E. Coli*. Biochem. Biophys. Res. Comm. 216, 549–553.

Ewing, D., 1997. Production of radiation-resistant *E. coli* strains by daily X-irradiation. Int. J. Radiat. Biol. 71, 253–258.

Fahr, H.J., 1968. On the influence of neutral interstellar matter on the upper atmosphere. Astrophys. Sp. Sci., 2. 474–495.

Fahr, H.J., Kausch, T., and Schere, H., 2000. A 5-fluid hydrodynamic approach to model the solar system-interstellar medium interaction. Astron. Astrophys. 357, 268–282.

Fano, U., 1963. Penetration of protons, alpha particles, and mesons. Ann. Rev. Nuclear Sci. 13, 1–66.

Farkas, J., 1998. Irradiation as a method for decontaminating food. Int. J. Food Microbiology. 44, 189–204.

Farquhar, J., Wing, B.A., McKeegan, K.D., Harris, J.W., Cartigny, P., Thiemens, M.H., 2002. Mass-independent sulfur of inclusions in diamond and sulfur recycling on early Earth. Science 298, 2369–2372.

Favata, F., Reale, F., Micela, G., Sciortino, S., Maggio, A., Matsumoto, H., 2000. An extreme X-ray flare observed on EV Lac by ASCA in July 1998. Astron. Astrophys. 353, 987–997.

Feder, M.E., Hofmann, G.E., 1999. Heat-shock proteins, molecular chaperones, and the stress response: Evolutionary and ecological physiology. Ann. Rev. Physiol. 61, 243–282.

L. E. Feinendegen, 2005. Br. J. Radiology. 78, 3.

Ferreira, A.C., Nobre, M.F., Moore, E., Rainey, F.A., Battista, J.R., da Costa, M.S., 1999. Characterization and radiation resistance of new isolates of *Rubrobacter radiotolerans* and *Rubrobacter xylanophilus*. Extremophiles. 3, 235–238.

Ferriera, S.E.S. and Potgeiter, M.S., 2004. Long-term cosmic-ray modulation in the heliosphere. Astrophys. J., 603. 744–752.

Ferrière, K.M., 2001. The interstellar environment of our galaxy. Rev. Mod. Phys., 73. 1031–1066.

Feynman, J., Spitale, G., Wang, J., Gabriel, S., 1993. J. Geophys. Res. 98, 13281.

Feynman, J., Ruzmaikin, A., Berdichevsky, V., 2002. J. Atmos. Solar-Terr. Phys. 64, 1679.

Fielden, E.M., and O'Neill, P., 1991. The Early Effects of Radiation on DNA. Springer, Berlin.

Fisher, R.A., 1958. The Genetical Theory of Natural Selection. Dover, NY.

Florinski, V., Pogorelov, N.V., Zank, G.P., Wood, B.E. and Cox, D.P., 2004. On the possibility of a strong magnetic field in the local interstellar medium. Astrophys. J., 604. 700–706.

Florinski, V., Zank, G.P., and Axford, W.I., 2003. The Solar System in a dense interstellar cloud: Implications for cosmic-ray fluxes at Earth and ^{10}Be records. Geophys. Res. Lett., 30. 2206–2210.

Florinski, V., Zank, G.P., and Pogorelov, N.V., 2003. Galactic cosmic ray transport in the global heliosphere. J. Geophys. Res., 108(A6). 1228–1243.

Forster, L., Forster, P., Lutz-Bonengel, S., Willkomm, H., and Brinkmann, B., 2002. Natural radioactivity and human mitochondrial DNA mutations. PNAS 99, 13950–13954.

Foukal, P., 1990. Solar Astrophysics. John Wiley & Sons, NY.

Fox, J.L., Victor, G.A., 1988. Electron energy deposition in N_2 gas. Plan. Sp. Sci. 36, 329–352.

Friedberg, E.C., 2003. DNA damage and repair. Nature. 421, 436–440.

Frisch, P.C., 2006. Introduction: Paleoheliosphere versus paleoLISM. http://arxiv.org/astro-ph/0601356.

Frisch, P.C., Muller, H.R., Zank, G.P. and Lopate, C., 2005. Galactic environment of the sun and stars: Interstellar and interplanetary material. In Astrophysics of Life, in press.

de la Fuente Marcos, R. and de la Fuente Marcos, C., 2004. On the recent star formation history of the Milky Way disk. New Astron., 9. 475–502.

Gallagher, P.T., Moon, Y.-J., Wang, H., 2002. Sol. Phys. 182, 497.

Garcia-Munoz, M., Mason, G.M., and Simpson, J.A., 1975. The anomalous ^{4}He component in the cosmic-ray spectrum at $\lesssim$ 50 MeV per nucleon during 1972–1974. Astrophys. J., 202. 265–275.

Gaustad, J.E. and Van Buren, D., 1993. The distribution of interstellar dust in the solar system. Pub. Astron. Soc. Pacific, 105. 1127–1140.

Gehrels, N., et al., 2003. Ozone depletion from nearby supernovae. Astrophys. J. 585, 1169–1176.

Gershberg, R.E., Katsova, M.M., Lovkaya, M., Terebizh, A.V., Shakhovskaya, N.I., 1999. Catalogue and bibliography of the UV Ceti-type flare stars and related objects in the solar vicinity. Astron. Astrophys. Suppl. Ser. 139, 555–558.

Gershberg, R.E., Shakhovskaya, N.I., 1983. Characteristics of activity energetics of the UV Ceti-type flare stars. Astrophys. Sp. Sci. 95, 235–253.

Getselev, I., et al., 2004. Adv. Sp. Res. 34, 1429.

Giacalone, J. and Jokipii, J.R., 1999. The transport of cosmic rays across a turbulent magnetic field. Astrophys. J., 520. 204–214.

Gillespie , J.H., 1998. Population Genetics: A Concise Guide. Johns Hopkins Univ. Press, Baltimore.

Giraud, A., Matic, I., Tenaillon, O., Clara, A., Radman, M., Fons, M., Taddei, F., 2001. Costs and benefits of high mutation rates: Adaptive evolution of bacteria in the mouse gut. Science 291, 2606–2608.

Golub, L., Pasachoff, J.M., 1997. The Solar Corona. Cambridge Univ. Press, NY.

Gombosi, T.I., 1998. Physics of the Space Environment. Cambridge Univ. Press, NY.

Gomez, F., Miikkulainen, R., 1997. Incremental evolution of complex general behavior. Adaptive Behavior 5, 317–342.

Gonzalez, G., Brownlee, D., Ward, P., 2001. The Galactic habitable zone: Galactic chemical evolution. Icarus 152, 185–200.

Gopalswamy, N., et al., 2005. J. Geophys. Res., 110, A09S00.

Gredel, R., Lepp, S., Dalgarno, A., Herbst, E., 1989. Cosmic-ray-induced photodissociation and photoionization rates of interstellar molecules. Astrophys. J. 347, 289–293.

Güdel, M., Audard, M., Kashyap, V.L., Drake, J.J., Guinan, E.F., 2003. Are coronae of magnetically active stars heated by flares? II. Extreme ultraviolet and X-ray flare statistics and the differential emission measure distribution. Astrophys. J. 582, 423–442.

Guinan, E.F., Ribas, I., 2002. Our changing sun: The role of solar nuclear evolution and magnetic activity on Earth's atmosphere and climate. In: Montesinos, B., Gimenez, A., Guinan, E.F. (Eds.), The Evolving Sun and its Influence on Planetary Environments. Vol. 269. Astro. Soc. Pac., San Francisco, pp. 85–106.

Gunell, H., Holstrom, M., Kallio, E., Janhunen, P., Dennerl, K., 2004. X rays from solar wind charge exchange at Mars: A comparison of simulations and observations. Geophys. Res. Lett. 31, L22801–L22804.

Haberle, R.M., McKay, C.P., Tyler, D., and Reynolds, R., 1994. Can synchronously rotating planets support an atmosphere? In Circumstellar Habitable Zones: Proceedings of the First International Conferrence, ed. L. Doyle, Travis House Publications, Menlo Park, CA, pp. 29–34.

Haberle, R.M., Tyler, D., McKay, C.P., Davis, W.L., 1994. A model for the evolution of CO_2 on Mars. Icarus 109, 102–120.

Haisch, K.E., Lada, E.A., and Lada, C.J., 2001. Disk frequencies and lifetimes in young clusters. Astrophys. J. Lett., 553. L153–L156.

Haisch, B., Strong, K.T., Rodono, M.A., 1991. Ann. Rev. Astron. Astrophys. 29, 275.

Hall, E.J., 2004. Int. J. Radiat. Biol., 80, 327.

Hammersley, J.M., Handscomb, D.C., 1979. Monte Carlo Methods. Chapman and Hall, London.

Hanslmeier, A., 2002. The Sun and Space Weather. Kluwer, Dordrecht.

Hartmann, D.L., 1993. "Radiative effects of clouds on the Earth's climate in aerosal-cloud-climate interactions." In P.V. Hobbs (ed.), Aerosol-Cloud-Climate Interactions, Academic Press, pp. 151.

Hawley, S.L., Pettersen, B.R., 1991. The great flare of 1985 April 12 on AD Leonis. Astrophys. J. 378, 725–741.

Heath, M.J., Doyle, L.R., Joshi, M.M., Haberle, R.M., 1999. Habitability of planets around red dwarf stars. Origins Life Evol. Biosphere 29, 405–424.

Henke, B.L., Gullikson, E.M., Davis, J.C., 1993. X-ray interactions: Photoabsorption, scattering, transmission, and reflection at E = 50-30,000 eV, Z = 1-92. Atomic Data and Nuclear Data Tables 54, 181–342.

Henry, T.J., Franz, O.G., Wasserman, L.H., Benedict, G.F., Shelus, P.J., Ianna, P.A., Kirkpatrick, J.D., and McCarthy, D.W., 1999. The optical mass-luminosity relation at the end of the main sequence (0.08–0.20 $M_{\odot}$). Astrophys. J., 512. 864–873.

Heyer, M.H., Carpenter, J.M., and Snell, R.L., 2001. The equilibrium state of molecular regions in the outer Galaxy. Astrophys. J., 551. 852–866.

Hillenbrand, L.A. and White, R.J., 2004. An assessment of dynamical mass constraints on pre-main-sequence evolutionary tracks. Astrophys. J., 604. 741–757.

Höflich, P., Wheeler, J.C., Khokhlov, A., 1998. Hard X-rays and gamma rays from type Ia supernovae. Astrophys. J. 492, 228–245.

Holzer, T.E., 1989. Interaction between the solar wind and the interstellar medium. Ann. Rev. Astron. Astrophys., 27. 199–234.

Hoyle, F., and Lyttleton, R.A., 1939. The effect of interstellar matter on climatic variations, Proc. Camb. Phil. Soc. Math. Phys. Sci., 35, 405–415.

Huber, K.P., Herzberg, G., 1979. Molecular Spectra and Molecular Structure. IV. Constants of Diatomic Molecules. van Nostrand Reinhold, NY.

Hudson, H.S., 1991. Solar flares, microflares, nanoflares, and coronal heating. Solar Phys. 133, 357–369.

Hut, P., Tremaine, S., 1985. Have interstellar clouds disrupted the Oort comet cloud? Astron. J., 90. 1548–1557.

Ingersoll, A.P., 1969. The Runaway Greenhouse: A History of Water on Venus. J. of Atmos. Sci. 26, 1191–1198.

Ip, W.-H. and Axford, W.I., 1985. Estimates of galactic cosmic ray spectra at low energies. Astron. Astrophys., 149. 7–10.

Isenberg, P.A., 1986. Interaction of the solar wind with interstellar neutral hydrogen: Three-fluid model. J. Geophys. Res., 91(A9). 9965–9972.

Itoh, T., Martin, W., Nei, M., 2002. Acceleration of genomic evolution caused by enhanced mutation rate in endocellular symbionts. Proc. Natl. Acad. Sci. 99, 12944–12948.

Jagger, J., 1985. Solar-UV actions on living cells. Prager Publ., NY.

Jakosky, B.M. and Phillips, R.J., 2001. Mars' Volatile and Climate History. Nature, 412, 237–244.

Johnson, A.S., Golightly, M.J., Weyland, M.D., Lin, T., Zapp, E.N., 2005. Adv. Sp. Res. 36, 2524.

Jokipii, J.R., 1999. Summary talk: The transport of Galactic and anomalous cosmic rays in the heliosphere. Adv. Sp. Res., 23. 617–626.

Jones, A.V.J., 1974. Aurora. Reidel, Dordrecht.

Joshi, M., 2003. Climate Model Studies of Synchronously Rotating Planets. Astrobiology 3, 415–428.

Joshi, M.M., Haberle, R.M., Reynolds, R.T., 1997. Simulations of the atmospheres of synchronously rotating terrestrial planets orbiting M dwarfs: Conditions for atmospheric collapse and the implications for habitability. Icarus 129, 450–465.

Kalas, P., Liu, M.C., Matthews, B.C., 2004. Discovery of a large dust disk around the nearby star AU Microscopii. Science, 303. 1990–1992.

Kallman, T.R., McCray, R., 1982. X-ray nebular models. Astrophys. J. Supp. 50, 263–317.

Kalos, M.H., Whitlock, P.A., 1986. Monte Carlo Methods, Vol. I: Basics. Wiley, NY.

Kanbach, G., Bertsch, D.L., Fichtel, C.E., and 7 others, 1993. Detection of a long-duration solar gamma-ray flare on June 11, 1991 with EGRET on COMPTON-GRO. Astron. Astrophys. Supp. 97, 349–353.

Karam, P.A., 2002. Gamma and neutrino radiation dose from gamma ray bursts and nearby supernovae. Health Physics 82, 491.

Kasting, J.F., 1988. Runaway and moist greenhouse atmospheres and the evolution of earth and Venus. Icarus 74, 472–494.

Kasting, J.F., Donahue, T.M., 1980. The evolution of atmospheric ozone. J. Geophys. Res. 85, 3255–3263.

Kasting, J.F., Holland, H.D., Pinto, J.P., 1985. Oxidant abundances in rainwater and the evolution of atmospheric oxygen. J. Geophys. Res. 90, 10497.

Kasting, J.F., Whitmire, D.P., Reynolds, R.T., 1993. Habitable zones around main sequence stars. Icarus 101, 108–128.

Kasturirangan, K., Rao, U.R., Rastogi, R.G., Chakravarty, S.C., Sharma, D.P., 1976. Ionospheric effects of transient celestial X-ray and gamma-ray events. Astrophys. and Sp. Sci. 42, 57–62.

Kewley, L.J., Geller, M.J., Jansen, R.A., 2004. [OII] as a star formation rate indicator. Astron. J. 127.

Kirkby, J., Mangini, A., Muller, R.A., 2004. The glacial cycles and cosmic rays. Earth Plan. Sci. Lett., submitted. (http://arxiv.org/physics/0407005)

Kolb, V.M., Dworkin, J.P., and Miller, S.L., 1994. Alternative bases in the RNA world: The prebiotic synthesis of urazole and its ribosides. J. Mol. Evol. 38, 549–557.

Kopylov, V.M., Bonch-Osmolovskaya, E.A., Svetlichnyi, V.A., Miroshnichenko, M.L., and Skobkin, V.S., 1993. Gamma-irradiation resistance and UV-sensitivity of extremely thermophilic archaebacteria and eubacteria. Mikrobiologiya. 62, 90–95.

Krucker, S., Lin, R.P., 2002. Relative timing and spectra of solar flare hard X-ray sources. Solar Phys. 210, 220–243.

Kulsrud, R.M., 2005. Plasma physics for astrophysics (Princeton).

Kulsrud, R., Pearce, W.P., 1969. The effect of wave-particle interactions on the propagations of cosmic rays. Astrophys. J., 156. 445–469.

Labrosse, S., 2004. Thermal and magnetic evolution of the Earth's core. Phys. Earth Plan. Int., 140. 127–143.

Labrosse, S., Poirier, J.-P., and Le Mouel, J.-L., 2001. The age of the inner core. Earth Plan. Sci. Lett., 190. 111–123.

Lammer, H., Selsis, F. Ribas, I., Guinan, E.F., Bauer, S.J., and Weiss, W.W. (2004) Atmospheric loss of exoplanets resulting from stellar X-ray and extreme-ultraviolet heating. Astrophys. J., 598. L121

Lang, K.R., 2000. The Sun from Space. Springer-Verlag, NY.

Larkin, A., Haigh, J.D., Djavidnia, S., 2000. The effect of solar UV irradiance variations on the Earth's atmosphere. Sp. Sci. Rev. 94, 199–214.

Larson, R.B., 1981. Turbulence and star formation in molecular clouds. Mon. Not. Roy. Astron. Soc., 194. 809–826.

Laughlin, G., Bodenheimer, P., and Adams, F.C., 2004. The core accretion model predicts few Jovian-mass planets orbiting red dwarfs. Astrophys. J., 612. L73–L76.

Laut, P., 2003. Solar activity and terrestrial climate: an analysis of some purported correlations, J. Atmos. Solar-Terrestrial Physics, 65. 801–812.

Leblanc, F., Johnson, R.E., 2001. Sputtering of the Martian atmosphere by solar wind pick-up ions. Plan. Sp. Sci. 49, 645–656.

Lee, M.A., 1997. "Effects of cosmic rays and interstellar gas on the dynamisc of a wind." In: Cosmic Winds and the Heliosphere. Jokipii, J.R., Sonett, C.P., Giampapa, M.S. (Eds.) (Arizona: Tucson), pp. 857–886.

Lee, T.T., Petrosian, V., and McTiernan, J.M., 1993. The distribution of flare parameters and implications for coronal heating. Astrophys. J.. 412, 401–409.

Leggett, S.K., Allard, F., Geballe, T.R., Hauschildt, P.H., and Schweitzer, A., 2001) Infrared spectra and spectral energy distributions of late M and L dwarfs. Astrophys. J., 548. 908–918.

Levy, M., Miller, S.L., 1998. The stability of the RNA bases: Implications for the origin of life. Proc. Natl. Acad. Sci. 95, 7933–7938.

Liebert, J., Kirkpatrick, J.D., Reid, I.N., Fisher, M.D., 1999. A 2MASS ultracool M dwarf observed in a spectacular flare. Astrophys. J. 519, 345–353.

Lin, R.P., Feffer, P.T., Schwartz, R.A., 2001. Solar hard X-ray bursts and electron acceleration down to 8 keV. Astrophys. J. Lett. 557, L125–128.

Lingenfelter, R.E., Hudson, H.S., 1980. In The Ancient Sun (Pergammon Press), pp. 69–79.

Lingenfelter, R.E., Rothschild, R.E., 2000. Gamma-ray and neutrino astronomy. In: Cox, A.N. (Ed.), Allen's Astrophysical Quantities. Springer, NY, pp. 215–234.

Liu, M.C., 2004. Substructure in the circumstellar disk around the young star AU Mic (GJ 803). Science, 305. 1442–1444.

Liu, M.C., Najita, J. and Tokunaga, A.T., 2003. A survey for circumstellar disks around young substellar objects. Astrophys. J., 585. 372–391.

Lodders, K., and Fegley, B., 1998. The Planetary Scientist's Companion. Oxford Univ. Press, NY.

Lofthus, A., Krupenie, P.H., 1977. The spectrum of molecular nitrogen. J. Phys. Chem. Ref. Data 6, 113–307.

Longair, M., 1992. High Energy Astrophysics (Cambridge Univ. Press).

Lu, Q.-B., Sanche, L., 2001. Effects of cosmic rays on atmospheric chlorofluorocarbon dissociation and ozone depletion. Phys. Rev. Lett., 87. 078507(1–4).

Luhmann, J.G., Johnson, R.E., and Zhang, M.G.H., 1992. Evolutionary Impact of Sputtering of the Martian Atmosphere by O+ Pick Up Ions. Geophys. Res. Lett. 19, 2151–2154.

Lynds, B.T., 1962. Catalogue of dark nebulae. Astrophys. J. Supp., 7. 1–60.

Maíz-Apellániz, J., 2001. The Origin of the Local Bubble. Astrophys. J., 560. L83–L86.

Mancinelli, R.L., and Klovstad, M., 2000. Martian soil and UV radiation: microbial viability assessment on spacecraft surfaces. Plan. Sp. Sci. 48, 1093–1097.

Marcy, G.W., Butler, R.P., Fischer, D., Vogt, S.S., Lissauer, J.J., and Rivera, E.J., 2001. A pair of resonant planets orbiting GJ 876. Astrophys. J., 556. 296–301.

Marsden, D. and Lingenfelter, R.E., 2003. Solar activity and cloud opacity variations: A modulated cosmic ray ionization model. J. Atmos. Sciences, 60. 626–636.

Marsh, N. and Svensmark, H., 2003. Solar influence on Earth's climate. Space Sci. Rev., 107. 317–325.

Martin, S.F., 1980. Solar Phys. 68, 217.

Matsumoto, M., Nishimura, T., 1998. A 623-dimensionally equidistributed uniform pseudo-random number generator. ACM Trans. on Modeling and Computer Simulation 8, 3–27.

McCracken, K.G., et al., 2001. J. Geophys. Res. 106, 21585.

McCrea, W.H., 1975. Ice ages and the Galaxy. Nature, 255. 607–609.

McKay, C.P., 1985. Noctilucent cloud formation and the effects of water vapor variability on temperatures in the middle atmosphere. Planet. Space Sci., 33. 761–771

McKay, C.P. and Thomas, G.E., 1978. Consequences of a past encounter of the Earth with an interstellar cloud. Geophys. Res. Lett., 5. 215–218.

Melott, A.L., Lieberman, B.S., Laird, C.M., Martin, L.D., Medvedev, M.V., Thomas, B.C., Cannizzo, J.K., Gehrels, N., Jackman, C.H., 2004. Did a gamma-ray burst initiate the late Ordovician mass extinction? Intl. J. Astrobio. in press.

Meyers, L.A. and Bull, J.J., 2002. Fighting change with change: adaptive variation in an uncertain world. Trends Ecol. Evol., 17. 551–557.

Michod, R.E., Wojciechowski, M.F., 1994. DNA repair and the evolution of transformation in the bacterium Bacillus subtilis. IV. DNA damage increases transformation. J. Evol. Bio. 7, 147–175.

Mileikowsky, C., Cucinotta, F.A., Wilson, J.W., and 7 others, 2000. Natural transfer of viable microbes in space. 1. From Mars to Earth and Earth to Mars. Icarus. 145, 391–427.

Miroshnichenko, L.I., 2003. Radiation Hazard in Space (Kluwer, Dordrecht).

Miroshnichenko, L.I., Mendoz, B., Perez Enriquez, R., 2001. Solar Phys. 202, 151.

Mitchner, M., Kruger, C.H., 1973. Partially Ionized Gases. John Wiley & Sons, NY.

Molina-Cuberos, G.J., Stumptner, W., Lammer, H., Komle, N.I., 2001. Cosmic ray and UV radiation models on the ancient Martian surface. Icarus 154, 216–222.

Mori, M., 1997. The Galactic diffuse gamma-ray spectrum from cosmic-ray proton interactions. Astrophys. J., 478. 223–232.

Moriarty, D.E., Miikkulainen, R., 1995. Discovering complex Othello strategies through evolutionary neural networks. Conn. Sci. 7, 195–209.

Moriarty, D.E., Miikkulainen, R., 1999. Learning sequential decision tasks through symbiotic evolution of neural networks. In: Honavar, V., Patel, M., Balakrishnan, K. (Eds.), Advances in the Evolutionary Synthesis of Neural Systems. MIT Press, Cambridge, pp. 367–382.

Moxon, E.R., Rainey, P.B., Nowak, M.A., Lenski, R.E., 1994. Adaptive evolution of highly mutable loci in pathogenic bacteria. Curr. Biol. 4, 23–33.

Mullan, D.J., Mathioudakis, M., 2000. Extreme-ultraviolet flares in an F2 star. Astrophys. J. 544, 475–480.

Muller, E.B. and Nisbet, R.M., 2000. Survival and production in variable resource environments. Bull. Math. Biol., 62. 1163–1189.

Nagylaki, T., 1992. Introduction to Theoretical Population Genetics. Springer-Verlag, NY.

Nilsson, A., 1996. Ultraviolet Reflections: Life under a Thinning Ozone Layer. Wiley & Sons, NY.

O'Brien, K., 2005. Adv. Sp. Res., 26, 1731.

Omongain, E., Baird, G.A., 1976. Ionospheric techniques for the detection of transient X- and gamma-ray bursts. Astrophys. and Sp. Sci. 42, 63–67.

Padoan, P. and Scalo, J., 2005. Confinement-driven spatial variations in the cosmic ray flux. Astrophys. J. Lett. 624, L97–L100.

Pagano, I., Ventura, R., Rodono, M., Peres, G., Micela, G., 1997. A major optical flare on the recently discovered X-ray active dMe star G 102-21. Astron. Astrophys. 318, 467–471.

Pallé, E., Butler, C.J., O'Brien, K., 2004. The possible connection between ionization in the atmosphere by cosmic rays and low level clouds. J. Atmos. Solar-Terr. Phys., 66, 1779–1790.

Parhi, S., Bieber, J.W., and Matthaeus, W.H., 2003. Toward an ab initio theory of the solar modulation of cosmic rays. Astrophys. J., 585. 502–515.

Parker, E.N., 1963. Interplanetary dynamical processes (NY: Wiley), pp. 113–128.

Parker, E.N., 1965. The passage of energetic charged particles through interplanetary space. Plan. Sp. Sci., 13. 9–49.

Paul, N.D., Gwynn-Jones, D., 2003. Ecological roles of solar UV radiation: Towards an integrated approach. Trends Ecology Evol. 18, 48–55.

Pauls, H.L., Zank, G.P., Williams, L.L., 1995. Interaction of the solar wind with the local interstellar medium. J. Geophys. Res., 100(A11). 21,595–21,604.

Pavlov, A.K., Blinov, A.V., Konstantinov, A.N., 2002. Sterilization of Martian surface by cosmic radiation. Plan Sp. Sci. 50, 669–673.

Pavlov, A.A., Pavlov, A.K., Mills, M.J., and Ostryakov, V.M., 2005a. Catastrophic ozone loss during passage of the Solar system through an interstellar cloud. Geophys. Res. Lett., 32. L01815–L01818.

Pavlov, A.A., Toon, O.B., Pavlov, A.K., Bally, J., and Pollard, D., 2005b. Passing through a giant molecular cloud: "Snowball" glaciations produced by interstellar dust. Geophys. Res. Lett., 32. L03705–L03708.

Peak, I.R.A., Jennings, M.P., Hood, D.W., Bisercic, M., Moxon, E.R., 1996. Tetrameric reeat units associated with virulence factor phase variation in Haemophilus also occur in Neisseria spp. and Moraxella catarrhalis. FEMS Microbiol. Lett. 137, 109.

Pearce, G., et al., 1993. Astrophys. Sp. Sci., 208, 99.

Peterson, W.K., Beaty, E.C., Opal, C.B., 1972. Measurements of energy and angular distributions of secondary electrons produced in electron-impact ionization of helium. Phys. Rev. A 5, 712–723.

Peterson, W.K., Opal, C.B., Beaty, E.C., 1971. Energy distributions of electrons ejected in ionizing collisions of electrons with helium. J. Physics B 4, 1020–1025.

Pinaud, R., Tremere, L.A., Penner, M.R., Hess, F.F., Robertson, H.A., Currie, R.W., 2002. Complexity of sensory environment drives the expression of candidate-plasticity gene, nerve growth factor induced-A. Neuroscience 112, 573–582.

Prasad, S.S., Tarafdar, S.P., 1983. UV radiation field inside dense clouds—its possible existence and chemical implications. Astrophys. J. 267, 603–609.

Preece, R.D., Briggs, M.S., Mallozzi, R.S., Pendleton, G.N., Paciesas, W.S., Band, D.L., 2000. The BATSE gamma-ray burst spectral catalog. I. High time resolution spectroscopy of bright bursts using high energy resolution data. Astrophys. J. Supp. 126, 19–36.

Press, W.H., Teukolsky, S.A., Vetterling, W.T., and Flannery, B.P., 1992. Numerical Recipes in C: The Art of Scientific Computing, 2nd ed., Cambridge Univ. Press, Cambridge, pp. 358–359.

Pugliucci, M., 2002. Buffer zone. Nature 417, 598.

Qiu, J., Liu, C., Gary, D.E., Nita, G.M., Wang, H., 2004. Hard X-ray and microwave observations of microflares. Astrophys. J.. 612, 530–545.

Quillardet, P., Rouffaud, M.A., and Bouige, P., 2003. DNA array analysis of gene expression in response to UV irradiation in *Escherichia Coli*. Res. Microbiol. 154, 559–572.

Radman, M., Matic, I., Taddei, F., 1999. Evolution of evolvability. Ann. NY Acad. Sci 870, 146–155.

Radman, M., Taddei, F., Matic, I., 2000. Evolution-driving genes. Res. Microbiol. 151, 91–95.

Rahmstorf, S. Archer, D. and 10 others, 2004. Cosmic rays, carbon dioxide and climate. Eos-Transactions AGU, 85. 38–41.

Rainey, P.B., Travisano, M., 1998. Adaptive radiation in a heterogeneous environment. Nature 394, 69–72.

Randall, C.E., Harvey, V.L., and 9 others, 2005. Stratospheric effects of energetic particle precipitation in 2003–2004. Geophys. Res. Lett, 32. L05802–L050805.

Ratkiewicz, R., 1992. An analytical solution for the heliopause boundary and its comparison with numerical solutions. Astron. Astrophys., 255. 383–387.

Reames, D.V., 1999. Sp. Sci. Rev. 90, 413.

Reames, D.V., et al., 1997. Astrophys. J. 491, 414.

Redfield, S., Linsky, J.L., 2000. The three-dimensional structure of the warm local interstellar medium. II. The Colorado model of the local interstellar cloud. Astrophys. J., 534. 825–837.

Reedy, R.C., 1996. In Solar Drivers of Interplanetary and Terrestrial Disturbances, K. S. Balasubramaniam, S. L. Kell, R. N. Smartt, Eds. (ASP Press, San Francisco), p. 429.

Reedy, R.C., Arnold, J.R., Lal, D., 1983. Cosmic-ray record in solar system matter. Science. 219, 127–135.

Reid, I.N., Gizis, J.E., and Hawley, S.L., 2002. The Palomar/MSU nearby star spectroscopic survey. IV. The luminosity functon in the solar neighborhood and M dwarf kinematics. Astron. J., 124. 2721–2738.

Reznick, D.N., Shaw, F.H., Rodd, F.H., Shaw, R.G., 1997. Evaluation of the rate of evolution in natural populations of guppies (*Poecilia reticulata*). Science 275, 1934–1937.

Rocha-Pinto, H.J., Flynn, C., Scalo, J., Hänninen, J., Maciel, W.J., and Hensler, G., 2004. Chemical enrichment and star formation in the Milky Way disk. III. Chemodynamical constraints. Astron. Astrophys., 423. 517–535.

Rohwer, R.G., 1984. Scrapie infectious agent is virus-like in size and susceptibility to inactivation. Nature. 308, 658–662.

Ross, R.R., 1979. Spectral formation in compact X-ray sources. Astrophys. J. 233, 334–343.

Ross, R.R., Fabian, A.C., 1993. The effects of photoionization on X-ray reflection spectra in active galactic nuclei. Mon. Not. Royal. Astron. Soc. 261, 74–82.

Ross, A.J., et al., 1997. In Shielding Strategies for Human Space Exploration, J. W. Wilson, J. Miller, A. Konradi, F. A. Cucinotta, Eds., NASA Conf. Pub. 3360 (1997), pp. 283–296.

Rothschild, L.J., 1999. Enigmatic microorganisms and life in extreme environments. In: Seckbach, J. (Ed.), Microbes and Radiation. Kluwer, Dordrecht, pp. 551–562.

Rubenstein, E.P., and Schaefer, B.E., 2000. Are superflares on solar analogues caused by extrasolar planets? Astrophys. J. 529, 1031–1033.

Ruderman, M.A., 1974. Possible consequences of nearby supernova explosions for atmospheric ozone and terrestrial life. Science 184, 1079–1081.

Russell, A.D., 1982. The destruction of bacterial spores. Academic Press, New York.

Rutherford, S.L., Lindquist, S., 1998. Hsp90 as a capacitor for morphological evolution. Nature 396, 336–342.

Ryan, J.M., 2000. Long-duration solar gamma-ray flares. Sp. Sci. Rev. 93, 581–610.

Sagan, C., Chyba, C., 1997. The early faint sun paradox: Organic shielding of ultraviolet-labile greenhouse gases. Science 276, 1217–1221.

Saganti, P.B., Cucinotta, F.A., Wilson, J.W., Simonsen, L.C., Zeitlin, C., 2004. Radiation climate map for analyzing risks to astronoauts on the Mars surface from galactic cosmic rays. Sp. Sci. Rev. 110, 143–156.

Sankaranarayanan, K., 1982. Genetic Effects of Ionizing Radiation in Multicellular Eukaryotes and the Assessment of Genetic Radiation Hazards in Man (Elsevier Biomedical, Amsterdam).

Sankaranarayanan, K., Chakraborty, R., 2000. Ionizing radiation and genetic risks. XI. The doubling dose estimates from the mid-1950s to present and the conceptual change to the use of human data on spontaneous mutation rates and mouse data on induced mutation rates for doubling dose calculations. Mutat. Res. 453, 107–127.

Sankaranarayanan, K., Chakraborty, R., 2001. Radiat. Res. 156, 648.

Satoh, C., et al., 1996. Environ. Health Perspect. 104, Suppl. 3, 511.

Scalo, J.M., 1985. Fragmentation and hierarchical structure in the interstellar medium. In *Protostars and Planets II*, ed. D.C. Black and M.S. Matthews, Univ. Ariz. Press, pp. 201–296.

Scalo, J.M. and Lazarian, A., 1996. Occlusion effects and the distribution of interstellar cloud sizes and masses. Astrophys. J., 469. 189–193.

Scalo, J., Wheeler, J.C., 2002. Astrophysical and astrobiological implications of gamma-ray burst properties. Astrophys. J. 566, 723–737.

Scalo, J., Wheeler, J.C., Williams, P., 2004. Intermittent jolts of galactic UV radiation: mutagenetic effects. In: Celnikier, L.M., Tron Thon Van, J. (Eds.), Frontiers of Life. Gioi, Vietnam, pp. 221–228.

Schaefer, B.E., King, J.R., Deliyannis, C.P., 2000. Superflares on ordinary solar-type stars. Astrophys. J. 529, 1026–1030.

Scherer, K., Fichtner, H., and Stawicki, O., 2002. Shielded by the wind: the influence of the interstellar medium on the environment of the Earth. J. Atmospher. Solar-Terr. Phys., 64. 795–804.

Schimmerling, W., Wilson, J.W., Nealy, J.E., Thibeault, S.A., Cucinotta, F.A., Shinn, J.L., Kim, M., Kiefer, R., 1996. Shielding against Galactic cosmic rays. Adv. Sp. Res. 17, (2)31–(2)36.

Schuerger, A.C., Mancinelli, R.L., Kern, R.G., Rothschild, L.J., McKay, C.P., 2003. Survival of endospores of Bacillus subtilis on spacecraft surfaces under simulated martian environments: Implications for the forward contamination of Mars. Icarus. 165, 253–276.

Schuster, A., 1905. Radiation through a foggy atmosphere. Astrophys. J. 21, 1–22.

Seager, S., Sasselov, D.D., 1998. Extrasolar giant planets under strong stellar irradiation. Astrophys. J. Lett. 502, L157–L161.

Setlow, R.B., Pollard, E.C., 1962. Molecular Biophysics. Addison-Wesley, Reading, MA.

Shakhovskaya, N.I., 1995. Flare activity among nearby stars. In: Greiner, J., Duerbeck, H.W., Gershberg, R.E. (Eds.), Flares and Flashes: Proc. IAU Colloq. Vol. 151. Springer, NY, pp. 61–62.

Shalchi, A., Bieber, J.W., and Matthaeus, W.H., 2004. Analytic forms of the perpendicular diffusion coefficient in magnetostatic turbulence. Astrophys. J., 604. 675–686.

Shapley, H., 1921. Note on a possible factor in changes of geological climate. J. Geology, 29.

Shaviv, N.J., 2002. Cosmic ray diffusion from the Galactic spiral arms, iron meteorites, and a possible climatic connection. Phys. Rev. Lett., 89. 051102.

Shaviv, N.J., 2003. The spiral structure of the Milky Way, cosmic rays, and ice age epochs on Earth. New Astron., 8. 39–77.

Shaviv, N.J., 2004. On climate response to changes in the cosmic ray flux and radiative budget. J. Geophys. Res., in press. (http://arxiv.org/physics/0409123)

Shaviv, N.J. and Veizer, J., 2003. Celestial driver of Phanerozoic climate? GSA Today, 13. 4–10.

Shea, M.A., Smart, D.F., 1990. Solar Phys. 127, 297.

Shea, M.A., Smart, D.F., 1996. Solar proton fluxes as a function of the observation location with respect to the parent solar activity. Adv. Space Res. 17, 225–228.

Shea, M.A., Smart, D.F., 2000. Sp. Sci. Rev. 93, 211.

Shklovskii, I.S., Sagan, C., 1966. Intelligent Life in the Universe. Holden-Day, San Francisco.

Shklovsky, I.S., 1969. Supernovae. John Wiley & Sons. Ltd, NY.

Simnett, G.M., 1993. Adv. Sp. Res. 13, 133.

Simnett, G.M., 1999. In The Many Faces of the Sun: A Summary of the Results from NASA's Solar Maximum Mission, K. T. Strong, J. L. R. Saba, B. M. Haisch, J. T. Schmelz, Eds. (Springer, NY), pp. 201-229.

Silberberg, R., Tsao, C.H., 1979. In Proc. 26th Int. Cosmic Ray Conf. (Kyoto, Japan), 5, 317.

Silberberg, R., et al., 1987. Adv. Space Res. 4, 143.

Smith, E.J., Marsden, R.G., and 10 others, 2003. The sun and heliosphere at solar maximum. Science, 302. 1165–1169.

Smith, D.S., Scalo, J., 2006. Statistics of galactic cosmic-ray modulation variations on habitable planets. Astrophys. J., in preparation .

Smith, D.S., Scalo, J., Wheeler, J.C., 2004a. Importance of biologically active aurora-like UV emission: Stochastic irradiation of Earth and Mars. Origins of Life and Evolution of the Biosphere, in press.

Smith, D.S., Scalo, J., Wheeler, J.C., 2004b. Transport of ionizing radiation in habitable exoplanet atmospheres. Icarus, 171, 229.

Sniegowski, P.D., Gerrish, P.J., Johnson, T., Shaver, A., 2000. The evolution of mutation rates: Separating causes from consequences. BioEssays 22, 1057–1066.

Sparrow, A.H., Underbrink, A.G., Sparrow, R.C., 1967. Chromosomes and cellular radiosensitivity. I. The relationship of D0 to chromosome volume and complexity in seventy-nine different organisms. Rad. Res. 31, 915–949.

Sparrow, A.H., Underbrink, A.G., Rossi, H.H., 1972. Mutations induced in Tradescantia by small doses of X-rays and neutrons: analysis of dose-response curves. Science. 176, 916–918.

Spitzer, L., 1962. Physics of Fully Ionized Gases. Wiley-Interscience, NY.

Spitzer, L., 1978. Physical processes in the interstellar medium. Wiley-Interscience, NY.

Stevenson, D.J., 2003. Planetary magnetic fields. Earth Plan. Sci. Lett. 208. 1–11.

Stone, E.C., Cummings, A.C., McDonald, F.B., Heikkila, B.C., Lal, N., Webber, W.R., 2005. Voyager 1 explores the termination shock region and the heliosheath beyond. Science, 309. 2017–2020.

Stothers, R., 1980. Giant solar flares in Antarctic ice. Nature. 287, 365–365.

Stozhkov, Y.I., 2003. The role of cosmic rays in the atmospheric processes. J. Phys. G: Nucl. Part. Phys., 29. 913–923.

Straume, T., Rugel, G., Marchetti, A.A., and 10 others, 2003. Measuring fast neutrons in Hiroshima at distances relevant to atomic-bomb survivors. Nature, 424. 539–542.

Sutherland, B.M., Bennett, P.V., Sidorkina, O., Laval, J., 2000. Clustered DNA damages induced in isolated DNA in human cells by low doses of ionizing radiation. Proc. Natl. Acad. Sci. 97, 103–108.

Svensmark, H., 2000. Cosmic rays and Earth's climate. Sp. Sci. Rev., 93. 175–185.

Svensmark, H., 2004. Cosmic rays and the evolution of Earth's climate during the Last 4.6 billion years. Submitted to Phys. Rev. Lett., 16 Jun 2003.

Svensmark, H., Friis-Christensen, E., 1997. Variation of cosmic ray flux and global cloud coverage—a missing link in solar-climate relationships. J. Atmos. Solar-Terr. Phys., 11, 1225–1232.

Swartz, W., Nisbet, J., Green, A., 1971. Analytic expression for the energy-transfer rate from photoelectrons to thermal-electrons. J. Geophys. Res. 76, 8425.

Talbot, R.J., Butler, D.M., and Newman, M.J., 1976. Climatic effects during passage of the Solar System through interstellar clouds. Nature, 262. 561–562.

Talbot, R.J. and Newman, M.J., 1977. Encounters between stars and dense interstellar clouds. Astrophys. J. Supp., 34. 295–308.

Tavani, M., Band, D., Ghirlanda, G., 2000. Time Resolved GRB Spectroscopy. In: Kippen, R.M., Mallozzi, R.S., Fishman, G.J. (Eds.), AIP Conf. Proc. 526: Gamma-ray Bursts, 5th Huntsville Symposium. pp. 185–189.

Tucker, W.H., Koren, M., 1971. Radiation from a high-temperature low-density plasma: The X-ray spectrum of the solar corona. Astrophys. J. 168, 283–312.

Turnbull, M.C., Tarter, J.C., 2003. Target selection for SETI. I. A catalog of nearby habitable stellar systems. Astrophys. J. Supp. 145, 181–198.

Turner, J.E., 1995. Atoms, Radiation, and Radiation Protection, 2nd ed., Wiley, NY.

UNSCEAR 2000 Report, Sources and effects of ionizing radiation. Annex B: Exposures from natural radiation sources. http://www.unscear.org/pdffiles/annexb.pdf

UNSCEAR Hereditary Effects of Radiation (United Nations, New York, 2001).

Usoskin, I.G., Gladysheva, O.G., and Kovaltsov, G.A., 2004. Cosmic ray-induced ionization in the atmosphere: spatial and temporal changes. J. Atmos. Solar-Terr. Phys., 66, 1791–1796.

van Belkum, A., Scherer, S., van Alphen, L., Verbrugh, H., 1998. Short-sequence DNA repeats in prokaryotic genomes. Microbiol. Mol. Biol. Rev. 62, 275–293.

Veronig, A., Temmer, M., Hanslmeier, A., Otruba, W., Messerotti, M., 2002. Temporal aspects and frequency distributions of solar soft X-ray flares. Astron. Astrophys. 382, 1010–1080.

Violot, D., M'kacher, R., Adjadj, E., Dossou, J., de Vathaire, F., Parmentier, C., 2005. Evidence of increased chromosomal abnormalities in French Polynesian thyroid cancer patients. Eur. J. Nucl. Med. Mol. Imaging. 32, 174–179.

Vogt, S.S., Marcy, G.W., Butler, R.P., and Apps, K., 2000. Six new planets from the Keck precision velocity survey. Astrophys. J., 536. 902–914.

von Sonntag, C., 1987. The chemical basis of radiation biology. Taylor & Francis, NY.

Wänke, H., Brückner, J., Dreibus, G., Rieder, R., Ryabchikov, I., 2001. Chemical composition of rocks and soils at the Pathfinder site. Sp. Sci. Rev. 96, 317–330.

Ward, J.F., 1997. In DNA Damage and Repair: Biochemistry, Genetics, and Cell Biology, Vol. II, J. A. Nickoloff, M. F. Hoekstra, Eds. (Humana Press, Totawa), pp. 65-84.

Ward, J.F., 1999. Ionizing radiation damage to DNA: A challenge to repair systems. In: Dizdaroglu, M., Karakaya, A.E. (Eds.), Advances in DNA damage and repair: Oxygen radical effects, cellular protection, and biological consequences. Kluwer/Plenum, NY, pp. 431–439.

Ward, P.D., Brownlee, D., 2000. Rare Earth: Why Complex Life is Uncommon in the Universe. Copernicus Books, NY.

Watson, A.M., Henney, W.J., 2001. An efficient Monte Carlo algorithm for a restricted class of scattering problems in radiation transfer. Revista Mexicana de Astronomia y Astrofisica 37, 221–236.

Webber, W.R., 1998. A new estimate of the local interstellar energy density and ionization rate of Galactic cosmic rays. Astrophys. J., 506. 329–334.

West, A.A., Hawley, S.L., and 9 others, 2004. Spectroscopic properties of cool stars in the Sloan Digital Sky Survey: An analysis of magnetic activity and a search for subdwarfs. Astron. J., 128. 426–436.

Wetherill, G.W., 1996. The formation and habitability of extra-solar planets. Icarus, 119. 219–238.

Whalen, J.A., O'Neil, R.R., Picard, R.H., 1985. The aurora. In: Jursa, A.S. (Ed.), Handbook of Geophysics and the Space Environment. pp. 12–34.

Whang, Y.C., Burlaga, L.F., Wang, Y.-M., and Sheeley, N.R., 2003. Solar wind speed and temperature outside 10 AU and the termination shock. Astrophys. J., 589. 635–643.

Wheatland, M.S., 2005. Space Weather. 3, S07003.

Wiechert, U.H., 2002. Earth's early atmosphere. Science 298, 2341–2342.

Wilson, J.W., Cucinotta, F.A., Kim, M.-H.Y., Schimmerling, W., 2001. Optimized shielding for space radiation protection. Physica Medica. XVII, 67–71.

Wilson, J.W., Clowdsley, M.S., Cucinotta, F.A., Tripathi, R.K., Nealy, J.E., De Angelis, G., 2004. Adv. Sp. Res. 34, 1281.

Wimmer-Schweingruber, R.F. and Bochsler, P., 2000. Is there a record of interstellar pick-up ions in lunar regolith? In *Acceleration and Transport of Energetic Particles Observed in the Heliosphere: AIP Conf. Proc.*, edited by R.A. Mewaldt et al., Melville, NY, pp. 270–273.

Wimmer-Schweingruber, R.F. and Bochsler, P., 2001. A non-solar origin of the "SEP" component in lunar soils. In *The Outer Heliosphere: The Next Frontiers, COSPAR Colloquia Ser. 11*, edited by K. Scherer, H. Fichtner, H.J. Fahr, and E. Marsch, Pergamon Press, Amsterdam, pp. 507–510.

Witt, A.N., 1977. Multiple scattering in reflection nebulae. I—A Monte Carlo approach. Astrophys. J. Supp. 35, 1–6.

Witte, M., 2004. Kinetic parameters of interstellar neutral helium: Review of results obtained during one solar cycle with the Ulysses/GAS-instrument. Astron. Astrophys., 426. 835–844.

Wood, B.E., Muller, H.R., Zank, G.P., Linsky, J.L., 2002. Measured mass-loss rates of solar-like stars as a function of age and activity. Astrophys. J. 574, 412–425.

Woods, T.N., Eparvier, F.G., Fontenla, J., Harder, J., Kopp, G., McClintock, W.E., Rottman, G., Smiley, B., and Snow, M., 2004. Solar irradiance variability during the October 2003 solar storm period. Geophys. Res. Lett. 31, L10802–10806.

Xu, Y., Ross, R.R., McCray, R., 1991. Comptonization of gamma rays by cold electrons. Astrophys. J. 371, 280–288.

Yabushita, S. and Allen, A.J., 1989. On the effect of accreted interstellar matter on the terrestrial environment. Mon. Not. Roy. Astron. Soc., 238. 1465–1478.

Yamazaki, T. and Oda, H., 2002. Orbital influence on Earth's magnetic field: 100,000-year periodicity in inclination. Science, 295. 2435–2438.

Yeghikyan, A. and Fahr, H., 2004a. Effects induced by the passage of the sun through dense molecular clouds. I. Flow outside of the compressed heliosphere. Astron. Astrophys., 415. 763–770.

Yeghikyan, A. and Fahr, H., 2004b. Terrestrial atmospheric effects induced by counter-streaming dense interstellar cloud material. Astron. Astrophys., 425. 1113–1118.

Yung, Y.L., DeMore, W.B., 1999. Photochemistry of planetary atmospheres. Oxford Univ. Press, NY.

Zank, G.P., 1999. Interaction of the solar wind with the local interstellar medium: A theoretical perspective. Sp. Sci. Rev., 89, 412–688.

Zank, G.P., Frisch, P.C., 1999. Consequences of a change in the Galactic environment of the sun. Astrophys. J. 518, 963–965.

Zirin, H., Sammis, I., Tang, F., 2000. The magnetic circumstances of large flares. In: Ramaty, R., Mandzhavidze, N. (Eds.), ASP Conf. Ser. 206: High Energy Solar Physics Workshop—Anticipating HESSI. pp. 37–42.

Vita

David Samuel Smith was born and raised in Northeast Texas, the son of James and Mary Smith. After graduating valedictorian of Commerce High School in 1997, he attended The University of Texas at Austin on full scholarship. In May 2001, he graduated with a B.S. in physics and a B.A. in astronomy and was named Dean's Honored Graduate in both departments. That fall, he entered graduate school at Harvard University and finished his A.M. in astronomy that year. In the summer of 2002, he returned to the University of Texas to finish his Ph.D. and marry his fiancée, Diana Carver.

Permanent Address: 2702 Rix St, Commerce, Texas 75428

This dissertation was typeset with LaTeX 2_ε[8] by the author.

[8] LaTeX 2_ε is an extension of LaTeX. LaTeX is a collection of macros for TeX. TeX is a trademark of the American Mathematical Society. The macros used in formatting this dissertation were written by Dinesh Das, Department of Computer Sciences, The University of Texas at Austin, and extended by Bert Kay, James A. Bednar, and Ayman El-Khashab.